Helsinki University of Technology Automation Technology
Series A: Research Reports No. 36
Espoo, November 2010

ESTIMATION OF UNKNOWN NODE POSITIONS OF A LOCALIZATION NETWORK WITH A MULTI-ROBOT SYSTEM

Mikko Elomaa

Aalto University
School of Science
and Technology

Aalto University
Automation Technology
Series A: Research Reports No. 36
Espoo, November 2010

Estimation of Unknown Node Positions of a Localization Network with a Multi-robot System

Mikko Elomaa

Doctoral dissertation for the degree of Doctor of Science in Techology to be presented with due permission of the Faculty of Electronics, Communications and Automation for public examination and debate in Auditorium TU2 at the Aalto University School of Science and Technology (Espoo, Finland) on the 3rd of December 2010 at 12 noon.

Aalto University
School of Science and Technology
Faculty of Electronics, Communications and Automation
Department of Automation and Systems Technology

Distribution:

Aalto University
School of Science and Technology
Faculty of Electronics, Communications and Automation
Department of Automation and Systems Technology
P.O. BOX 11000
FI-00076 AALTO
FINLAND

e-mail: Mikko.Elomaa@tkk.fi
Tel. +358 9 470 23778
Fax +358 9 470 23308

ISBN 978-952-60-3440-9 (printed)
ISBN 978-952-60-3441-6 (pdf)
ISSN 0783-5477

Aalto-Print
Helsinki 2010

Aalto University

ABSTRACT OF DOCTORAL DISSERTATION	AALTO UNIVERSITY SCHOOL OF SCIENCE AND TECHNOLOGY P.O. BOX 11000, FI-00076 AALTO http://www.aalto.fi

Author Mikko Elomaa

Name of the dissertation

Estimation of Unknown Node Positions of a Localization Network with a Multi-robot System

Manuscript submitted 14.6.2010	Manuscript revised 28.10.2010
Date of the defence 3.12.2010	
☒ Monograph	☐ Article dissertation (summary + original articles)

Faculty	Faculty of Electronics, Communications and Automation
Department	Department of Automation and Systems Technology
Field of research	Mobile robotics
Opponent(s)	Professor Pekka Appelqvist
Supervisor	Professor Aarne Halme
Instructor	

Abstract

In this thesis, a novel method for estimating the node positions of a localization network is presented. A multi-robot system is used to map the positions of the network nodes, while the robots track their own position simultaneously. It is an application of simultaneous localization and mapping (SLAM). The localization is based on bearing angle measurements between a robot and a network node. Hence, the method used for the localization can be called bearing-only SLAM.

The localization method is based on a probabilistic approach. All the measurement data are collected to a centralized Kalman Filter. As a result of the non-linear measurement equation, the Extended Kalman Filter (EKF) algorithm is used. The centralized structure maintains the covariances between all the entities and thus takes full advantage of the cooperation in a multi-robot system. The algorithm is shown to work with a sparse distribution of landmarks. A robot makes a bearing angle measurement to only one landmark at a time. Therefore, the computational complexity of the Kalman filter stays low.

The Radio Frequency Identification (RFID) technology is used in the case study presented in this thesis. It is shown that passive RFID tags can serve as landmarks with a unique ID. The inexpensive, maintenance-free RFID tags can easily be distributed over the intended working area of the robots to form a localization network. The bearing angle measurements to the RFID tags do not need to be highly accurate as the proposed algorithm can handle uncertain measurements. Simulations and laboratory experiments are used in order to prove the performance of the proposed method.

Keywords SLAM, Localization network, RFID	
ISBN (printed) 978-952-60-3440-9	ISSN (printed) 0783-5477
ISBN (pdf) 978-952-60-3441-6	ISSN (pdf)
Language English	Number of pages 129
Publisher Aalto University, Department of Automation and Systems Technology	
Print distribution Aalto University, Department of Automation and Systems Technology	
☒ The dissertation can be read at http://lib.tkk.fi/Diss/2010/isbn9789526034416	

Aalto-yliopisto

VÄITÖSKIRJAN TIIVISTELMÄ	AALTO-YLIOPISTO TEKNILLINEN KORKEAKOULU PL 11000, 00076 AALTO http://www.aalto.fi

Tekijä Mikko Elomaa

Väitöskirjan nimi

Paikannusverkon solmukohtien paikannus monirobottijärjestelmällä

Käsikirjoituksen päivämäärä 14.6.2010	Korjatun käsikirjoituksen päivämäärä 28.10.2010
Väitöstilaisuuden ajankohta 3.12.2010	
☒ Monografia	☐ Yhdistelmäväitöskirja (yhteenveto + erillisartikkelit)

Tiedekunta	Elektroniikan, tietoliikenteen ja automaation tiedekunta
Laitos	Automaatio- ja Systeemitekniikanlaitos
Tutkimusala	Liikkuvat robotit
Vastaväittäjä(t)	Professori Pekka Appelqvist
Työn valvoja	Professori Aarne Halme
Työn ohjaaja	

Tiivistelmä

Tässä väitöskirjassa esitetään uusi menetelmä paikannusverkon solmukohtien paikantamiseksi. Monirobottijärjestelmää käytetään verkoston solmukohtien paikantamiseen. Samalla robotit huolehtivat oman paikkatiedon ylläpitämisestä. Kyseessä on samanaikaisen paikannuksen ja kartoituksen sovellus. Paikannus perustuu robotin ja solmukohdan välisen suuntiman mittaamiseen.

Menetelmässä käytetään todennäköisyyslaskuun perustuvaa lähestymistapaa. Kaikki mittatieto kerätään yhteen keskitettyyn Kalman suotimeen. Koska suuntakulmiin perustuva mittaus johtaa epälineaarisiin mittausyhtälöihin, käytetään menetelmässä laajennettua Kalman suodinta. Keskitetyn ratkaisun avulla pystytään pitämään kirjaa robottien ja maamerkkien välisistä vuorovaikutussuhteista. Näin voidaan hyödyntää robottien välinen yhteistyö mahdollisimman hyvin. Paikannusalgoritmin osoitetaan toimivan maamerkkien ollessa harvassa. Robotit suuntivat yhtä maamerkkiä kerrallaan. Näin ollen algoritmi on laskennallisesti kevyt.

Väitöskirjassa esitetyssä sovelluksessa käytetään radiotaajuista tunnistetekniikkaa. Sovelluksella osoitetaan, että passiivisia tunnisteita voidaan käyttää maamerkkeinä, joilla on yksilöllinen tunnus. Passiiviset tunnisteet ovat halpoja eivätkä ne vaadi huoltoa. Niistä voidaan helposti muodostaa paikannusverkko robottien työskentelyalueelle. Maamerkkeihin tehtyjen suuntimien ei tarvitse olla erityisen tarkkoja, koska paikannus algoritmi sisältää mittausepävarmuuden huomioon ottavan mekanismin. Menetelmän toimivuus osoitetaan simulaatioiden ja laboratoriokokeiden avulla.

Asiasanat	Samanaikainen paikannus ja kartoitus, paikannusverkko, radiotaajuinen tunnistetekniikka		
ISBN (painettu)	978-952-60-3440-9	ISSN (painettu)	0783-5477
ISBN (pdf)	978-952-60-3441-6	ISSN (pdf)	
Kieli	Englanti	Sivumäärä	129
Julkaisija	Aalto-yliopisto, Automaatio- ja systeemitekniikan laitos		
Painetun väitöskirjan jakelu	Aalto-yliopisto, Automaatio- ja systeemitekniikan laitos		
☒ Luettavissa verkossa osoitteessa http://lib.tkk.fi/Diss/2010/isbn9789526034416			

Preface

This research was conducted in the Automation Technology Laboratory and was mostly funded by the Finnish Centre of Excellence in Generic Intelligent Machines Research (GIM). My one-year visit to the Laboratoire d'electronique et de technologie de l'information, CEA, France, was funded by the Finnish Cultural Foundation.

I am grateful to Professor Aarne Halme, my supervisor, for all the guidance throughout the years of this thesis project and for his help in arranging my visit to CEA.

I also wish to express my gratitude towards Dr. François Vacherand for welcoming me to France and helping me to find the right people to work with. Sincere thanks for the comments on my thesis as well. Thanks go also to my other pre-examiner Professor Kalevi Hyyppä.

Many thanks go to Dr. Elisabeth Crochon, Dr. Serge Bories and Dr. Benoit Lépine, who helped me with the RFID technology during my stay in France.

The following people at the Automation Technology Laboratory have provided me with valuable help and advice on various matters: Marek Matusiak with robot platforms, Sami Kielosto and Kalle Rosenblad with electronics, Janne Paanajärvi with mathematics, Antti Maula with programming, Seppo Heikkilä and Jari Saarinen with research methods and laboratory experiments, Matti Öhman with algorithms and Tapio Leppänen with mechanics. Big thanks go to the whole staff of the Automation Technology Laboratory for the easy going atmosphere.

My friends have kept me sane and provided the motivation to strive for better solutions. Thanks especially to Hakamäki group and to the members of the band Vitriolic Swipe. With you, I was able to take a break from work and, for a moment, focus on completely different matters.

I am also grateful to my family for the support and guidance I have received during my whole life. This achievement would not have been possible without your help.

Finally, I want to express the biggest thanks to Vicky Wong for frequent discussions and advice on scientific and linguistic matters, but most of all for the tremendous support during the final years of this project. It made all the difference to have someone like you by my side.

Espoo, November 2010

Mikko Elomaa

Contents

Nomenclature

2D	Two-dimensional
(x_r, y_r)	Robot position in 2D-coordinate frame
(x_t, y_t)	Target (e.g. landmark) position in 2D-coordinate frame
α	Polarization angle between reader and tag antennas
γ	Mutual angle between two bearing angles
δ	Partial derivative
ϵ	Error term, used with specifying subscript (e.g. ϵ_{syst} for systematic error)
η	Bisector angle of two bearing angle measurements
θ	Heading angle of a robot
λ	Measured bearing angle or wavelength
π	Mathematical constant, pi
σ	Standard deviation of a random variable
σ^2	Variance of a random variable
v	Measurement noise
ϕ	Azimuth angle to an object
ψ	Direction of robot movement with respect to the previous heading angle estimate
ω	Model noise
atan2(y,x)	A function, that gives an angle in radians, $(-\pi...\pi]$, between the positive x-axis and the point (x,y) specified
$f(\hat{x}_{k-1}, u_k, 0)$	Prototype of Kalman filter motion model
$h(\hat{x}_k^-, 0)$	Prototype of Kalman filter measurement model
k	Sample index
u_k	Control vector at instant k
x_k	State at instant k
$\hat{x}_k$	Estimate of state at instant k
$\hat{x}_k^-$	Priori of state at instant k
z_k	Measurement at instant k
A	System matrix
B	Control matrix
H	Measurement matrix
I	Identity matrix
K	Kalman gain
$\mathcal{N}(0, 1)$	Normal distribution with zero mean and variance of 1
O(N)	Complexity of an algorithm

P_k	Error covariance matrix at instant k
P(λ)	Landmark detection probability
Q	Model noise covariance matrix
R	Measurement noise covariance matrix
U	Control noise covariance matrix
CEA	Commissariat a l'energie atomique, a French research center
CL	Cooperative localization
CST	A company, "Computer Simulation Technology"
dB	Decibel, logarithmic unit expressing relative quantity
dBi	Gain of an antenna compared to a theoretical isotropic antenna
dBm	Power measurement relative to 1 milliwatt
DOA	Direction of Arrival
EKF	Extended Kalman Filter
EPC	Electronic Product Code, an ID number of an RFID tag
ERP	Effective Radiated Power
EIRP	Effective Isotropic Radiated Power
F/B-ratio	Front-to-back ratio. The ratio of power gain between the front and back of a directional antenna
FR-4	Material containing fiberglass and epoxy. Used for PCBs
GIM	Finnish centre of excellence in Generic Intelligent Machines research
GPS	Global Positioning System
HF	High Frequency, 3-30 MHz range in radio frequencies
LETI	Laboratoire d'Electronique et de Technologie de l'Information
PC	Personal Computer
PCB	Printed Circuit Board
PWM	Pulse-Width Modulation
RF	Radio Frequency, electromagnetic radiation of frequency range 3kHz-300GHz
RFID	Radio Frequency Identification
RS-232	A standard for serial binary data signals (used in PC serial ports)
RSSI	Received Signal Strength Indication
SLAM	Simultaneous localization and mapping
UHF	Ultra High Frequency, 300-3000 MHz range in radio frequencies
USB	Universal Serial Bus
VNA	Vector Network Analyzer

List of Figures

List of Tables

Chapter 1

Introduction

1.1 Overview

The localization of a mobile robot is of the utmost importance for efficient task execution. The field has been well studied and a lot of different methods have been proposed. These methods can be roughly divided into two categories: one with methods relying only on internal sensors measuring the movement of a robot directly and the other with methods using external infrastructure such as beacons, landmarks, etc. A robot relying only on its proprioceptive sensors, such as wheel encoders, gyroscopes or accelerometers, can work in environments without any external infrastructure. However, when it is moving in an unknown environment the uncertainty in the robot's position estimate increases over time, because the robot does not have any absolute reference for its position.

The benefit of using external infrastructure is that a robot can always estimate its position within bounded error. The robot measures its position relative to a known location, that of a landmark, and the resulting position estimate does not depend on the history of the robot. The accuracy of the position estimate of a robot only depends on the measurement error and the error in the position data of the landmark. Hence, the accuracy of the position estimate of a robot is bounded by the limits of the measurement error and the landmark position error.

An intermediate solution between the aforementioned methods is simultaneous localization and mapping (SLAM). The idea of SLAM is to observe static features in the surroundings of the robot and use them to build a map. The features are not predefined, so the sensor has to extract them from the environment and localize them. The sensor has to be able to make recurrent measurements to the features in order to correct the accumulated estimation error in the pose of the robot. The features can be natural or artificial, depending on the sensor used.

1.2 Motivation and aims for the study

The benefits of external reference points for the localization of a robot are clear. Unfortunately, the natural existence of such reference points cannot be guaranteed. The deployment and maintenance costs of artificial landmarks for reference points are often too high. This research aims to find a novel method for providing external reference points, i.e. landmarks either completely without human participation or with minimum human effort in the deployment and localization of the landmarks.

When the landmarks are small and easy to deploy (e.g. RFID tags) the robots can place them autonomously. The RFID tags used in the case study of this research are like stickers and a simple mechanism for attaching them to walls would be sufficient. If the price of a landmark is only a few cents, the number of landmarks does not need to be optimized and they can be deployed in abundance. Thus the system is expected to function properly, regardless of a few badly placed landmarks, a result of the limited environment sensing capability of the robots. With this approach humans are only needed to launch the robots.

Humans can also deploy the landmarks easily, when the location of each landmark does not need to be known at the moment of deployment. If landmarks are deployed in advance, they can contain messages for robots, such as the limits of a work area or other mission related information.

The aim of this study is to show how a group of robots can be used in the localization of landmarks. A multi-robot approach is expected to offer better overall performance. Cooperating robots can maintain more accurate pose estimates, when the information sharing is sufficient. Additionally, when multiple robots operate simultaneously, the time required for the localization of the landmarks with a certain accuracy is a fraction of the time required with a single robot.

The approach used in the case example is also very minimalistic in the sense of high technology sensors. The system has been tested using only cheap, commercially available sensors.

1.3 Scientific contribution of the dissertation

The main contribution of this dissertation is the novel method for the estimation of the node positions in a localization network. A localization network is a collection of usually static nodes, that provide location information over the coverage area of the network. In order to provide localization related information, the nodes have to be localized.

In this study it is shown that:

- robots can autonomously initialize and expand a support system for localization. Previously unknown positions of nodes in a localization

network are estimated with a probabilistic algorithm, while robots track their own pose simultaneously;

- there are benefits of using multiple robots for localization instead of a single robot. Information sharing between the robots results in a better overall performance.

The use of the Radio Frequency Identification (RFID) technology in localization is also examined. A novel application using passive RFID tags as landmarks is presented. The accuracy of the localization system is shown to be sufficient for indoor localization in an office environment. The case study in this dissertation proposes a novel application:

- bearing-only SLAM with passive RFID tags as landmarks

Previous work exists, in which passive RFID tags are used as landmarks (Hahnel et al., 2004; Kulyukin et al., 2004; Bohn, 2006; Kleiner et al., 2006), but the novel method in this study uses an unprecedented approach to localization and is the first RFID localization method that makes use of the benefits of a multi-robot system. The approach is minimalistic in terms of its economic and computation costs.

1.4 Outline of the dissertation

This dissertation has the following structure:

- Chapter 1: Short introduction and aims of the research
- Chapter 2: Literature review on the state of the art of multi-robot localization
- Chapter 3: A novel method for distributed node position estimate using a multi-robot system is presented
- Chapter 4: The setup of the simulation experiments is explained
- Chapter 5: The setup of the laboratory experiments is explained
- Chapter 6: The results of the simulations and laboratory experiments are presented and discussed
- Chapter 7: The summary of the research results

1.5 Author's contribution

The development of the algorithm as well as the design and implementation of the bearing angle measurement unit based on the RFID technology was carried out by the author. The simulations and laboratory experiments were also designed and conducted by the author. All the analysis and conclusions are made by the author. The robot platform and the software for operating a robot was developed in the Generic Intelligent Machines (GIM) research group. The robot hardware team was led by Marek Matusiak and the software team by Antti Maula.

1.6 Declaration of previous work

Publications have been made at various stages of the research.

- The concept was first published in (Elomaa et al., 2008)
- The full algorithm with early results was published in (Elomaa and Halme, 2009)
- The final results are published in (Elomaa and Halme, 2010)

Chapter 2

State of the art in multi-robot localization

2.1 Description of localization

The basis of localization is a coordinate frame, where all the objects of interest are to be located. Depending on the application, the coordinate frame may have one, two or three axes. A two-axis coordinate frame is typical in navigation at sea or mobile robotics, whereas a three-dimensional coordinate frame is used with aircraft or underwater applications. In global localization the objects are localized with respect to the origin of a common coordinate frame. Therefore, the relative positions of two known objects can always be solved. Figure 2.1 shows two objects located in a two-dimensional coordinate frame. The vectors r_A and r_B define the displacements of the objects from the origin of the coordinate frame.

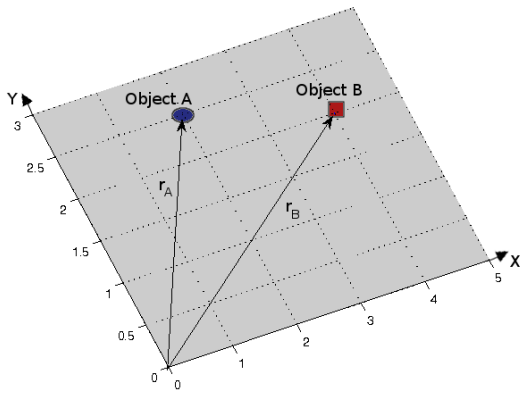

Figure 2.1: 2D coordinate frame

2.2 Navigation

Even though ships have been used for transportation and trade for at least 4000 years, navigation on the open seas only started to develop in the middle of the second millennium Anno Domini. Earlier, ships had to navigate along a visible coastline or use the sun or the North Star to keep the correct heading during the short passages, where the land could not be used for navigation. Estimates of the heading and the time that had elapsed made it possible to calculate the relative movement of a ship by dead reckoning. However, errors in the measurements and other factors such as sea currents and wind, cause inaccuracies in the estimate of the motion of a ship. The development of the compass increased the accuracy of heading estimates, but could not compensate for the other sources of error.

When methods for measuring the angle between the horizon and the sun or certain stars were developed the latitude of the ship could be estimated, regardless of the time or the course traveled. The latitude indicates the position of the ship in a north-south direction in degrees from the equator towards a pole. Later with the invention of the seagoing chronometer, the longitude (position in an east-west direction) could also be determined.

2.3 Mobile robot localization methods

A mobile robot can use its own proprioceptive and exteroceptive sensors for localization without the help of an external localization system. However, if an external system is available it can usually reduce the uncertainty in the robot's pose and maintain it within finite bounds over time.

2.3.1 Internal sensors only

In mobile robot localization the simplest approach is to use encoders on the wheels or motors of a robot. The encoder pulses represent a discrete step of a fixed distance, usually a fraction of a millimeter. By integrating from the pulses of the robot's wheel encoders, the relative translation and rotation of the robot can be calculated when the mechanics of the robot are known. However, the measurement errors accumulate over time and the uncertainty of the pose estimate increases without bounds. For example, a small wheel slippage may cause inaccuracy in the heading angle estimate of a robot, which over time leads to a considerable position error. The mechanical structure of the robot may have a considerable effect on the accuracy of the odometry. For a two-wheel differential-drive robot with proper calibration the accuracy can be relatively good (Papadopoulos and Misailidis, 2007). A thorough overview of different mechanical constructions and calibration methods can be found in (Borenstein et al., 1996). Additional

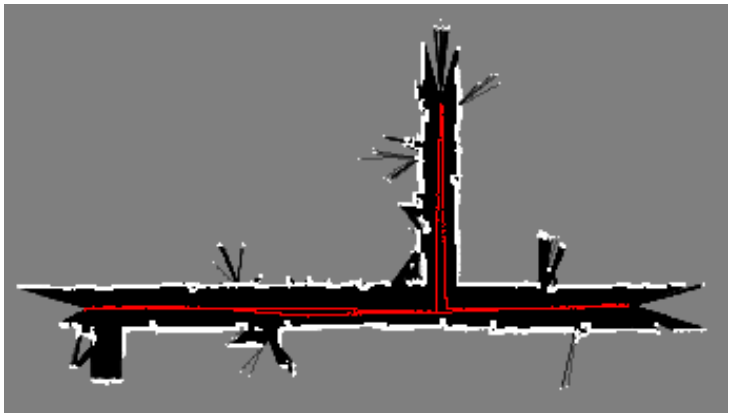

Figure 2.2: An example of the SLAM method. A scan matching algorithm with a laser scanner and odometry measurements were used.

sensors, such as a gyroscope and compass can reduce the error in the heading angle, but they also involve sources of error. A gyroscope drifts over time and a compass is sensitive to magnetic disturbances (Heikkilä, 2005).

Nowadays, the most common approach to the localization of a mobile robot is the method called Simultaneous Localization And Mapping (SLAM). The idea of SLAM is to build a map by observing static features in the surrounding environment. In order to position the features correctly with respect to each other, the location of the sensor (i.e. the location of the robot) has to be estimated during each observation. Thus, localization has to be solved simultaneously. The same sensors are used for both mapping and localization. Hence, the mapping and pose uncertainties are correlated. The complexity of the SLAM problem has been shown to be O(N^2), N being the number of landmarks in the map (Nerurkar and Roumeliotis, 2007). An example of the SLAM method is illustrated in Figure 2.2.

The identification of the natural features is not trivial. Often there are a large number of features that look very similar to the sensor. This is especially true in human-made environments, such as office buildings or hospitals. The difficulty of identifying two separate observations of the same feature is a typical problem in multi-robot SLAM, but it also appears in a single robot scenario, when the robot returns to a previously mapped place from a new direction. This is called the loop-closing problem.

Several different variations of the SLAM method exist in order to best address different problems. The most common ones are the approaches, which use particle filter or Kalman filter algorithms and a 2D laser scanner as their measurement hardware. A solution based on an extended Kalman filter was introduced as long ago as two decades ago (Smith et al., 1990). Since then, several improvements have been proposed by different researches concen-

trating on some particular problem in the SLAM localization method. Newman and Ho address the loop-closing problem by combining the observations of visual features with laser scanner data (Newman and Ho, 2005). In (Williams et al., 2002a) sub maps are used to keep the computational burden from increasing over time. Fast SLAM algorithms have been developed to cope with a large number of landmarks (Montemerlo, 2002) or real-time constraints (Montemerlo et al., 2003).

2.3.2 External localization systems

When a robot is integrating its position estimate from relative measurements, sooner or later the position error will grow to such proportions that the task execution becomes impossible. For long-term operation, it is important that the robot can correct the accumulated error periodically and keep the error in the position estimate within finite bounds. This can be done using external infrastructure.

The benefit of using external infrastructure is that the accuracy of the position estimate of a robot stays within certain bounds, regardless of the time that has elapsed. The measurements to the landmarks are independent of each other and have inaccuracies that only depend on the measurement system used. Additionally, with an absolute positioning system, the robot does not need to be told its pose after power-up, because it can localize itself with the available measurements. In some systems the measurements to the static external objects are the only source of information, but in mobile robotics it is common to use a combination of sensors measuring the internal state of a robot and the environment.

A well-known example of a localization system with external infrastructure is the Global Positioning System (GPS). Whenever a GPS device is turned on, it can calculate its pose in the global coordinate frame provided that at least three satellites are visible. However, in an indoor environment the metallic structures of the building usually prevent the use of GPS for localization. Additionally, the accuracy of a satellite-based system may not be adequate for robotic systems that require accurate positioning. Similar kinds of localization systems can be built on a smaller scale by placing beacons inside a building. A commonly used approach is to measure the distance between a robot and beacons with ultrasound sensors (Priyantha et al., 2000; Marantos et al., 2008). When the localization is based on the range measurements to known landmarks, it is called trilateration. Relative angle measurements to known landmark positions can also be used for localization (Shimshoni, 2002; Briechle and Hanebeck, 2004; Kim and Hmam, 2009). This method is called triangulation. Both methods normally assume that the distance or bearing to at least three landmarks can be measured, when the localization is performed, but even then the existence of a singular solution is not always guaranteed (Cohen and Koss, 1992).

The major drawbacks of using an external infrastructure are deployment and maintenance costs and the need for initial localization of each beacon before it can be used. Active beacons need a power supply, which means wiring during the installation phase or periodic recharging of the batteries. The initial localization can be done during the installation phase if an accurate map of the environment exists and if the beacons are installed at locations that can be recognized on the map. These constraints cannot always be satisfied.

2.3.3 Bearing-only SLAM

When a robot moves in a 2D plane its pose is defined by three variables: x and y-coordinates and the heading angle θ. The position coordinates of each landmark are defined by two variables. If the tracking of relative changes in the pose of a robot is to be performed without odometry sensors, there are 3M+2N unknowns to be solved. M is the number of different locations of the robot for measurements and N is the number of landmarks. In order to solve the unknowns the number of landmarks and measurements from different locations is defined by:

$$MN + 4 > 3M + 2N. \tag{2.1}$$

This states that at least four landmarks have to be visible simultaneously when the tracking of the robot is performed (Deans and Hebert, 2001).

When distance measurements to a landmark are combined with odometry, localization can be achieved with just one landmark. However, it does not necessarily provide a unique solution as shown in (Bais et al., 2006). Two consecutive range-only measurements to a single landmark will give two possible positions for a robot. Non-linear motion will solve this ambiguity. Additionally, an a priori estimate of the position of the robot may be used to choose the closer alternative.

If odometry data are combined with bearing angle measurements to a single landmark from two arbitrary points, a unique solution for the relative displacement can be obtained. The two positions of the robot and the intersection of the two bearing angles form a triangle. The angles of the triangle can be solved using the measured bearing angles. The scale of the triangle is solved using the distance between the two robot positions, measured with the odometry system. Systematic error in the odometry measurement cannot be corrected with bearing-only SLAM as the system scales according to the measured odometry (Deans and Hebert, 2001).

2.4 Multi-robot localization

Multi-robot systems have become a major research field in robotics over the past 15 years.. As early as in 1995 McLurkin experimented with a homogeneous robot society with 21 robots called Ants (McLurkin, 1995). In (Dellaert et al., 2002) a multi-robot system with one "mother ship" robot and several smaller and identical robots is introduced. The idea is that the bigger robot can carry a host of small robots and unleash them at places, where they may be useful. Examples of heterogeneous robot societies are presented in several papers by L.E. Parker et al. (Parker, 1998; Parker et al., 2003, 2004). Dudek et al. introduce a taxonomy for classifying multi-robot systems depending on various aspects (Dudek et al., 1996).

A group of robots faces the same problem of spatial awareness as a single mobile robot does. In order to successfully complete a task, each robot has to know at least its relative position with respect to the other robots and key points in the surrounding environment. If the group of robots is working together to accomplish a certain task they can move as a team, but in many applications the robots are required to be able to navigate independently, when necessary. In a multi-robot scenario there are several approaches to cooperative localization. These can be roughly divided into three categories: continuous cooperation between robots staying together, continuous cooperation between robots sharing localization-related information and occasional cooperation between two individual robots when they detect each other.

2.4.1 Relative measurements between robots

One of the earliest methods for cooperative localization was developed by Kurazume et al.. Their idea was to divide the robot team into two groups. While one group moves, the other one serves as a set of stationary reference points, i.e. landmarks. By constantly changing the roles of the groups, the team can advance step by step (Kurazume et al., 1994). A simplified version of the same method is to have a pair of robots moving together and improving their individual pose estimates with relative measurements between the two robots. If one robot can measure the distance and relative bearing angle to the other robot it can estimate the position of the other robot relative to its own pose. If the robot can also measure the relative heading angle of the other robot it can estimate its pose. An example of this kind of approach is a robot with a laser scanner tracking another robot with a three plane target mounted on it (Rekleitis et al., 2003). With the data provided by the laser scanner, the translation and rotation between the two robots can be calculated. In order to minimize the effects of odometry errors in the pose estimates, only one robot moves at a time, while the other one serves as a stationary beacon. The robots exchange localization related information

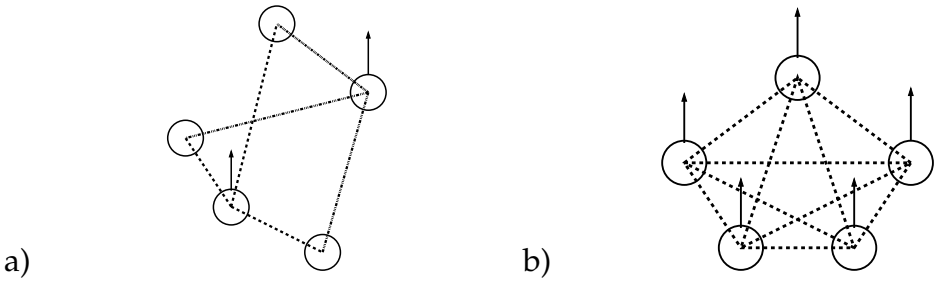

Figure 2.3: Relative measurements between a) robots alternating as static landmarks and moving units (marked with arrows) and b) robots moving in a formation

continuously, so both robots benefit from the relative measurements made by the robot with the laser scanner. This concept can be extended to a larger group of robots, where at least one robot has a suitable sensor for tracking the other robots. A similar idea has been used in several other research studies, where some members of the robot team act as stationary targets while one or more members move (Rekleitis et al., 1997; Grabowski et al., 2000; Howard et al., 2003; Spletzer and Taylor, 2003).

Another approach based on relative measurements in a group is mimicking formation flying. Robots drive in a formation, while each robot detects changes in the poses of the other robots. The shape of the formation has a considerable effect on the accumulated uncertainty in the robot poses (Hidaka et al., 2005; Andersson and Nygards, 2008). A heterogeneous robot group moving as a formation is introduced in (Parker et al., 2003). Two helper robots are used to steer two mobile sensor nodes, which are not capable of navigating on their own. The helper robots are equipped with suitable sensors for the localization and guidance of the mobile sensor nodes. One helper robot has a laser scanner and it provides the global localization for the group. Another helper robot has a vision system which can detect colored markers on the other members of the group. Therefore, it can follow the other helper robot and also control the mobile sensor nodes. Two different methods based on relative measurements between robots are illustrated in Figure 2.3.

2.4.2 Multi-Robot SLAM

The strict constraint on robots staying together may be too limiting in some scenarios. Then the robots can be allowed to explore independently and share localization information only when they meet. The simultaneous localization and mapping described in Section 2.3.1 can be adapted to a scenario with multiple robots. In a multi-robot case, the point of interest is the translation and rotation matrices between the coordinate frames of individual robots. When two robots share location related information, they have

to present it in a common coordinate frame. Therefore, the relation of the robot coordinate frames has to be solved. Many approaches assume that the robots know their relative poses right from the start, i.e. they start at a known pose in a common frame of reference. (Burgard et al., 2000; Simmons et al., 2000) In this case the multi-robot SLAM problem does not really differ from the distributed approach to single-robot SLAM described in (Williams et al., 2002b). Because of the analogy with single-robot approaches, systems of this kind are not considered in this chapter.

Other approaches deal with the uncertainty about relative poses by using various methods. The most popular one is to let the robots explore independently until a pair of robots manage to estimate their relative poses. The relative poses can be estimated by direct measurements between robots, when one robot incidentally detects another one (Howard et al., 2004; Chang et al., 2007; Zhou and Roumeliotis, 2006). The problem with this approach is that two robots can explore large overlapping areas before they detect each other. Thus the efficiency of the mapping task could be low.

Another method uses a map provided by previous robots for the initial localization of each additional robot (Fenwick et al., 2002; Williams et al., 2002b; Marco et al., 2003). This restricts the starting point of each new robot to the area of an existing map. A more versatile approach is introduced in (Ko et al., 2003) and developed further in (Fox et al., 2006). In this approach, the robots constantly try to exchange sensor and control information through wireless communication. The robots collect the available information from the sensors of other robots and try to localize the other robots on their own maps. When the partial maps of two robots overlap, the relative pose of the robots can be estimated and a meeting at a common point can be arranged. The meeting verifies the correctness of the relative pose estimate. A brute force approach was introduced by Howard et al.. It is based on the idea that all robots broadcast all the measurement data and thus, each robot can run a separate particle filter for every robot in order to know their poses. This clearly requires significant computational resources, but is very robust and simple.

Some approaches use only the landmarks on the overlapping parts of the local maps of different robots in order to align the maps (Thrun and Liu, 2003; Martinez-Cantin et al., 2007). This can be done, for example, by finding corresponding sets of landmarks based on the group geometry or by the direct feature matching of two landmarks. The benefit of this approach is that the robots do not need to meet and do not need sensors to measure their relative poses.

The different approaches presented here use both Bayesian (Fox et al., 2006; Zhou and Roumeliotis, 2006; Marco et al., 2003; Thrun and Liu, 2003) and non-Bayesian (Chang et al., 2007) algorithms. The most common algorithms are different variations of the Markov localization method using a particle filter or Kalman filtering techniques.

2.4.3 Collective Localization

A collective approach uses a single Kalman filter that collects data from all the robots and calculates estimates for each one (Roumeliotis and Bekey, 2002). The Kalman filter can be decomposed into a number of communication filters run by individual robots. Each robot moves independently and localizes itself with the available sensors. When two robots meet, they measure their relative poses and exchange information. Both robots benefit from the information exchange. In (Jo and Lee, 2007) the correlation of the error in the position estimates of multiple GPS receivers is used to achieve a more accurate position estimate than could be obtained with one GPS receiver only. The method is similar to differential GPS. It has been shown that cooperative localization is superior to single-robot localization using odometry and GPS. The cooperation between robots is achieved by sharing the position-related data between the robots.

2.5 RFID technology in localization

The Radio Frequency Identification (RFID) technology is used for localization in the case study in this research. An overview of the RFID technology and the applications of the RFID technology in localization now follows.

The RFID technology dates back to the 1940's, when the technology was used to identify approaching airplanes. Only after advances in semiconductor technology were the first commercial products launched in the 1980's. An RFID system contains one or more readers (or interrogators) and several tags (or labels). The tags can be passive, semi-passive or active. Passive tags have no power source, but get their operating power from the electric field provided by the reader antenna. Back-scattering of the electromagnetic waves that are received is used for the communication between a reader and a passive RFID tag. Semi-passive tags have a power supply, but no transmitter. Back-scattering is used for communication, but the communication range is greater than with passive tags and the tag remains operational outside the field of the reader. Active tags have a power supply and a transmitter. Therefore, they are able to communicate over distances far greater than the tags using back scattering.

The original purpose of the RFID tags was to provide unique identification. Recently more memory for information storage and different kinds of sensors have been integrated into the tags.

There have been a number of approaches using an RFID system for the localization of a mobile object. These approaches can be divided into two groups according to the type of RFID device (reader or tag) on the mobile object to be localized. Stationary reader(s) and mobile tags were used in (Hightower et al., 2000; Ni and Liu, 2004; Kim et al., 2004) whereas systems with a mobile reader and stationary tags are introduced in (Hahnel et al.,

2004; Bohn, 2006; Herianto et al., 2007; Kleiner et al., 2006; Kubitz et al., 1997; Kim and Chong, 2009). The aforementioned systems localizing mobile tags use active transponders. Systems with stationary tags use passive RFID tags, except in (Kim and Chong, 2009).

2.5.1 System with a mobile tag

In (Ni and Liu, 2004) a system called Landmarc is introduced. It is based on active RFID tags and multiple readers. The readers are placed around the area where localization is needed. Several active tags are placed in known locations to act as reference points, i.e. landmarks. The stationary readers are equipped with the Received Signal Strength Indication (RSSI). When the signal strength received from the tag to be localized is compared with the signal strength received from the reference tags, an estimate of the location of the tag can be computed. With four RFID readers and 16 reference tags in an area of $20m^2$, the average error in the position estimate of a mobile tag is approximately one meter. Another system using multiple stationary readers and an active mobile tag is described in (Hightower et al., 2000). The position estimate is based on the received signal strength of the readers. No reference tags are used. The position estimate is given as a 3 x 3 m square.

Signal strength and direction is used for the localization of a mobile tag in (Kim et al., 2004). The measurement of the relative distance between the reader and the tag is based on time-of-flight and phase shift methods. The direction of the tag is estimated using a 3-axis orthogonal array antenna. The research is based on simulation only. The simulations indicate good accuracy at distances up to three meters.

2.5.2 System with a mobile reader

An approach with a mobile reader is introduced in (Hahnel et al., 2004). The system uses passive tags as landmarks. 100 tags are attached to the walls of an office space measuring 28 x 28 m. A robot with an RFID reader, wheel encoders and a laser scanner is used to localize the landmarks. The RFID reader uses two patch antennas (20 x 20 cm), which provide a reading distance of 6 meters. The antennas are mounted perpendicularly to each other, one pointing forwards and to the left and the other forwards and to the right. The robot navigates around the office and localizes itself using the laser scanner with a SLAM algorithm. As it detects tags it creates a map of the tag positions with a probabilistic method. Both antennas have a probabilistic sensor model. When a tag is detected for the first time, its position is estimated by a discrete set of samples around the robot. Each further detection then refines the weights of the samples according to the sensor model. It is shown that after 200 measurements the position estimate of the landmark has converged towards a clearly distinguished position. In

some cases this may not happen if the robot cannot get measurements to the landmark from all the necessary directions. When the landmarks are localized the robot can navigate by just using the map of the RFID tags.

A floor filled with RFID tags (39 to 128 tags/m2) is used for localization in (Bohn, 2006). The system operates on an HF frequency and detects only tags directly underneath the robot. In tracing mode a robot is pushed along a trajectory, which is memorized by the tags and can later be followed autonomously. The data stored into the tags includes a trace-specific ID and a trace counter defining the order of the trace markers in local scope. A following robot then looks for tags with the given trace ID and increasing values of the trace counter. Hence, it follows the trace towards the tags with a higher value of the trace counter. In mapping mode the robot uses dead reckoning-based location information to record the position of each tag it encounters. Mapping with multiple robots is mentioned, but not implemented. A somewhat similar system is presented in (Herianto et al., 2007). RFID tags are placed on the floor and used as artificial pheromone sources. The use of a pheromone track for navigation is mentioned, but no actual results are presented.

Kleiner et al. introduce a multi-robot system where robots distribute RFID tags, while exploring new areas and use them for localization and data sharing. However, the prototype robot relied mostly on a laser scanner for navigation, while the RFID tags were used for developing globally consistent maps with the algorithms introduced by Lu and Milios (Lu and Milios, 1997). Multi-robot systems are discussed, but no actual experiments were performed with more than one robot (Kleiner et al., 2006). Similarly Kubitz et al. used the RFID technology to be able to divide a global map of a large area into smaller pieces, which were given to a robot on demand. RFID tags served as landmarks and gave the robot a rough estimate of its position in the global frame of reference. Then the robot matched the local map (obtained using laser or ultrasonic ranging) to the part of the global map representing the area around the RFID tag (Kubitz et al., 1997).

The idea of a multi-axis array antenna introduced in (Kim et al., 2004) is developed further in (Kim and Chong, 2009), where a mobile robot is guided towards a recharging station. The recharging station is equipped with an active RFID transponder and the robot has a 2-axis antenna. With the dual-directional antenna the robot can estimate the direction of the transponder using the direction of arrival (DOA) method. The system does not estimate the position of the robot, but only indicates the direction towards a target marked with an active RFID transponder.

In (Kurth et al., 2003) a radio ranging system is used for SLAM. It is not based on the RFID technology, but the same methods could be implemented in an RFID system. Instead of RFID tags, small active radio tags are placed around a test area and localized with a mobile radio ranging device. Tags that have already been localized are used as landmarks when

localizing new tags or when moving around. The localization is based on range-only SLAM. The range is determined as a function of the time that elapses between a query to a tag and the reply being received. The localization of the tags was done by a single robot following a non-linear path. Nine working tags were placed in an area of approximately 40 meters by 30 meters. It is shown that the range measurements had acceptable variance, when the range was approximately between 4 meters and 30 meters. Measurements too close to a tag were not reliable and had to be filtered out. With the SLAM method the tags are localized with an average error of 1.01 m. The robot position estimate has an average error of 0.40 m.

2.6 Sensor networks

Localization in a sensor network deals with an array of sensor nodes, which normally have at least partially overlapping detection ranges. The number of nodes is usually considerable and the position of most of the nodes is unknown at the beginning. In order to use the sensor array for localization purposes the sensor nodes need to be localized. Several methods exist for the initial localization process. Some methods use mutual localization, where sensor nodes measure distances or bearings to other nodes. A quantitative comparison is given in (Langendoen and Reijers, 2003). Other approaches use a mobile node which moves among the stationary nodes and acts as a common target for all the stationary nodes (Cevher and McClellan, 2001; Pathirana et al., 2005; Galstyan et al., 2004; Olson et al., 2006). The task is somewhat simpler, if the mobile node can keep track of its own position (Cevher and McClellan, 2001; Pathirana et al., 2005; Olson et al., 2006), but localization of the stationary nodes has also been shown to be possible with an arbitrarily moving mobile node (Taylor et al., 2006). The aforementioned studies show that the accuracy of the localization depends heavily on the measurement method. Nodes equipped with an ultrasound ranging system can an achieve accuracy of a few centimeters, whereas systems based on RSSI measurements may only have a localization accuracy of one meter. The density of the sensor nodes has also been shown to have a considerable effect on the localization accuracy.

A system that was already mentioned in the section dealing with formation flying has been used to deploy mobile sensor nodes (Parker et al., 2003). The helper robots steer mobile sensor nodes to their assigned positions. A sensor node is capable of acoustic sensing and can have an estimate of its position given by the helper robots deploying it. A sensor node also has a color marker with a unique ID and stripes for detection of its vertical orientation. Thus, it can be used as a landmark for vision-based localization systems.

2.7 Influence

The research presented in this thesis has been inspired mostly by the works by Hahnel et al. and Kurth et al.. Both of these represent a scenario where a single robot localizes landmarks with unique IDs. The robots also localize themselves at the same time using internal sensor measurements.

In (Hahnel et al., 2004) a robot with an accurate localization system, based on a laser scanner, is used for the localization of the robot. As the laser scanner may not provide accurate localization in environments with a low number of suitable features it may not be the optimal solution. The price of a laser scanner may also be an issue in systems aiming for the lowest possible cost.

A range-only SLAM approach is presented in (Kurth et al., 2003). A single robot localizes active RF beacons while estimating its own pose simultaneously. The robot had multiple beacons visible all the time it was moving. The position estimates of individual landmarks were not very accurate, but the fact that there was a sufficient number of landmarks helped to keep the error in the position estimate at an acceptable level throughout the duration of the test run.

Chapter 3

Distributed estimation of a node position

In this chapter a distributed method for the estimation of the node positions in a localization network with the help of a multi-robot system is explained. All the coordinate frames are two-dimensional, having an x- and a y-axis. The robot's sensor for landmark detection is assumed to be located at the origin of the robot's coordinate frame. The robot coordinate axes are labeled u and v instead of x and y in order to distinguish the robot coordinate frame from the global coordinate frame. The positive u-axis of the robot coordinate frame points forward, marking the direction of the heading angle, θ. The heading angle of the robot in the global coordinate frame is expressed in engineering format, i.e. a zero angle points towards the positive x-axis, with counter-clockwise being the positive direction. The bearing angle measurements (λ) are expressed as an angle relative to the robots heading angle, with counter-clockwise as the positive direction (Figure 3.1).

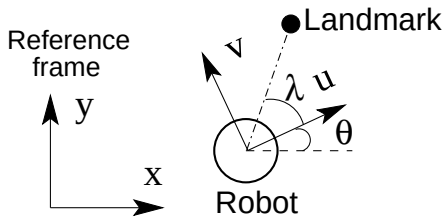

Figure 3.1: Coordinate frames and related angles

3.1 Dead reckoning

In robotics odometry means estimating a movement on the basis of the turning of the wheels of the robot. It is used as a basis for localization in many mobile robot systems. For example, in a system where the visibility of a sufficient number of external landmarks cannot be guaranteed at all instants in time, the robot's movement between measurements to the landmarks can

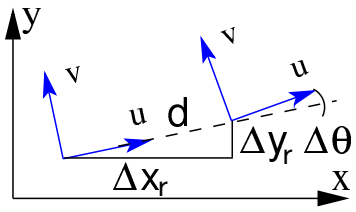

Figure 3.2: Relative change in the pose of a robot

be based on the direct information acquired from an odometry system. In order to calculate the change in the robot's pose the odometry system uses a method called dead reckoning. In dead reckoning a relative movement with respect to a starting point is calculated (Figure 3.2). Therefore, it is not an absolute localization method. This method is best known from its applications at sea. The change in the position of a ship is estimated by calculating the distance traveled using the average speed and time that has elapsed and assuming linear motion in the direction obtained as a function of a compass reading. In mobile robotics, dead reckoning also means that the changes in the position of the robot are considered as small linear movements, measured with suitable sensors. The changes in the heading angle of the robot are measured or calculated according to the structure of the robot. As the updating of a robot's pose can be done very frequently (several times in a second), the assumption of a linear path, even for a robot traveling along an arc, causes an error of insignificant magnitude in comparison to the other sources of error.

For a differential drive robot, the dead reckoning can be calculated using the data received from the encoders indicating the turning of the driven wheels. The encoders can be directly connected to the axis of a driven wheel. This ensures that the encoder pulses really represent the true movement of the wheel, but makes control harder because there may be a slight delay between the movement of the motor and the actual turning of the wheel. Additionally, the resolution of the encoders has to be high in order to have a sufficient number of pulses per revolution of the wheel. A more common approach is to connect the encoders to the axis of the electric motor that is driving the wheel. This gives a greater number of encoder pulses per full revolution of the wheel, but also introduces error sources such as backlash in the gears. The accuracy of the odometry can be further improved by separate encoder wheels, that are not actuated or by pulling an encoder trailer behind the robot (Borenstein et al., 1996).

The necessary equations for the calculation of the change in the pose of a differential drive robot are presented in Equations 3.1 - 3.4, where b is the wheel base of the robot and d_{rw} and d_{lw} are the incremental distances traveled by the right- and left-hand wheels, obtained from the encoder readings.

$$
\begin{aligned}
d &= \frac{d_{rw} + d_{lw}}{2} && (3.1)\\
\Delta x_r &= d \cdot \cos(\theta) && (3.2)\\
\Delta y_r &= d \cdot \sin(\theta) && (3.3)\\
\Delta\theta &= \frac{d_{rw} - d_{lw}}{b} && (3.4)
\end{aligned}
$$

3.2 Bearing-only localization

If the robot is equipped with sensors to measure both the distance and heading to a landmark, the estimate of the location of the landmark can be calculated after each measurement. As the relative distance d_m is measured and the absolute bearing angle can be calculated as a function of the robot's heading angle θ and the measured bearing λ, the landmark position estimate (x_t, y_t) in a global coordinate frame can be solved with Equation 3.5, where (x_r, y_r) denotes the position estimate of the robot.

$$
\begin{aligned}
x_t &= x_r + d_m \cdot cos(\theta + \lambda)\\
y_t &= y_r + d_m \cdot sin(\theta + \lambda) && (3.5)
\end{aligned}
$$

With range-only measurements, localization with a single landmark is not possible, if the robot moves along a straight line (Olson et al., 2006). In this case there would always be two possible locations for the landmark, one on either side of the robot. Driving the robot along a non-linear path would solve this problem, but in many situations it is an undesirable practice.

However, if the robot can measure the bearing angles to a single landmark, an estimate can be calculated for the relative displacement between the landmark and the robot, provided that the robot has basic odometry sensors. In bearing-only localization, the robot makes at least two bearing angle measurements to the landmark from different locations. An estimate of the relative position of the landmark can be found at the intersection of the two bearing angle measurements.

Figure 3.3 shows a robot making two bearing angle measurements at locations R_k and R_{k+1}. The distance d_r between the two locations is measured with wheel encoders. The two bearing angle measurements λ_1 and λ_2 are measured with a suitable sensor. The distance d_m can be solved as follows:

$$\gamma = \lambda_2 - \lambda_1 \quad (3.6)$$

$$d_m = \frac{d_r \cdot sin(\lambda_1)}{sin(\gamma)} \quad (3.7)$$

The estimated heading angle (θ) of the robot can be based on wheel encoders, if no additional sensor data are available. The robot's heading angle

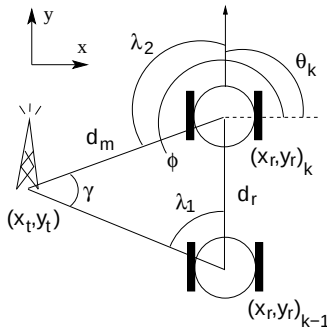

Figure 3.3: Estimation of the landmark position. A robot makes two bearing angle measurements (λ_1 and λ_2) from two different locations.

together with a bearing angle measurement yields an azimuth angle ϕ:

$$\phi = \theta + \lambda_2 \tag{3.8}$$

The distance estimate d_m and the azimuth angle estimate ϕ define the position of the landmark in polar coordinates relative to the origin of the robot's local coordinate frame. Hence, the displacement between the robot and the landmark in the global Cartesian coordinates can be calculated as indicated by the following equations:

$$\begin{aligned} \Delta x_m &= d_m \cdot cos(\phi) \\ \Delta y_m &= d_m \cdot sin(\phi) \end{aligned} \tag{3.9}$$

3.2.1 Localization uncertainty

The measurement noise affects the uncertainty of the estimated displacement in terms of x- and y-coordinates. If the displacement estimate is calculated as described above, both position coordinates have an uncertainty, which depends on the measurement noise v, the relative distance d_m between the robot and the landmark, the bisector angle η of the two bearings and the mutual angle γ between the two bearing angles.

The measurement noise indicates how uncertain the estimated bearing angle to the landmark is. The measurement noise, together with the estimated bearing, defines the sector in which the correct bearing angle probably lies. If the bearing angle measurement is too noisy for the required localization purposes, the measurement noise may be reduced by making multiple measurements from the same location and calculating the average value for the bearing angle estimate at that point. This holds good if the noise is due to random factors in the measurement process. Systematic errors should be removed with a calibration process.

The relative distance between the robot and the landmark affects the uncertainty of the position estimate, as the error perpendicular to the bearing

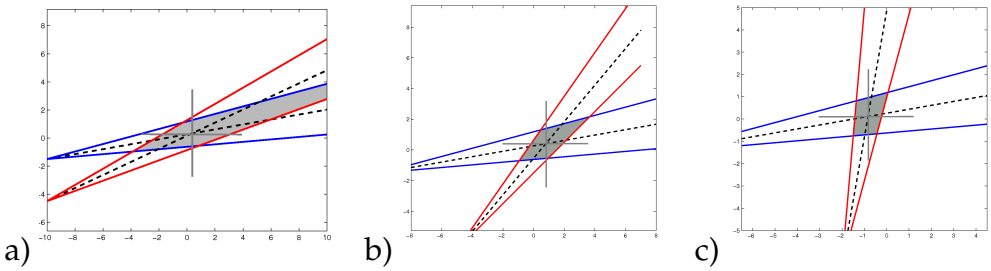

Figure 3.4: Two intersecting bearing angle measurements (dashed lines) with a) a 15° b) a 40° and c) a 70° mutual angle. The localization uncertainty region is formed by the intersection of two measurement sectors (blue and red) marked with solid lines around the estimated bearings.

angle is a linear function of the distance. However, depending on the measurement method used for bearing angle, the measurement noise may be inversely proportional to the relative distance between the robot and the landmark. The correlation between these two sources of uncertainty may have a significant effect on the overall uncertainty, but as this does not hold good for all systems, the uncertainties are here assumed to be uncorrelated.

The mutual angle between the two bearing angles affects the shape of the uncertainty region. Perpendicular measurements cause an almost symmetric uncertainty region, but bearing angles that are close to parallel form a long and narrow region.

As the uncertainty region is asymmetric, the bisector angle of the bearings affects the weight distribution of the uncertainty on the x and y coordinates of the landmark. The bisector angle is a bearing angle exactly half-way between the two measurements.

In Figure 3.4 the effect of the mutual angle on the shape of the uncertainty region is illustrated. The two bearing angle measurements are drawn with dashed lines. Their intersection indicates the estimated position of the landmark. The solid lines next to the dashed lines form two sectors that indicate the magnitude of the measurement noise in a bearing angle measurement. The two sectors intercept and form a region around the estimated position of the landmark. The shape of the region changes from a long and narrow one to a roughly symmetrical form, as the mutual angle between the measurements increases. For the asymmetrical uncertainty regions the long dimension is parallel to the bisector angle η.

For the sake of computational simplicity this region can be estimated approximately with an ellipse, as shown in Figure 3.5. The dimensions of the ellipse depend on the same factors as the uncertainty. The length of the minor axis b only depends on the distance to the landmark d_m and the measurement noise v. The length of the major axis a also depends on the mutual angle γ between the bearing angle measurements. The bisector angle η indicates the angle between the major axis of the ellipse and the positive x-axis

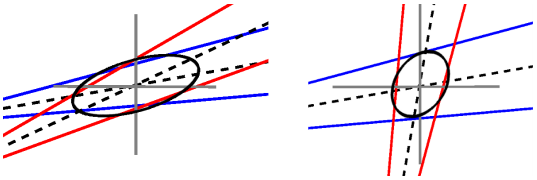

Figure 3.5: Displacement measurement uncertainty described with an ellipse for a mutual angle of 15° and 70°

of the global coordinate frame. The parameters describing an elliptical uncertainty region around the intersection of the bearing angle measurements can be calculated as follows:

$$\begin{aligned} a &= d_m \cdot \tan(v) \cdot (1 + 2 \cdot \cos(\gamma)) \\ b &= d_m \cdot \tan(v) \\ \eta &= \phi - \frac{\gamma}{2} \end{aligned} \tag{3.10}$$

With each new angle measurement, the robot can calculate the displacement estimates for the landmark using all the previous angle measurements to that same landmark. Thus after two measurements the robot has one estimate for the landmark location, while N measurements will give $C(N, 2)$ combinations, i.e. there are 1+2+3+...+ (N-1) measurement pairs to calculate the position estimates. Figure 3.6 shows landmark position estimates for five bearing angle measurements. All the position estimates of a single landmark can be fused using a probabilistic method, where the weight of each position estimate depends on the related uncertainty. The estimates based on almost parallel bearing angle measurements may show considerable error, but their uncertainties are also large. Hence, the effect of such measurements on the final estimate of the landmark position is small. When a Kalman filter is used the measurements are not handled as pairs. Instead, the values of the state vector reflect all the measurements in the history and each measurement provides a correction to these values. This will be explained thoroughly in the following sections.

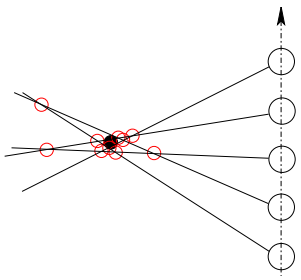

Figure 3.6: Estimation of landmark position using all the intersections of the bearing angle measurements from five different locations

3.3 Kalman Filter

In (Maybeck, 1979), Maybeck defines a Kalman filter as an optimal recursive data-processing algorithm. The Kalman filter uses a priori information and data to estimate an unknown value that a variable had at the moment the data were taken. Unlike Bayesian methods, the Kalman filter does not assume normal distribution, but operates as a minimum variance estimator.

One aspect that makes the Kalman filter an optimal estimator is that it takes into account all the information available:

- initial knowledge of the values of the variables to be estimated
- dynamics of the system and measurements
- uncertainties of the system and the measurements as noise

It is a recursive estimator, which means that all the prior information is contained in the previous estimate. Hence, the amount of memory required does not change over time, but is static as long as the number of variables to be estimated does not change.

The standard Kalman filter can be used with a linear motion model and linear measurement equation. A non-linear motion model or measurement equation requires the implementation of an extended Kalman filter, which uses linearization for non-linear equations. A Kalman filter with a correct prediction model maintains the first two moments, the mean and the variance, of the state distribution (Welch and Bishop, 1995).

$$E[x_k] = \hat{x}_k \tag{3.11}$$

$$E[(x_k - \hat{x}_k)(x_k - \hat{x}_k)^T] = P_k \tag{3.12}$$

As the Kalman filter is generally implemented as program code running on a digital processor, a discrete-time format is needed. When a discrete-time Kalman filter is used, the motion model is presented with a discrete-time state-space representation (Equations 3.13-3.14). The state vector x_k represents the estimate of the system variables at the time instant k. The state vector is updated at each time step. The dynamics of the system are described by the matrix A_k. It defines the change of each element of the state vector during one time step according to the dynamic model of the system. The matrix A_k may change over time, but in many applications the dynamic model is assumed to be time-invariant. The matrix B_k defines the effect of the control vector u_k on each element of the state vector. The matrix B_k can also be assumed to be time-invariant in many applications. The estimated output of the system z_k depends on the system variables in the state vector. The matrix H_k is called the measurement matrix and it defines the output vector as a function of the state vector. Vectors ω_k and v_k represent the process and measurement noise, respectively.

$$x_{k+1} = A_k x_k + B_k u_{k+1} + \omega_k \quad (3.13)$$
$$z_k = H_k x_k + v_k \quad (3.14)$$

A general form for Kalman filter equations for the estimate in the case where matrices A, B and H are constants is shown in Table 3.1. Q_k represents the process noise covariance and R_k represents the measurement noise covariance. The noise in the external control u_k is contained in the covariance matrix U_k.

Table 3.1: Kalman filter equations

a priori state	$\hat{x}_k^- = A\hat{x}_{k-1} + Bu_k$
a priori estimate error covariance	$P_k^- = AP_{k-1}A^T + BU_kB^T + Q_k$
a posterior state	$\hat{x}_k = \hat{x}_k^- + K_k(z_k - H\hat{x}_k^-)$
a posterior estimate error covariance	$P_k = (I - K_kH)P_k^-$
Kalman gain	$K_k = P_k^- H^T(HP_k^- H^T + R_k)^{-1}$

If the matrices A, B, U, Q, H and R are constants, the estimate error covariance P_k and the Kalman gain K_k stabilize to a constant value. These constant values can be calculated in advance and used for the estimation of the posterior of the state vector. This reduces the computational complexity of the update phase, as there is no longer any need to calculate the inverse matrix in the Kalman gain equation.

The initial conditions for the state vector and the estimate error covariance matrix affect the speed and accuracy of the convergence. These should be selected with the best method available.

3.3.1 Extended Kalman Filter

In bearing-only localization, the only measurement is the bearing angle to the target. The robot displacement between measurements can be considered as external control. When calculating the position of the robot or the landmark, on the basis of bearing angle measurements, non-linear equations are needed. The Extended Kalman Filter (EKF) can use a non-linear measurement equation h, but the measurement matrix H has to be the Jacobian matrix composed of partial derivatives of h with respect to the elements of the state vector x. Depending on the motion model of the system, the a priori estimate of the state vector may need to be calculated with a non-linear function f. Then the a priori covariance matrix is calculated using the matrix A, which is a Jacobian matrix of partial derivatives of f with respect to the elements of the state vector x. If external input u_k exists, the noise covariance matrix U_k of the external input has to be incorporated into the

covariance matrix calculation using the matrix B, which is a Jacobian matrix of f with respect to the elements of the control vector u_k. As the Jacobian matrices are always calculated for the current values of the state vector and the control vector, the Kalman gain has to be recalculated for every update. Thus the complexity of the filter depends on the dimensions of the estimate error covariance matrix P_k and the number of simultaneous measurements during one update. The linearization at the estimated operating point may cause instability of the filter if the estimation error is considerable. However, with this algorithm no such behavior was detected in either the simulations or laboratory experiments. The equations for the Extended Kalman Filter are shown in Equations 3.15-3.19.

$$\hat{x}_k^- = f(\hat{x}_{k-1}, u_k, 0) \tag{3.15}$$

$$P_k^- = A_k P_{k-1} A_k^T + B_k U_k B_k^T + Q_k \tag{3.16}$$

$$\hat{x}_k = \hat{x}_k^- + K_k(z_k - h(\hat{x}_k^-, 0)) \tag{3.17}$$

$$P_k = (I - K_k H_k) P_k^- \tag{3.18}$$

$$K_k = P_k^- H_k^T (H_k P_k^- H_k^T + R_k)^{-1} \tag{3.19}$$

The a priori estimate of the state vector $\hat{x}_k^-$ is calculated using Equation 3.15. It states that given the previous estimate of the state vector $\hat{x}_{k-1}$ and the current control vector u_k, a prediction for the current value of the state vector can be calculated, using the non-linear function f. The third parameter of the function f is the error in the process update. Of course, the actual value of the error cannot be known, but it can be assumed to follow a distribution with zero mean, hence the zero as the third parameter. The variance of the distribution describing the random valued error is contained in the process noise covariance matrix Q and used in Equation 3.16, where an error covariance matrix for the predicted state vector is calculated. Similarly, the error in the measurement cannot be known, but it can be modeled with a zero mean distribution with a non-zero variance. The mean of this distribution is used as the second parameter of the measurement equation $h(\hat{x}_k^-, 0)$ and the variance is used in the measurement noise covariance matrix R.

As the Extended Kalman Filter uses linearization it differs from the original algorithm and cannot be shown mathematically to be optimal.

3.4 Localization algorithm

In robot localization, the state-space model can estimate the robot's position on the basis of the motion measured by the wheel encoders. As a result of wheel slippage and other measurement errors, the model gives increasingly bad position estimates, i.e. the position error increases over time. With the Kalman filter, a correction to this position estimate can be applied, if external positioning data such as triangulation or trilateration to landmarks are

available. The Kalman filter can combine the information received from the encoders and from the external measurements to landmarks. The process noise covariance matrix Q and the measurement noise covariance matrix R are used to tune the Kalman filter for the best possible performance in the operating environment. The process noise increases the uncertainty of the robot's position estimate at each step at which the Kalman filter is updated. The amount of process noise depends on the environment, the mechanics of the robot and the quality of the sensors, such as wheel encoders, used for measuring the movement of the robot directly. The measurement noise depends on the environment and the quality of the sensors used for obtaining the external positioning data.

3.4.1 Simultaneous localization and pose correction

Usually, the measurement to an external reference point, such as a landmark, is used for correcting the pose of the robot. The same measurement can also be used the other way around and the location of the landmark relative to the location of the robot can be estimated. Instead of a position estimate for the landmark being calculated directly, as described in Chapter 3.2, an estimate of the bearing angle to the landmark given the current estimates of the positions of the robot and landmark is calculated. Then the estimated bearing is compared with the related bearing angle measurement and both the robot and landmark position estimates are corrected according to the residual and the uncertainties of the estimates of the pose of the robot and position of the landmark. For this method to work, estimates of both the pose of the robot and position of the landmark have to exist. The estimate of the pose of the robot is initialized when the robot is deployed. The estimate of the position of the landmark is initialized at the first detection of the landmark. The initialization can be done using consecutive measurements or with a single measurement if a reasonable estimate for the range can be obtained, for example, from the expected detection distance of the landmark. The latter method was used in this study. The expected detection distance of a landmark could be estimated because of the limited range of the measurement system. The initial variance of an estimate has to be given an appropriate value, according to the initial localization method. Here, the uncertainty of the detection distance and the uncertainty of the bearing angle estimate were taken into account when defining the initial variance for the landmark position estimate.

In the case of one robot localizing with one landmark, the state vector x has five elements: the x- and y-coordinates of the robot (x_r, y_r), the heading angle of the robot θ and the x- and y-coordinates of the landmark (x_t, y_t).

$$x = \begin{bmatrix} x_r \\ y_r \\ \theta \\ x_t \\ y_t \end{bmatrix} \tag{3.20}$$

The uncertainty of each element of the state vector x is presented by the corresponding diagonal element of the covariance matrix P, where the diagonal elements are the variances of the random variables of the state vector. The non-diagonal elements indicate the correlation between different elements of the state vector. In this example, the state vector x contains estimates for the pose of a robot and the position of a landmark. As long as the robot has not made any measurements to the landmark, the correlation between the pose of the robot and the position of the landmark is zero. For example, the bottom left-hand element of the covariance matrix P $cov(y_t, x_r)$ is the covariance of the y-coordinate of the landmark, y_t and the x-coordinate of the robot, x_r. When the robot makes a measurement to the landmark, the estimates of x_r and y_t become correlated and the related covariances $cov(x_r, y_t)$ and $cov(y_t, x_r)$ become non-zero.

$$P = \begin{bmatrix} \sigma_{x_r}^2 & cov(x_r, y_r) & cov(x_r, \theta) & cov(x_r, x_t) & cov(x_r, y_t) \\ cov(y_r, x_r) & \sigma_{y_r}^2 & cov(y_r, \theta) & cov(y_r, x_t) & cov(y_r, y_t) \\ cov(\theta, x_r) & cov(\theta, y_r) & \sigma_{\theta}^2 & cov(\theta, x_t) & cov(\theta, y_t) \\ cov(x_t, x_r) & cov(x_t, y_r) & cov(x_t, \theta) & \sigma_{x_t}^2 & cov(x_t, y_t) \\ cov(y_t, x_r) & cov(y_t, y_r) & cov(y_t, \theta) & cov(y_t, x_t) & \sigma_{y_t}^2 \end{bmatrix} \tag{3.21}$$

Prediction equations

In many applications the robot can be assumed to be stationary while measuring the bearing angle to the landmark and the movement of the robot between measurements can be given by a separate odometry system. As no considerable dynamics exist, the movement of the robot can be defined by a control vector u_k. For this application the prediction can be calculated as shown in Equation 3.22, where $\Delta x_r, \Delta y_r$ and $\Delta\theta$ indicate the change in the robot's pose given by the odometry system. The landmark is static and therefore, the elements of the control vector related to the landmark coordinates are zeros.

$$\hat{x}_k^- = \hat{x}_{k-1} + \begin{bmatrix} \Delta x_r \\ \Delta y_r \\ \Delta\theta \\ 0 \\ 0 \end{bmatrix} \tag{3.22}$$

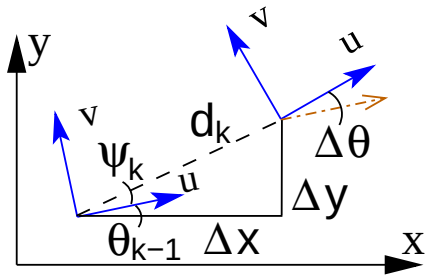

Figure 3.7: Change in the robot's pose as measured by the odometry system

As Δx_r and Δy_r depend on the heading angle estimate of the robot, it is better to express the change in the position of the robot as a vector relative to the previous pose. The vector has length d_k and direction $\theta_{k-1} + \psi_k$. This is illustrated in Figure 3.7. The control vector u_k is then as shown in Equation 3.23. The uncertainty in the length of the step and the uncertainty in the angle ψ_k do not depend on the heading angle of the robot. The prediction update $x_k^- = f(\hat{x}_{k-1}, u_k, 0)$ is computed with a set of non-linear equations for the predicted position (Equations 3.24-3.25) and the linear transform of the heading angle (Equation 3.26).

$$u_k = \begin{bmatrix} d_k \\ \psi_k \\ \Delta\theta \\ 0 \\ 0 \end{bmatrix} \tag{3.23}$$

$$\hat{x}_{r,k} = f_x(\hat{x}_{k-1}, u_k) = \hat{x}_{r,k-1} + d_k \cdot cos(\hat{\theta}_{k-1} + \psi_k) \tag{3.24}$$

$$\hat{y}_{r,k} = f_y(\hat{x}_{k-1}, u_k) = \hat{y}_{r,k-1} + d_k \cdot sin(\hat{\theta}_{k-1} + \psi_k) \tag{3.25}$$

$$\hat{\theta}_k = f_\theta(\hat{x}_{k-1}, u_k) = \hat{\theta}_{k-1} + \Delta\theta \tag{3.26}$$

The base of the Jacobian matrix A for the a priori covariance update is an identity matrix, because the predicted value of each element of the state vector depends on the previous value of that element. Additionally the estimated change in the position coordinates of the robot depend on the estimated heading angle. Therefore, the uncertainty of the heading angle affects the uncertainty of the position coordinates. These terms are calculated as partial derivatives of the coordinate update equations (Equations 3.29-3.30). Equations 3.27-3.28 show how the change in the position coordinates of the robot $(\Delta x, \Delta y)$ is related to the first two elements of the control vector u_k. In Equation 3.27 *atan2* is a two-argument function, that gives an angle between a vector and the positive x-axis of the coordinate frame in the range of $(-\pi..\pi]$. The first argument of the function is the difference in the y-coordinates of the initial and terminal points of the vector. The second argument is the difference in the x-coordinates.

$$\psi_k = atan2(\Delta y, \Delta x) - \hat{\theta}_{k-1} \tag{3.27}$$

$$d_k = \sqrt{\Delta x^2 + \Delta y^2} \tag{3.28}$$

$$\frac{\delta f_x}{\delta \theta} = -d_k \cdot \sin(\hat{\theta}_{k-1} + \psi_k) = -\Delta y \tag{3.29}$$

$$\frac{\delta f_y}{\delta \theta} = d_k \cdot \cos(\hat{\theta}_{k-1} + \psi_k) = \Delta x \tag{3.30}$$

In an example case with a state vector containing a pose estimate of one robot and a position estimate of one landmark, the Jacobian matrix A_k is as follows:

$$A_k = \begin{bmatrix} 1 & 0 & -\Delta y & 0 & 0 \\ 0 & 1 & \Delta x & 0 & 0 \\ 0 & 0 & 1 & 0 & 0 \\ 0 & 0 & 0 & 1 & 0 \\ 0 & 0 & 0 & 0 & 1 \end{bmatrix} \tag{3.31}$$

The Jacobian matrix B_k is calculated as partial derivatives of $f(\hat{x}_{k-1}, u_k, 0)$ with respect to the input vector u_k:

$$B_k = \begin{bmatrix} \cos(\hat{\theta}_{k-1} + \psi_k) & -\Delta y & 0 & 0 & 0 \\ \sin(\hat{\theta}_{k-1} + \psi_k) & \Delta x & 0 & 0 & 0 \\ 0 & 0 & 1 & 0 & 0 \\ 0 & 0 & 0 & 0 & 0 \\ 0 & 0 & 0 & 0 & 0 \end{bmatrix} \tag{3.32}$$

The noise covariance matrix of the external input U_k represents the noise in the odometry system of the robot caused by measurement inaccuracies. The noise parameters can be chosen according to the calibration results of the robot and they can be used to tune the Kalman filter for optimal performance. The covariance matrix of the process noise Q_k represents the uncertainty caused by unknown factors. These mostly depend on the environment, where the robot is operating and should be chosen accordingly. The landmark is static and thus has no motion noise.

Correction equations

For the sake of readability, the notation presented in Equations 3.33-3.34 is used in Equations 3.35 and 3.36 to describe the relative difference in the estimated position coordinates of the robot $(\hat{x}_r^-, \hat{y}_r^-)$ and the landmark $(\hat{x}_t^-, \hat{y}_t^-)$. This is also illustrated in Figure 3.8

$$\Delta x = \hat{x}_t^- - \hat{x}_r^- \tag{3.33}$$

$$\Delta y = \hat{y}_t^- - \hat{y}_r^- \tag{3.34}$$

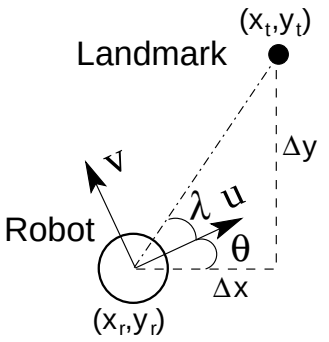

Figure 3.8: Bearing angle measurement to a landmark

The measurement equation $h(\hat{x}_k^-, 0)$ is a function of a robot pose and a landmark position (Equation 3.35). The position coordinates yield a bearing angle from the robot to the landmark in the global coordinate frame. The heading angle of the robot is then used to calculate an expected value for the bearing with respect to the robot coordinate system, which is the quantity that is being measured.

$$h(\hat{x}_k^-, 0) = atan2\left(\frac{\Delta y}{\Delta x}\right) - \theta \tag{3.35}$$

The Jacobian matrix H is a matrix of all the partial derivatives of the measurement functions. Here only one measurement is used and hence, only one measurement function $h(\hat{x}_k^-, 0)$ exists. In this case the Jacobian matrix becomes a vector:

$$H = \begin{bmatrix} \frac{-\Delta y}{(\Delta y)^2+(\Delta x)^2} & \frac{\Delta x}{(\Delta y)^2+(\Delta x)^2} & -1 & \frac{\Delta y}{(\Delta y)^2+(\Delta x)^2} & \frac{-\Delta x}{(\Delta y)^2+(\Delta x)^2} \end{bmatrix} \tag{3.36}$$

The Jacobian matrix H indicates how the measurement is related to each element of the state vector. As the measured quantity is the bearing angle with respect to the heading angle of the robot, the measurement is directly related to the heading angle of the robot, as indicated by a constant -1 as the third element of the vector H. The other elements of the state vector are the position coordinates of the robot and the landmark. As explained in Section 3.2, the direction of the bearing angle with respect to the global coordinate frame affects the weight distribution of the uncertainty on the estimated position coordinates. This can be seen in the numerators of the position-related elements of the vector H, where the coefficients for the x coordinates depend on Δy and the coefficients for the y-coordinates depend on Δx. The denominators for all the elements of vector H that are related to the position coordinates are identical. The denominator is the square of the distance between the robot and the landmark. It indicates that the weight of the measurement on each position-related element of the state vector depends on the relative distance between the robot and the landmark. The vector H

is used with the covariance matrix P and the measurement noise covariance matrix R to compute a vector K known as the Kalman gain (Equation 3.19). The Kalman gain defines the weight of the residual on each element of the state vector. It is also used to update the covariance matrix P, which contains the uncertainties and correlations of the elements of the state vector.

When more and more measurements made by one robot are combined with the Kalman filter, the estimate of the relative position of the landmark becomes more accurate since the effect of measurement errors decreases. However, the position estimate of the landmark in the global coordinate frame is based on the estimate of the robot's own pose. Therefore, the error in the pose of the robot is directly inherited by the position estimate of the landmark. A single robot can pass a landmark several times and correct its own pose estimate and the position estimate of the landmark, but the initial inaccuracies in the robot position estimate inherited by the landmark will still be there. Even if the robot were to return to the starting point and start localization again from a reference point, its pose estimate would be subjected to the same structure-related error as in previous runs. Thus localization runs made by a single robot are always correlated. To cope with this, measurements from multiple independent sources, i.e. from different robots, are required.

3.5 Distributed estimation

When a single robot estimates the position of a landmark the estimate is biased by the inaccuracies in the robot's own position and heading angle estimate. Filtering the different measurements of a single robot helps to reduce the effect of measurement errors, but not the effect of the inaccuracies in the robot's own pose estimate. However, if different robots are estimating the position of a landmark, the position estimate is based on several independent groups of measurements. When multiple robots pass a landmark, they each have a different estimation error and uncertainty in their own position estimate. This is due to the mechanical differences between the robots, the individual calibration parameters and the differences in the actions they have taken so far. Of course, the poses of robots using the same landmarks for localization will become correlated over time. This implies that less and less new information is available as time passes and the location estimates of the landmarks will become more and more static. When the localization network reaches a mature state the cooperation between the robots is no longer needed for localization. The landmarks will provide a common frame of reference for all the robots operating in the area of the coverage.

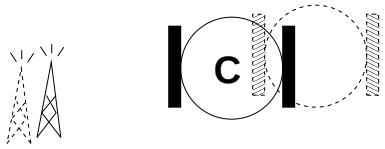

Figure 3.9: Robot "C" updating its pose estimate and the position estimate of a landmark

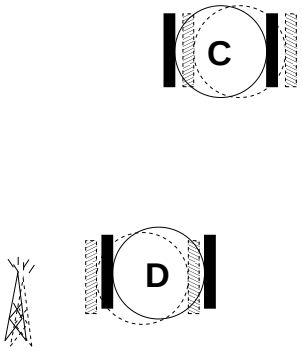

Figure 3.10: Robot "D" passing the landmark and informing robot "C" of the new estimate of the landmark position

3.5.1 Cooperation

The robots have to use the same global coordinate frame in order to cooperate. If the robots start at a common location, they share a common view of the global coordinate frame right from the start. Otherwise, the robots need to use a hierarchical method to determine which global coordinate frame they should adapt to, when detecting landmarks that have already been localized by robots using a different global coordinate frame. The previous estimate of the position of the landmark and the related uncertainty have to be available for a robot calculating new estimates. This can be done by storing the related information to the memory of the landmark or by broadcasting all new estimates to the other robots. The landmark position estimate contains all the information provided by the robots that have already passed the landmark. Therefore, each robot passing the landmark benefits from the position information of all the previous robots.

When a robot localizes a landmark, its pose becomes correlated with the position of the landmark (Figure 3.9). If the covariance information is not discarded, a robot can also benefit from the localization information of the following robots, making the position estimate of the landmark more accurate. If the robot has passed a landmark recently, its pose is highly correlated with the landmark. Then, if another robot improves the landmark estimate, the first robot can recalculate its own pose estimate according to the new position estimate of the landmark and the information about the correlation of the landmark position and the robot pose (Figure 3.10).

A straightforward way of making good use of all the available information is to use a centralized Kalman filter. All the information from all the robots is collected into one filter, which makes sure that all the correlations are maintained correctly. The downside is that the complexity of the estimate calculation grows, as the Kalman filter matrices expand with the number of robots and landmarks. A scenario with M robots and N landmarks uses a state vector with 3M+2N elements:

$$X = \begin{pmatrix} x_{r1} \\ y_{r1} \\ \theta_{r1} \\ \vdots \\ x_{rM} \\ y_{rM} \\ \theta_{rM} \\ x_{t1} \\ y_{t1} \\ \vdots \\ x_{tN} \\ y_{tN} \end{pmatrix} \tag{3.37}$$

The calculation of the inverse matrix in the Kalman gain equation affects the computation complexity of the algorithm. If there is a small number of simultaneous measurements, the dimensions of the denominator matrix are small and the computational complexity of the matrix inversion is low. An example of the matrices of an extended Kalman filter in a case with two robots and two landmarks is provided in Appendix A

Another downside is the communication bandwidth required for transmitting all the information to the central unit. If the number of robots and landmarks is relatively small, neither of these downsides is of critical importance. In Section 3.6 an application of sparsely distributed landmarks is presented. For applications with communication restrictions or a larger number of robots or landmarks, a distributed or sparse filter structure can be used (Thrun and Liu, 2003; Liu and Thrun, 2003; Kroetsch and Clark, 2005). As this problem is a research topic in its own right, it is not addressed here.

3.6 Case Study: Measuring bearing to an RFID tag

An RFID system using passive tags offers some very interesting possibilities. As mentioned in Chapter 2 some research has been conducted into using RFID systems for localization. The approach introduced in this thesis is a minimalistic one, which uses a very low number of tags per surface area.

In RFID systems the antennas have a very important role, especially in systems using passive tags. The system used in this case study uses commercial tags, which can be selected from the available designs. The reader antenna had to be designed exclusively for this application, because there seemed to be no antennas on the market that would fulfill the necessary requirements. In a passive RFID system, besides communication, the antennas are used for transferring power to the electronics of the tags. Normally, this is a far more demanding task than the actual information transfer between the reader and the tag. Thus it effectively stipulates the operating range of the system.

3.6.1 Antenna theory

When alternating current is applied to an antenna, it creates both magnetic and electric fields. As the distance d to the antenna increases the strength of the magnetic field decreases rapidly as a factor of $1/d^3$ and thus it is not practical for far-field operation. The strength of the electric field decreases as a factor of $1/d$, which makes it far more suitable for applications requiring a longer operating range. In an RFID system using passive tags, the electric field needs to be strong enough to provide energy for the electronics of the tag. If the tag is close enough to be powered by the reader antenna, then the back-scattered data can easily be received by the reader antenna. The amount of power needed by the tag depends on the components of the tag. The Friis transmission equation gives a theoretical relation between transmitted and received power, under ideal conditions. In its simplest form it does not take into account the effects of polarization and other attenuating factors, such as reflection or absorption. The basic form is presented in Equation 3.38, where P_r is the received power, P_t is the transmitted power, G_t is the linear gain of the transmitting antenna, G_r is the gain of the receiving antenna, λ is the wavelength and R_{tr} is the distance between the two antennas.

$$\frac{P_r}{P_t} = G_t G_r \left(\frac{\lambda}{4\pi R_{tr}} \right)^2 \tag{3.38}$$

Antenna gain and transmitted power may also be expressed in decibel format. Antenna gain is given in the direction of maximal radiation and

is often expressed relative to a theoretical isotropic antenna. The unit used is dBi. An isotropic antenna cannot exist in reality, but it gives a common reference point for comparing various real antennas. The transmitted or received power can be expressed as power relative to 1 milliwatt. Then the unit used is dBm:

$$P[dBm] = log_{10}(P[mW]) \tag{3.39}$$

Local regulations usually control the field strengths of RF devices. For example, the European regulations (European RFID standard EN 302 208) limit the effective isotropic radiated power (EIRP) of RF devices operating in the 865.6-867.6 MHz frequency band to a maximum of 3.8W (35.8dBm). The effective isotropic radiated power can be calculated as indicated in Equation 3.40, where P_t is the transmitted power in dBm, L_c represents the cable losses in dB and G_t is the gain of the transmitting antenna in dBi, relative to an isotropic reference antenna.

$$EIRP = P_t - L_c + G_t \tag{3.40}$$

3.6.2 Reader antenna type

In this application, a directional antenna is required in order to have a constrained beam to measure the bearing angle of the tag. The side and back lobes have to be sufficiently small, for a tag not to respond outside the main beam area. The directivity also increases the gain of the antenna in the direction of the main lobe and hence gives a longer detection range.

The directivity can be achieved by in several ways, such as using a reflector, a horn, an array of antennas or a radiating element with a specific shape. In this application, the antenna should also be as small as possible. Therefore, an array of several antennas would not be a sensible solution. The selected frequency often states the minimum size of at least one of the dimensions of the antenna. The length of an efficient horn antenna is several wavelengths and parabolic antennas have a radius of at least one wavelength. However, in certain designs all the antenna dimensions can be less than $\lambda/2$, which is half of the wavelength. Two different types of antennas can satisfy this constraint and still be sufficiently directive. One is a three-element Yagi-Uda antenna and the other is a helical antenna (Figure 3.11).

The Yagi-Uda antenna was developed in 1926 by Shintaro Uda of Tohoku Imperial University, Sendai, Japan, with the collaboration of Hidetsugu Yagi. It is based on a dipole radiating element which has a reflector element on one side and one or more directors on the other side. The shape, size and position of each element can vary, depending on the purpose of the antenna. Probably the best-known examples of Yagi-Uda antennas are regular television antennas. The Yagi-Uda antenna can be built using a PCB

a)  b) 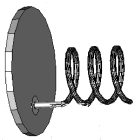

Figure 3.11: a) 4-element Yagi-Uda antenna b) Helical antenna

design. Then all the elements have to be planar, with their thickness defined by the thickness of the copper of the selected PCB material. The simplest design has a ground plane with the negative half of the dipole connected to it on one side of the PCB and the positive half of the dipole (with the feed line) and a director on the other side of the PCB. There also has to be an impedance-matching network to provide correct matching with the connected transmitter. Fortunately, in many applications the impedance matching can be done simply by using the proper type of connector.

A helical antenna is constructed of a wire shaped like a spring. Very often a ground plane is also used at one end of the cylinder-like structure. If the circumference of the antenna is much less than one wavelength, the antenna operates like a monopole. A helical antenna with a circumference of at least one wavelength is a wave-guide antenna and it has a true circular polarization. In the latter case the radiation is directed along the axis of the antenna. The direction of the polarization (left or right) depends on the winding direction of the wire.

Both antennas have the following benefits:

- all dimensions smaller than $\lambda/2$
- high F/B-ratio

In the comparison between these two antennas the Yagi-Uda antenna has two advantages over the helical antenna. It is a flat antenna, i.e. one dimension is very small and it is easy to make on a PCB. The advantage of a helical antenna is that it has circular polarization instead of the linear polarization of the Yagi-Uda antenna. This gives more freedom in the orientation of the tags.

The Yagi-Uda antenna design was chosen for this application because of its ease of manufacturing and flat outline. Additionally, it has a slightly narrower half-power bandwidth (HPBW) and, in consequence, higher gain than a helical antenna with the same dimensions.

3.6.3 Bearing angle measurement

The relative angle between an RFID reader antenna and a passive RFID tag is measured by consecutive interrogations to the tag while the reader antenna is being turned. Thus the electric field of the antenna sweeps over the

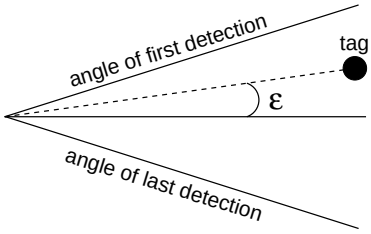

Figure 3.12: Bearing angle measurement

surroundings of the reader. A tag can only respond, when it is in an electric field strong enough to provide the minimum power needed. The sector where the tag is detected is recorded and used for estimating the bearing of the tag. The basis of the bearing angle estimation can be the middle of the detected sector. An offset can then be used to compensate for the systematic error ϵ, caused by different error sources (Figure 3.12).

Passive tags need to draw the necessary operating power from the electric field of the reader antenna. When a tag has not been in an electric field for a while, its energy storage capacitor is empty. Hence, it may take a bit longer for the tag to respond to the first call when it enters the electric field. If the timeout for a tag response is set to be very short this small additional delay may bias the angle measurement. It can be taken into account in the bearing angle calculation or accepted as measurement noise.

Chapter 4

Simulations

A simulation model for the multi-robot localization system was built in the Matlab environment. With the simulations, the effects of inaccuracies in different measurements can be observed. Scenarios with different number of robots and landmarks can also be simulated. For this purpose it is very important that the simulator resembles some real-world application. This means that the different error sources have to be tuned according to the available information from the laboratory measurements.

4.1 Scenario 1: Effects of various inaccuracies

The system presented here simulates a scenario where a single landmark is localized by a group of robots passing the landmark one by one. The robots estimate their own pose simultaneously in a common (global) coordinate frame. Each robot has random error in its estimated position and heading angle. Each bearing angle measurement also contains a random error. After each bearing angle measurement, an extended Kalman filter is used to compute new estimates for the location of the landmark and the pose of the robot.

4.1.1 Simulator parameters

The simulation model permits the setting of several parameters. The robot pose error depends on two components. The first one is the original error after localization at the reference point, i.e. when the robot is deployed and attached to the common coordinate frame. The other is the error that has accumulated while the robot has been moving. Both are set separately for each robot as random numbers, controlled with appropriate parameters. When a robot arrives near a landmark, the uncertainty in the robot's pose estimate ($var_{rx}, var_{ry}, var_{\theta}$) is initialized with a calculated pose uncertainty. The pose uncertainty and the accumulated error depend on a random number ρ_t, representing the length of the trajectory that the robot has traveled since the reference localization. The position and heading angle errors inherited from the reference localization have small, fixed uncertainties. The actual

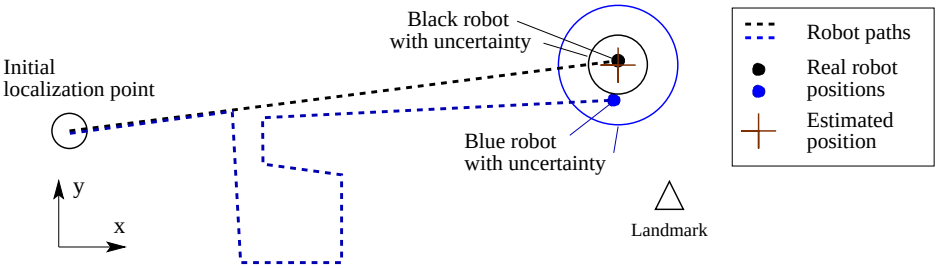

Figure 4.1: Accumulated robot error and uncertainty

error in the pose of each robot is a product of the error coefficient representing the standard deviation of the error and a random number $\rho_{x,y,\theta}$ sampled from a standard normal distribution $(\mathcal{N}(0,1))$. For example, the error in the x-coordinate of the robot's position can be calculated according to Equation 4.1. The random number describing the robot trajectory length (ρ_t) is sampled from a uniform distribution. The random variables are assumed to be independent of each other, so the expected value and the variance of the error ϵ_x can be calculated as shown in Equations 4.2-4.3.

$$\begin{aligned} \epsilon_x &= (\epsilon_{orig} + \rho_t \cdot \epsilon_{accu}) \cdot \rho_x && (4.1) \\ E[\epsilon_x] &= (\epsilon_{orig} + E[\rho_t] \cdot \epsilon_{accu}) \cdot E[\rho_x] && (4.2) \\ E[(\epsilon_x - \hat{\epsilon}_x)^2] &= (\epsilon_{orig}^2 \cdot Var[\rho_x] + \epsilon_{accu}^2 \cdot Var[\rho_t \rho_x] \\ &\quad + \epsilon_{orig} \cdot \epsilon_{accu} \cdot Cov[\rho_x, \rho_t \rho_x]) && (4.3) \end{aligned}$$

When the random numbers are expected to be independent and the limits for the uniform distribution are set to $\rho_t \in [1,2]$, the expected value and the variance of the error ϵ_x have values according to Equations 4.4-4.5. As can be seen, the error term has zero-mean distribution with variance controlled by the parameters representing the original and the accumulated error.

$$\begin{aligned} E[\epsilon_x] &= (\epsilon_{orig} + \frac{3}{2} \cdot \epsilon_{accu}) \cdot 0 && (4.4) \\ E[(\epsilon_x - \hat{\epsilon}_x)^2] &= \left(\epsilon_{orig}^2 + \frac{7}{3} \cdot \epsilon_{accu}^2 + 3 \cdot \epsilon_{orig} \cdot \epsilon_{accu} \right) && (4.5) \end{aligned}$$

Figure 4.1 illustrates how two robots get the original pose at a reference localization point with fixed uncertainty. Then one robot travels straight to the vicinity of the landmark, while the other robot travels along a complex path that is approximately twice as long as the direct path to the landmark. Consequently, the uncertainty (and in this illustration the pose error) of the second robot is clearly larger than that of the first robot.

At this point the error in the pose of a robot is independent of the other robots, i.e. there is no correlation between the pose estimates of different robots. This follows from the assumption that the reference localization point defines the common coordinate frame and thus is accurately localized. The original error in the pose of a robot only depends on the accuracy of the reference localization method.

The landmark detection was modeled as a function of the distance Δd between the robot and the landmark. If the robot was within the inner limit, the landmark detection probability was 1 and if the robot was outside the inner limit, but inside the outer limit, the landmark detection probability was 0.5. The inner limit was set to 0.9 m and the outer limit to 1.5 m.

$$P(\lambda) = \begin{cases} 1 & , \Delta d < 0.9m \\ 0.5 & , 0.9m \leq \Delta d < 1.5m \end{cases}$$

4.1.2 Test procedure

Simulations were run in order to discover how different error sources affect the accuracy of the landmark position and robot pose estimates. Each simulation consists of 1000 independent runs, each having 20 robots passing a landmark. As a result, the average estimation errors in the landmark position and robot pose are computed. The landmark position is recorded after each passing robot. Thus the effect of an error source on robot groups of different sizes can be analyzed. Additionally, the pose estimate of each robot is recorded right after it has passed the landmark. This allows a comparison to be made between the individual and group-based corrections. The error sources under consideration are:

- inaccurate bearing angle measurement;
- inaccurate position estimate of a robot;
- inaccurate heading angle estimate of a robot.

4.2 Scenario 2: System performance

In this scenario, the overall system performance with different number of robots and landmarks is observed. First, an office-like environment with two perpendicular corridors and small rooms is considered. The length of the main corridor is approximately 30 meters and that of the side corridor is 10 meters. The number of rooms visited by the robots is 0-3. There are three main points of interest that are being observed with these simulation runs:

- the landmark position error as a function of the distance from the starting point and the number of robots

- a comparison of localization with single and multiple robots
- the robot pose accuracy with respect to the other robots, i.e. how well the robots share a common frame of reference.

Additionally, simulations are used to observe the capability of the robots to expand their working area. The robots first localize one set of landmarks and then move to another area with a new set of landmarks. The expansion adds approximately 15 meters to the main corridor and two more side corridors. Another variation of the office environment is used to test loop-closing. This is known to be difficult for SLAM algorithms (Newman and Ho, 2005). With external landmarks that have unique IDs the loop-closing should not cause problems, but should offer the benefit of correcting the accumulated error using a landmark localized much earlier. With this test the magnitude of the landmark position error as a function of the distance from the starting point is observed again.

4.2.1 Simulator parameters

The simulator parameters are adjusted in such a manner that the simulator should resemble a real-world application as closely as possible. Laboratory experiments conducted with homogeneous robots equipped with an RFID measurement system were used as a reference system for this simulation scenario. The laboratory experiment setup is described in detail in Chapter 5. The following parameters were adjusted according to the information received from the laboratory experiments:

- bearing angle measurement error
- landmark detection distance and reliability
- accumulated error in heading angle
- systematic error in heading angle

The bearing angle measurement error is due to the inaccuracy of the measurement method that was used in the environment that was selected. The landmark detection distance and reliability also depend on the measurement system that is selected. In this simulation, a scenario using passive RFID tags as landmarks is used. The measurement error and detection characteristics are as recorded in the laboratory experiments.

The accumulated error in the heading angle of a robot is due to the random error introduced, when the robot is moving. This can be caused by backlash in gears, uneven ground, local variation in the wheel radius or wheelbase, encoder accuracy, etc. It is non-systematic and cannot be predicted or compensated for. The systematic error caused by errors in the measurements of the critical dimensions of the robot should be removed by

accurate calibration of the robot. As the calibration cannot be perfect and may even change over time, a small systematic error has to be taken into account.

Original and accumulated error

Just as in the first scenario, there is original and accumulated error in the robot pose. At the starting point the robots either localize themselves or they are localized by another entity deploying them. In both cases the robots get a starting point in a common frame of reference. The pose error of the reference localization is simulated with a small difference between a robot's estimated and real pose at the starting point. The procedure is the same as described in Section 4.1.

The accumulated error of a robot depends on its trajectory. When driving towards a target, the robot calculates the necessary adjustment to its heading angle at each update, in order to face the target point (Equation 4.6).

$$\Delta\theta_k = \texttt{atan2}(\Delta y, \Delta x) - \hat{\theta}_{k-1} \tag{4.6}$$

where

$$\begin{aligned} \Delta x &= x_{target} - \hat{x}_{rk-1} \\ \Delta y &= y_{target} - \hat{y}_{rk-1} \end{aligned} \tag{4.7}$$

When a robot turns, an error is introduced into the heading angle. This error is simulated as a function of systematic and random error and scaled according to the change in the robot's heading angle:

$$\epsilon_{\theta_k} = (\epsilon_{rand} \cdot \rho_k + \epsilon_{syst}) \cdot \Delta\theta_k, \tag{4.8}$$

where ρ_k is a random number sampled from the standard normal distribution. The error terms ϵ_{rand} and ϵ_{syst} are robot-specific constant coefficients of random and systematic error.

The new heading angle estimate $\hat{\theta}_k$ and the robot's true heading angle θ_k are

$$\begin{aligned} \hat{\theta}_k &= \hat{\theta}_{k-1} + \Delta\theta_k \\ \theta_k &= \theta_{k-1} + \Delta\theta_k + \epsilon_\theta \end{aligned} \tag{4.9}$$

The accumulated error in the position coordinates of a robot is assumed to be entirely due to the heading angle error, as the error in the linear distance traveled was found to be negligible for properly calibrated robots in an office environment.

4.2.2 Test procedure

Each robot is given a list of target points and an individual start time. Thus the robots start driving one after another and follow the paths assigned to them. There is no collision detection or collision avoidance algorithm in the simulations. The paths of the robots are planned in such a way that they always drive on the right-hand side of the centerline of the corridor. Hence, the robots going in opposite directions should not collide. This behavior was implemented, because it directly affects the distance between a robot and the landmarks along the walls of the corridors and, therefore, the detection of the landmarks. In reality many things (a badly planned path, localization error, intersections) can cause collisions, so some sort of collision avoidance system needs to be implemented.

As the robots interact during the simulation run, the effect of group size on the performance of the system has to be tested with separate simulations that have different number of robots cooperating. Each simulation consists of 1000 independent runs with the selected number of robots following predefined paths. The landmark and robot positions are recorded after all the robots have completed their runs. In some experiments, the robot position estimates and their true positions are also recorded at intermediate points.

Chapter 5

Laboratory experiments

In order to have realistic parameters for the simulation runs, laboratory experiments were conducted. The bearing angle measurement system was first tested in a protected environment in order to see, how it can perform in optimal conditions. Then an office-like environment was used to record the performance of the complete multi-robot system.

5.1 Hardware

A marsupial robot society has been developed in the Automation Technology Laboratory of Aalto University to support several different multi-robot studies. These marsupial robots also served as a platform for the laboratory experiments of this research. The bearing angle measurement system was designed using a commercial RFID technology. Only the antennas of the RFID readers had to be designed and manufactured especially for this purpose.

5.1.1 MarsuBot

The robots used for the laboratory experiments were small, mechanically homogeneous differential drive robots called MarsuBots (Figure 5.1). Depending on the structure and the weight distribution of a robot, the center of gravity of the robot may not be at the geometrical center of the robot. This would affect the turning of the robot. In these differential drive robots the origin of the robot coordinate frame is fixed to the middle of the line connecting the two driven wheels. The actual center of gravity of the robot is very close to this point, so the robot odometry system can use the equations introduced in Chapter 3. The important dimensions of a MarsuBot

Table 5.1: Dimensions of a MarsuBot robot

Wheel diameter	158 mm
Wheelbase	164 mm

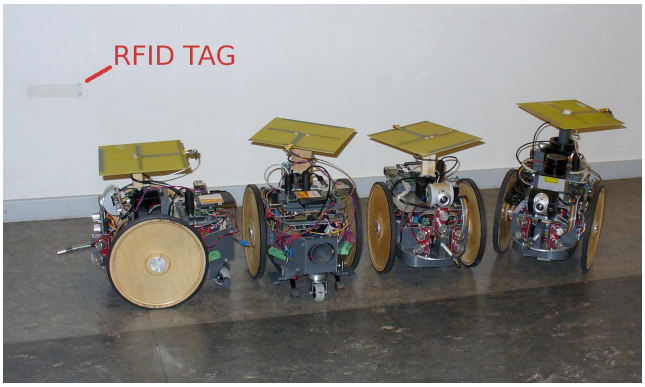

Figure 5.1: The MarsuBot robots (Danny, Emma, Fiona and Hugo) used in the laboratory experiments. An RFID tag serving as a landmark is visible in the background.

robot are shown in Table 5.1. The relatively big wheels, accurate mechanical design and suitable encoders make the odometry system of the robots reliable enough for these experiments. However, the rather narrow wheelbase makes the robot odometry prone to error in the heading angle. This offers a challenge for the algorithm introduced in this thesis.

5.1.2 Bearing angle measurement unit

As explained in Chapter 3, the bearing angle is measured by turning the antenna of the RFID reader and making subsequent calls to an RFID tag. The sector where the tag responds is then used to compute the bearing to the tag. The parts of the bearing angle measurement unit are a microcontroller, an RFID reader, a reader antenna and a servo. The microcontroller controls the measurement process. The RFID reader and the servo are connected to the microcontroller and the antenna is mechanically attached to the servo. The microcontroller uses pulse-width modulation (PWM) to control the angle of the servo. There is no feedback from the servo. When a measurement command is received, the microcontroller sweeps the antenna from side to side in steps and makes requests, one per step, to the RFID reader to detect tags. If a tag is detected during the sweep, the microcontroller returns an estimated bearing angle to the tag and the ID of the tag, which is a part of the Electronic Product Code (EPC) of the tag.

5.1.3 RFID reader

The two most widely used frequency bands in RFID applications are the so-called HF and UHF bands. HF applications operate on the globally accepted 13.56 MHz frequency, whereas UHF uses slightly different frequencies, depending on the continent. The locally used UHF frequencies can range from

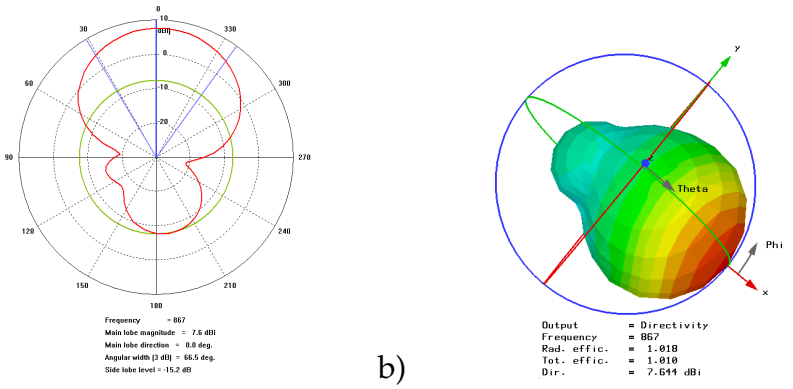

Figure 5.2: Radiation pattern of the simulated antenna a) in polar coordinates in the horizontal plane and b) in a 3D representation

860 MHz to 960 MHz.

As mentioned in Chapter 3, electric coupling is preferred in order to have a sufficient tag detection distance for bearing-only SLAM. The dimensions of the antennas required for this far-field type of operation depend on the frequency used. For directional antennas the largest dimensions are approximately half of the wave length. For a system operating in the HF band this would mean that the antenna dimensions would be over 10 meters and therefore HF band systems are only used for near-field operation with magnetic coupling. Thus a system working in the UHF band was selected for these experiments. Another benefit of the UHF band is that standardized communication protocols exist (e.g. EPC Class 1), which ensure that a reader can communicate with tags from many different manufacturers.

5.1.4 Reader antenna

The commercial antennas available for UHF RFID readers were found to be unsuitable for this application as a result of the compromise between the size of the antenna and the reading range. As the antenna is the most important part of the bearing angle measurement unit, its characteristics are explained here.

First, simulations were used to ensure that the requirements of the reader antenna could be met with a three-element Yagi-Uda antenna constructed on a printed circuit board (PCB). The antenna needs to have all its dimensions smaller than 20 cm in order to fit comfortably on the small robot platforms used in this research. The antenna also needs to have sufficient gain (>7dBi) for the maximum reading range. The simulation of the antenna design was run in CST Microwave Studio. A three-dimensional model was built using the characteristics of a printed circuit board made out of FR-4 glass epoxy. The substrate thickness of the PCB was selected to be 1.6 mm and the thickness of the copper layer 0.036 mm. A 50 Ohm coaxial connector

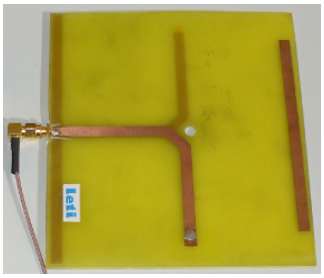

Figure 5.3: Three-element Yagi-Uda antenna on a PCB

was also included into the simulation model. It was placed at the reflector end of the PCB. With the simulations, appropriate values for the antenna parameters were found. The important parameters were the length of each element, the gaps between the elements and the shape and width of the feed lines.

All the elements were designed as 6 mm-wide copper strips. The 50 Ohm coaxial connector was placed behind the reflector so that its centerpiece met with the positive feed line. Figure 5.2 illustrates the characteristics of the simulated antenna. The main lobe gain was found to be 7.6 dBi and the F/B-ratio 15.2 dB. The half-power beam width was found to be 66.5 degrees in a horizontal plane. As these qualities meet the requirements, a prototype was built.

The Yagi-Uda antenna was made on a double-sided PCB that matched the characteristics of the simulated PCB material. The positive side of the dipole and the director were in the top layer. These can be seen as clearer lines in Figure 5.3. The negative side of the dipole and the reflector are seen through the epoxy and thus appear as softer lines. The antenna dimensions are shown in Table 5.2.

Table 5.2: Dimension of the Yagi-Uda antenna

Reflector length	146 mm
Gap 1 (reflector-driven element)	62 mm
Driven element length	128.5 mm
Gap 2 (director-driven element)	54 mm
Director length	113.5 mm
Copper strip width	6 mm

The antenna properties were verified according to the following measurements:

- S-parameters (reflected / radiated power)
- Gain pattern (main axis gain, half-power beam width, F/B-ratio)

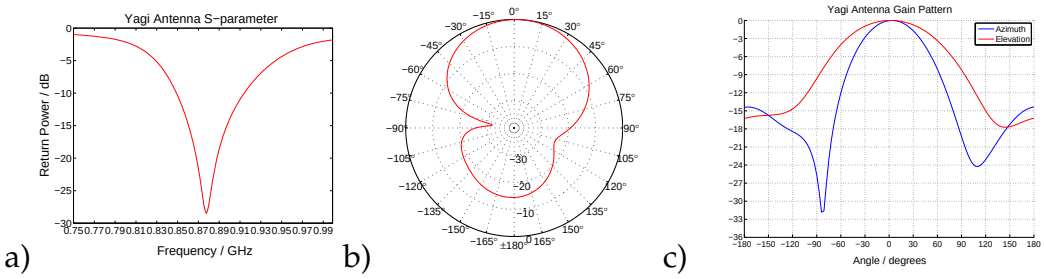

Figure 5.4: a) The frequency matching of the PCB antenna (s-parameter) and the radiation pattern b) in polar coordinates in the horizontal plane c) in Cartesian coordinates as a function of elevation and azimuth.

The antenna was tested in an anechoic chamber (an echo-free room for testing RF devices) in order to measure its characteristics accurately (Figure 5.5). A Vector Network Analyzer (VNA) was used for the measurements.

Figure 5.4a shows that at the frequency of 877 MHz the reflected power is at its minimum. The small amount of reflected power means, that almost all the power is radiated by the antenna and this would be the optimal operating frequency for the antenna. Another important quality of the antenna is the bandwidth. One way to describe the bandwidth of the antenna is the range, where the reflected power is less than -10 dB, i.e. more than 90% of the power is radiated. For the PCB antenna that was constructed the bandwidth is found to be 850 MHz - 914 MHz. On the European operating frequency for UHF band RFID devices (867 MHz), the reflected power is -19.5 dB, which means that 98.9% of the power is radiated. Even though the RFID reader operates in a very narrow band of 865.7-867.9MHz, it is good to have an antenna with a wider bandwidth, because conductive surfaces around the antenna may slightly change the tuning of the antenna and thus alter the optimal operating frequency.

The second characteristic that was measured was the radiation pattern of the antenna. The pattern was measured both in a horizontal (azimuth) and vertical (elevation) plane. In Figure 5.4c the antenna radiation pattern at the 870MHz frequency can be seen. The half-power (-3 dB) beam width (HPBW) in the azimuth plane is 68 degrees and in the elevation plane it is 115 degrees. Figure 5.4b shows the azimuth plane radiation pattern in polar coordinates. Both figures also reveal that there is a small offset between the center of the main lobe and the geometrical centerline of the antenna. This offset can be compensated with an appropriate calibration of the measurement system.

The rather large 115-degree HPBW in the elevation plane allows the reader to detect RFID tags at various heights. Thus the placement of the RFID tags does not need to be executed with great accuracy and reader antennas mounted at different heights can detect the same tags. However, when the antenna is mounted on top of a robot, the mounting height with

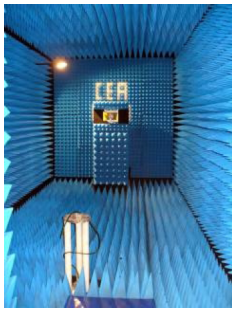

Figure 5.5: Anechoic chamber at the CEA

respect to the body of the robot and the material of the body may have a significant effect on the actual radiation pattern of the antenna. Hence, RFID tags placed a long way below the height of the antenna might not be detected. As a rule of thumb, the RFID tags should be placed approximately at the height of the highest-mounted antenna detecting them.

5.2 Software

The software controlling the different operations of the robots is divided between one central computer and a main processor and two microcontrollers on the robot. The central computer gives a robot all the high-level commands and stores the measurement data. The main processor of the robot takes care of the communication link and the distribution of the commands that have been received to the appropriate microcontrollers. One microcontroller is dedicated to the propulsion and odometry operations of the robot and the other controls the bearing angle measurement system. An overview of the high-level architecture of the software is provided in Appendix B.

5.3 Test environment

The bearing angle measurement was tested both in an anechoic chamber and in an office environment. The node position estimation experiments were run in the office environment.

5.3.1 Anechoic chamber

The anechoic chamber experiments were performed in the facilities of CEA-LETI in Grenoble, France. An anechoic chamber was used in order to find out the optimal performance of the bearing angle measurement system. A passive RFID tag was placed on top of a column. The column was made of a material with a very low dielectric constant. The reader antenna was placed on another column attached to a turn table. The rest of the equipment were

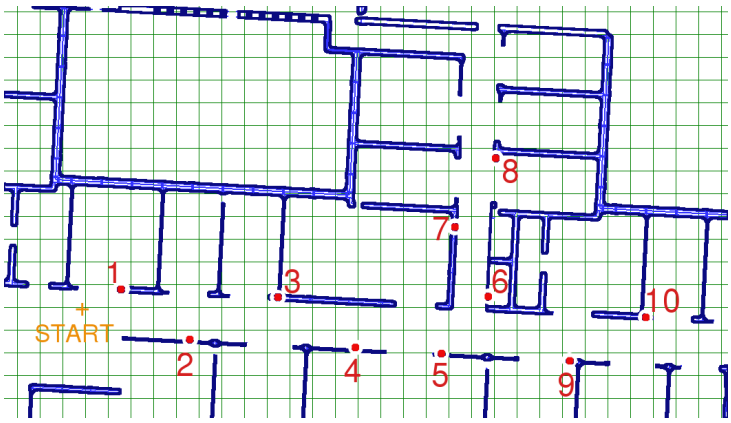

Figure 5.6: Landmark placement and the starting point of the robots in an office environment. The grid resolution is one meter.

placed outside the anechoic chamber. The turn table and RFID reader were controlled with a PC program allowing automated bearing angle measurements. The turning step size was set with a parameter.

5.3.2 Office building

The office environment used for the laboratory experiments was in the building of the Automation and Systems Technology department of Aalto University. The test environment consisted of a main corridor, a side corridor and rooms. The dimensions of the environment that was used were approximately 20 m x 15 m. The floor material is smooth vinyl with good friction. Ten RFID tags were placed on the walls of the two corridors. No tags were placed into the rooms. Figure 5.6 shows the placement of the tags. The width of the main corridor is two meters and that of the side corridor is approximately 1.7 meters. Figure 5.8 shows the MarsuBot robots in the office environment used in the laboratory experiments.

5.4 Calibration

The odometry system of each robot was calibrated in two steps. First, the average wheel circumference was calibrated by driving straight and comparing the measured and estimated distance. Then the wheelbase and wheel diameter ratio of the driven wheels were calibrated, using the bidirectional square-path experiment also known as the University of Michigan Benchmark (UMBmark) (Borenstein et al., 1996).

The bearing angle measurement system was calibrated by making multiple measurements from various known locations to a tag in a known lo-

cation. Each measured bearing was compared to the correct angle and an average error was calculated. A robot-specific offset was determined to minimize the average error in the bearing angle measurements. The turning direction of the antenna was also recorded, in order to compensate for the direction-dependent inaccuracy of the antenna turning system. This inaccuracy was due to the dead zone of the servo that was used to turn the antenna.

5.5 Test procedure

The test runs in the office environment were carried out with one robot at a time. A robot was placed on a marker, which aligned the robot approximately with the main corridor. Then the robot was given the task of driving to a target point using odometry and collecting data along the way. In the log file each line of data contains the odometry-based pose estimate of the robot, the ID of the landmark detected, the measured bearing angle to the landmark and the turning direction of the antenna. If no landmark was detected, the last three numbers were zeros.

When the robot reached a target point, it was given a new target until the desired path had been traveled. Each robot made several runs, following approximately the path shown in Figure 5.7. In the majority of the tests the path only followed the corridors, but the direction of the traffic was alternated. In addition, some test runs were made with a path including a visit to one or two office rooms.

The tags serving as landmarks were placed sparsely. Hence, only one tag at a time was visible to a robot. The bearing angle measurements were made at constant intervals, while the robot was passing a landmark. For each measurement the robot had to stop. The requirement to stop for the measurement is due to the somewhat slow scanning process of the bearing angle measurement system. This inconvenience is particular to this specific measurement system and can be avoided by using another kind of system for bearing angle measurements.

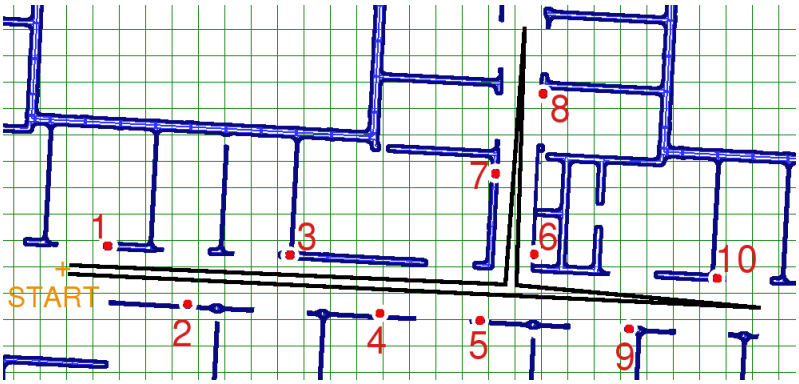

Figure 5.7: The path followed by the robots during the main test runs

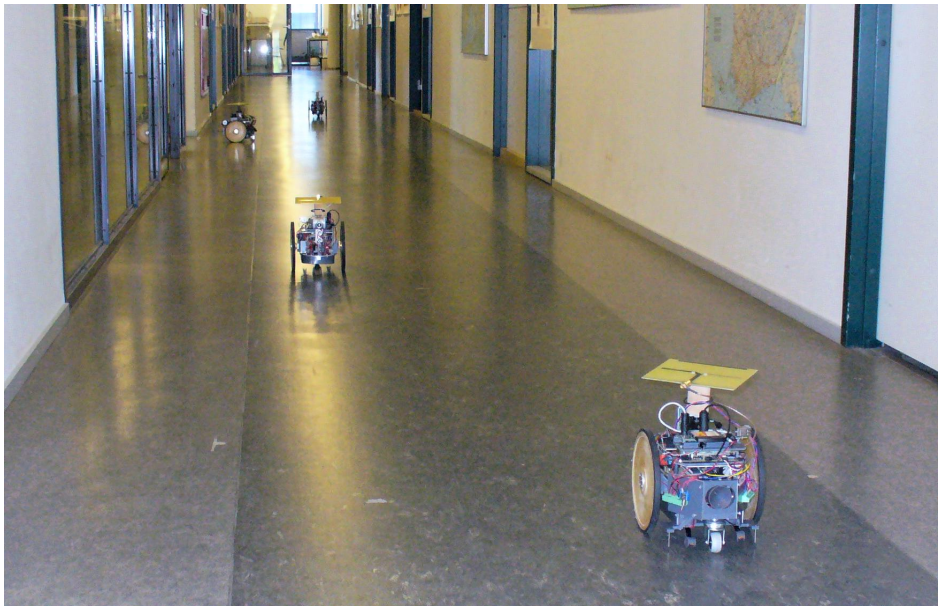

Figure 5.8: MarsuBot robots in the office environment

Chapter 6

Results

6.1 Effects of various inaccuracies on localization

The effects of different measurement inaccuracies on the estimates of the robot pose and the landmark position were tested with simulations. Several parameters were set to control the simulation process and the localization algorithm. During each simulation run, the parameter being tested was given various predefined values, while the rest of the parameters had their default values. The parameters and their default values are listed in Table 6.1.

Table 6.1: Default values for simulation parameters. Error parameters are based on the observations made during the laboratory experiments, as mentioned in Chapter 5.

Standard deviation of original error in robot's x-coordinate	ϵ_{orig_x}	0.04 m
Standard deviation of original error in robot's y-coordinate	ϵ_{orig_y}	0.04 m
Standard deviation of original error in robot's heading	ϵ_{orig_θ}	0.017 rad (1°)
Standard deviation for accumulated error in robot's x-coordinate	ϵ_{accu_x}	0.02 m
Standard deviation for accumulated error in robot's y-coordinate	ϵ_{accu_y}	0.02 m
Standard deviation for accumulated error in robot's heading	ϵ_{accu_θ}	0.017 rad (1°)
Standard deviation of error in measured bearing angle	ϵ_λ	0.10 rad (6°)
Standard deviation of heading error introduced when turning 2π	ϵ_θ	0.035 rad (2°)
Distance between consecutive measurements	*step*	0.2 m

The initial error in the robot pose is calculated as a function of the aforementioned parameters and random numbers ρ_t and $\rho_{xy\theta}$. The random number ρ_t represents the length of the path the robot has traveled since the original reference localization and is a common term for the errors in the position coordinates and in the heading angle of the robot. The calculation of the initial error in a robot pose estimate is presented in Equations 6.1-6.3.

$$\epsilon_x = (\epsilon_{orig_x} + \rho_t \cdot \epsilon_{accu_x}) \cdot \rho_x \quad (6.1)$$

$$\epsilon_y = (\epsilon_{orig_y} + \rho_t \cdot \epsilon_{accu_y}) \cdot \rho_y \quad (6.2)$$

$$\epsilon_\theta = (\epsilon_{orig_\theta} + \rho_t \cdot \epsilon_{accu_\theta}) \cdot \rho_\theta \quad (6.3)$$

The noise parameters for the model noise and the measurement noise of the Kalman filter were adjusted according to the error parameters. For a real application the error characteristics of the system are assumed to be known through a calibration process. Therefore, realistic noise parameters can be selected for the simulations.

In this simulation scenario the robots pass one landmark, making bearing angle measurements at constant intervals defined by the variable '*step*'. After they are out of range of the landmark, they do not move or make measurements. Thus, they do not affect the performance of the following robots. However, the following robots affect the position estimates of all the previous robots through the estimation error covariance matrix, which maintains the correlations between the robots and landmarks. Each robot managed to make approximately six bearing angle measurements, while passing the landmark. All the robots have the same error parameters. As explained in Chapter 3, all the measurements are processed with a centralized Kalman filter and the successful communication of the information is assumed.

6.1.1 Inaccurate bearing angle measurement

The error in the bearing angle measurement depends on the accuracy of the measurement system and the method used. Simulations were run in order to test the effect of the bearing angle measurement error on the robot and landmark position estimates. For each simulation run a different value for the standard deviation of the error distribution was used. The values for the standard deviation in the bearing angle measurement error were 0, 2, 4, 8, 16, 32 and 48 degrees. The actual error for each measurement was sampled from a normal distribution with the given standard deviation. The expected accuracy of the measurement system is assumed to be known. Hence, in these simulations the measurement noise followed the parameter controlling the standard deviation of the bearing angle measurement.

In Figure 6.1a the effect of the bearing angle measurement error on the accuracy of the position estimate of the robot is illustrated. The line with markers shows the average error in the robot's position after passing the

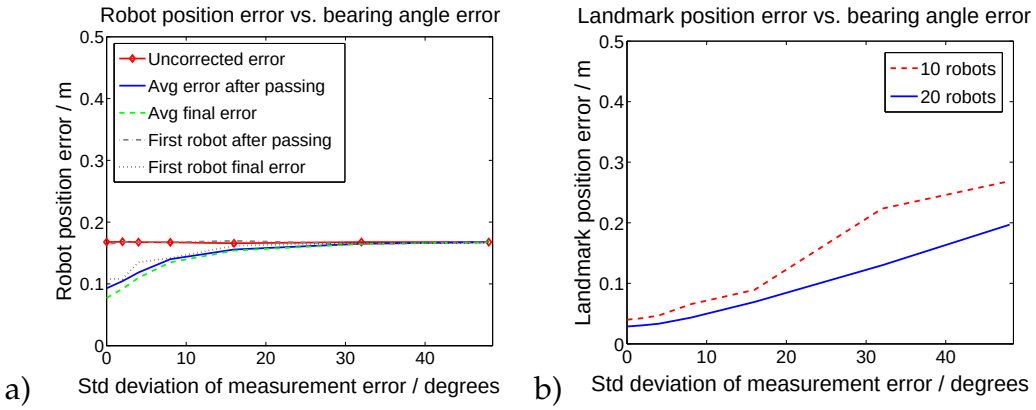

Figure 6.1: Effect of the bearing angle measurement error on a) robot position estimate b) landmark position estimate

landmark without making any measurements. As expected, it does not depend on the accuracy of the measurement system, but is constant. The solid line illustrates the average position error of a robot right after it has passed the landmark. This means that the following robots have not yet affected the position estimate of the robot and it is only based on the information left by earlier robots. The dashed line marks the average position error of a robot after the whole group of 20 robots has passed the landmark.

As the error in the bearing angle measurement increases, the corrected robot position estimate approaches the uncorrected estimate of the robot position. This implies that when the accuracy of the measurement system decreases (and consequently the measurement noise increases), the system can no longer provide useful information for the localization of a robot.

Figure 6.1b shows the effect of the bearing angle measurement error on the estimated position of the landmark. The dashed line illustrates the error distance between the absolute and the estimated position of the landmark after 10 robots have passed. The solid line shows the estimation error after all 20 robots have passed. As can be seen, the accuracy of the landmark position estimate decreases steadily as the measurement error increases. Nevertheless, the landmark position estimate seems to be less sensitive to the bearing angle measurement error than the localization of a robot. This is because the estimate of the landmark is based on a greater number of measurements. Each robot makes bearing angle measurements from six locations only (on average), while passing a landmark. When the measurement uncertainty is high, the weight of the measurements is not big enough to have a significant effect on the pose estimate of the robot. However, the position estimate of a landmark is based on all the robots that have passed. After ten robots the expected number of position estimate updates (i.e. successful bearing angle measurements) is 60 and after all 20 robots have passed, the number of updates is 120. With large variance in the bearing angle measurement, the variance of the landmark position estimate converges slowly

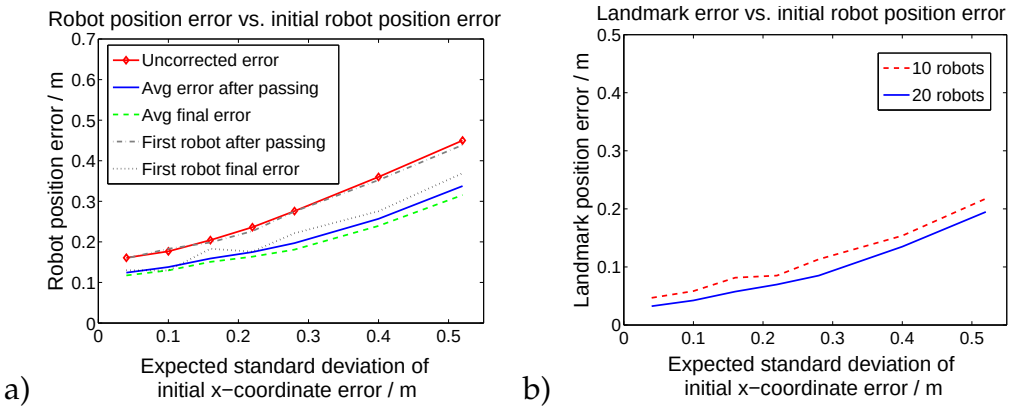

Figure 6.2: Effect of the initial error in the robot position on a) robot position estimate b) landmark position estimate

and the additional information provided by the measurements of even the last robot is still valuable. This can be seen when comparing the accuracy of the landmark position estimates after 10 and 20 robots. The difference in the accuracy grows as the measurement uncertainty grows.

6.1.2 Inaccurate initial position estimate of a robot

An inaccurate initial position estimate of a robot affects the accuracy of the position estimate of the robot after it has passed the landmark, as well as the accuracy of the position estimate of the landmark itself. Again, simulations were run with different values of the parameter describing the initial inaccuracy of the position estimate of the robot. The parameter affected the expected value of the standard deviation of the distribution used for sampling the actual initial position error in the x-coordinate of the robot. The actual parameter that was altered was the standard deviation for the accumulated error in the x-coordinate of the robot. As the robot-specific distribution depended on a random variable representing the distance traveled by the robot, only the expected value for the standard deviation of the distribution can be presented. The values for the expected standard deviation of the distribution of the initial position error in the x-coordinate of the position estimate of the robot were 0.04, 0.10, 0.16, 0.22, 0.28, 0.40 and 0.52 meters. The standard deviation for the distribution of the error in the y-coordinate had the default value.

In Figure 6.2a the effect of an inaccurate initial position estimate of a robot on the position estimate of the robot after it has passed the landmark is presented. The same markings are used for different plots as were used with the bearing angle measurement error. Here it can be seen that the average error of the first robot just after passing the landmark (dash-dot line) is approximately the same as the average of the uncorrected error. This implies that the first robot cannot correct its position estimate, as there is no new

information available for it at this point. It only estimates the previously unknown position of the landmark, which serves as a connection between the first robot and all the following ones. The dotted line illustrates the estimation error in the position of the first robot after all the robots have passed the landmark. It is very clear how the following robots can improve the position estimate of the first robot on the basis of the measurements to a common landmark. The average error of all the robots right after passing the landmark (solid line) is only slightly larger than the average position error of the robots after all have passed the landmark (dashed line). This implies that the robots that pass benefit from the previous robots and can already correct their position estimate, when passing the landmark. Additionally, for each passing robot there is less and less new information provided by the following robots as the number of robots is limited. The variance of the position estimates of a robot group is considerably smaller when all the information is shared. The difference grows as the standard deviation of the initial position error grows. For the highest tested value the variance for the individual robots right after passing the landmark was over twice the variance of the final position estimates after all the robots had passed.

Overall, the inaccuracy in the initial position estimate cannot be corrected completely by passing a single landmark and the remaining position error increases as the initial error increases. However, after a robot passes the landmark the position estimate of the robot is clearly more accurate than the uncorrected estimate.

The accuracy of the landmark position estimate decreases as the initial error in the robot position increases. Figure 6.2b shows how the error is inherited by the landmark position estimate. It can also be noted that the increase in the number of robots passing the landmark does not improve the estimate significantly.

6.1.3 Inaccurate initial heading angle of a robot

The effects of an inaccurate initial heading angle estimate of a robot were also tested by simulations. The values for the parameter controlling the standard deviation of the accumulated heading angle error of the robot were given in radians. The accurate values for the expected standard deviation of the normal distribution were 0.02, 0.0275, 0.035, 0.0462, 0.0688, 0.095 and 0.125 rad and the approximate values in degrees were 1.1, 1.6, 2.0, 2.6, 3.9, 5.4 and 7.2 degrees.

Figure 6.3a shows how the error in a robot's heading angle after it has passed a landmark depends on the initial heading angle error. Once again the different plots are marked in the same way as previously explained. The average heading angle error of the first robot right after passing the landmark (dash-dot line) is approximately the same as the uncorrected error, but the following robots provide improvements and after all the robots

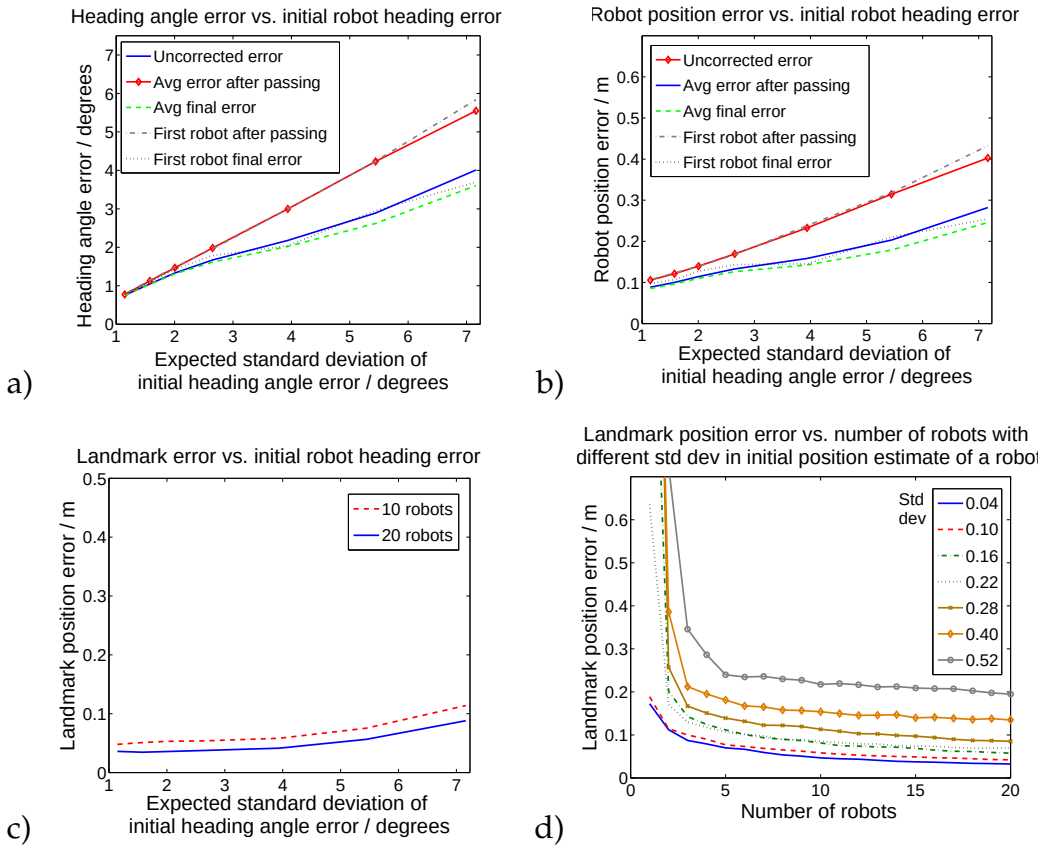

Figure 6.3: Effect of the error in the initial heading angle of a robot on a) robot heading angle error b) robot position estimate and c) landmark position estimate. d) The convergence of a landmark position estimate.

have passed the heading angle error of the first robot (dotted line) is close to the average error of all the robots. The average heading angle error of the individual robots right after they have passed the landmark (solid line) is slightly greater than the average error after all the robots have passed (dashed line). Similarly to the case with the initial position error, the variance in the heading angle estimates of different robots is significantly smaller for the final position estimates than for the individual robots after they have passed the landmark. The accuracy of the position estimate of the robot follows the accuracy of the heading angle estimate closely, as can be seen by comparing Figures 6.3a and 6.3b. The relative effect of the other error sources is rather small as the heading angle error increases. Therefore, the position error depends almost entirely on the heading angle error.

The landmark position estimate is quite immune to the heading angle error as the heading angle errors of different robots are sampled from a zero mean distribution with relatively small standard deviation. An increase in the number of robots from 10 to 20 does not provide a significant improvement in the landmark position estimate (Figure 6.3c).

6.1.4 Convergence of a landmark position estimate

The convergence of a landmark position estimate is illustrated in Figure 6.3d. The different plots represent different values of standard deviation in the initial position estimate of a robot. For all the plots the improvement in the landmark position estimate is greater for the first five robots. After that only a moderate improvement in the landmark position estimate appears. As more and more robots pass, the uncertainty of the landmark decreases and the effect of new measurement data becomes smaller. In this simulation all the major error sources are sampled from a normal distribution and no systematic error is present. With a real application the convergence is expected to be somewhat slower, as the error sources may be less ideal.

6.1.5 Summary

The estimation of a landmark position relative to the position of a robot is not very sensitive to the inaccuracy of the bearing angle measurement system as long as the total number of measurements made by all the passing robots is sufficient. The correction of the position estimate of an individual robot is based only on the measurements that the robot makes while passing the landmark. Therefore, if the measurement accuracy is low, the robot has to make measurements with a smaller interval in order to accumulate a sufficient number of measurements.

The inaccuracies in the position estimates of the robots are partly inherited by the landmark. The uncertainty of the landmark position estimate decreases as the number of estimate updates, i.e. measurements increases. Hence, an increase in the number of robots has less and less effect on the convergence of the landmark position estimate. A large standard deviation in the initial position estimates of the robots may result in a biased estimate of the landmark position, because the average position error of the first robots may be considerable and the convergence of the landmark position estimate would require an excessive number of separate measurement runs.

An inaccurate heading angle estimate will cause an increasing estimation error in the position estimate of a robot. With measurements to a landmark the estimate of the heading angle of a robot becomes more accurate, but the initial error can be corrected only partially when passing one landmark. Therefore, it is important to have a suitable landmark density. The landmark position estimate is not directly very sensitive to the heading angle error, as the measurement distance is rather short. However, when the accuracy of the position estimate of a robot decreases the landmark position estimates also become less accurate.

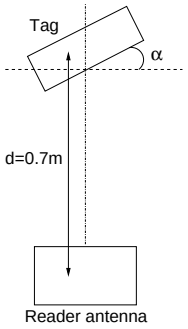

Figure 6.4: Bearing angle measurement setup in an anechoic chamber

6.2 Laboratory experiments

Laboratory experiments were conducted in order to evaluate the real performance of the bearing angle measurement system and to find realistic error parameters for large-scale system simulation.

6.2.1 Bearing angle measurement

The bearing angle measurement unit was tested in an anechoic chamber in order to observe its performance in optimal conditions. An RFID tag was placed 0.7 m away from the reader antenna. When dipole antennas are used the system is sensitive to the mutual angle α between the tag and the reader antenna. Four different configurations were tested in order to see how the polarization angle affects the measurement accuracy. The measurement setup is illustrated in Figure 6.4. For each configuration 20 measurements were made. The transmitting power of the reader was 19 dBm and the measurement step was 3° (i.e. the reader antenna was turned 3° between consecutive calls for the tag).

The measurement results are presented in Table 6.2. The standard deviation for all the measurements was below one degree. The system was calibrated with an angle offset parameter, making the average error of the first measurement zero. When the polarization angle (or polarization mis-

Table 6.2: Bearing angle measurements in an anechoic chamber. Average error, standard deviation and tag detection sector width are presented for various polarization angles (α).

α	Avg error	Std dev	Sector
0°	0°	0°	96°
30°	2.28°	0.54°	69°
45°	4.00°	0°	54°
−25°	1.10°	0.73°	83°

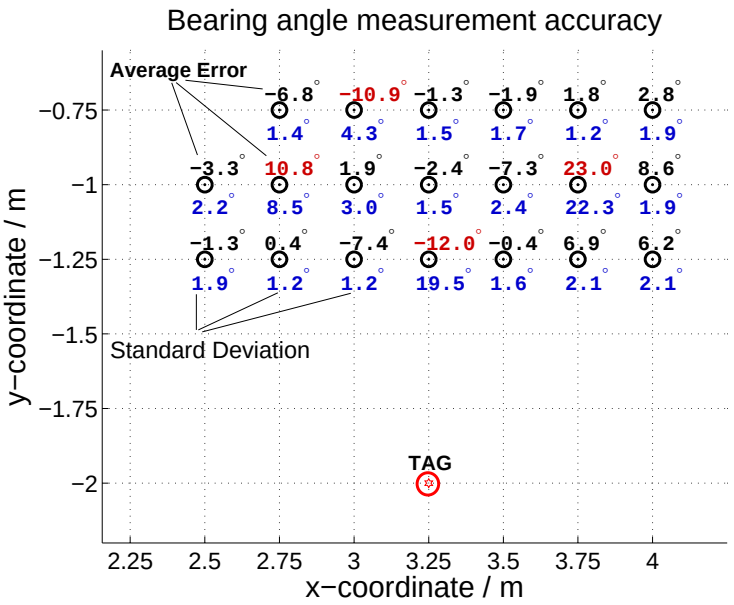

Figure 6.5: Bearing angle measurements from various locations to an RFID tag

match) α between the tag and the reader antenna increased, an error of a few degrees was introduced to the bearing angle measurement. This will increase the variance of the measurements performed by a passing robot, as the mutual angle changes while the robot moves.

The bearing angle measurement unit was also tested when mounted on a MarsuBot robot. The robot was placed on the floor of an office corridor. A localization grid was marked on the floor so that the exact location and heading of the robot were known with the help of a positioning rig. An RFID tag was placed on the wall of the corridor. The bearing angle measurement unit made ten measurements from each location where it was tested. The transmitting power of the RFID reader was 17 dBm and the measurement step was 5°. With the calibration process the systematic error is removed and the average error of the measurements is zero. The standard deviation of the measurements was 5.85°. This value is higher than when the system was tested in the anechoic chamber. This is due to the bigger measurement step size and the influence of the environment. Significant variations between different measurement positions were noted. In certain positions the measurement error and standard deviation of the measurements were considerably larger than the average values. This implies that the reflections and interference caused by the environment may have a significant effect on the accuracy of the bearing angle measurement unit. The reader antenna and the RFID tags are at a height of approximately 25 cm from the ground because of the small size of the MarsuBot robots. As the reader antenna beam width is rather large in the elevation plane (HPBW of

115°), the system is sensitive to interference caused by ground reflections.

In Figure 6.5 bearing angle measurement results from various positions to an RFID tag are shown. Above each measurement position the average error of the measurements is marked. Below each measurement position the standard deviation of the successful measurements is marked. In these measurements the robot's heading angle was zero (i.e. its right-hand side was facing towards the tag). Another set of measurements was made with the robot facing the other way.

The bearing angle measurement system was calibrated with two parameters. Accurate alignment of the zero angle of the servo and the actual main lobe direction of the antenna is demanding, because the main lobe direction cannot be determined visually. Misalignment causes systematic offset on the bearing angle measurement. One calibration parameter was used to cancel the offset in the measurement caused by the inaccurate installation of the antenna on the servo.

The servo that was used to turn the antenna did not have an encoder, but the estimate of the angular position of the servo was based on the control signal. The servo uses hysteresis in its internal feedback to ensure stability with a constant control signal. This causes a small dead zone when changing the direction of the rotation, which in turn leads to rotation direction-dependent angle position estimates. This behavior is systematic and it was compensated with the second calibration parameter.

In addition to the main lobe, the three-element Yagi-Uda antenna has a small but clear back lobe. This means that some energy is radiated in the opposite direction to the main lobe. The robot is expected to maintain some distance between the landmarks and itself. During the calibration the minimum distance between the landmark and the robot was 75 cm, which guaranteed that the back lobe would not cause problems. However, during a measurement run the robot might edge very close to a landmark. Then the back lobe of the antenna can be powerful enough to wake up a passive RFID tag. This, of course, would result in a 180° error in the bearing angle estimate. This happened a couple of times during the measurement runs of the laboratory experiments, but it did not seem to cause problems to the overall performance. Additionally, if an estimate of the landmark position exists the measurements with large errors can be filtered out.

6.2.2 Node position estimation

Four robots were used for the laboratory experiments. The robots collected measurement data one at a time and the actual localization algorithm was run offline. When multi-robot localization is being run offline, the robots start at fixed intervals and the measurement data are read simultaneously for each moving robot. The test environment was as explained in Chapter 5. Two modes of operation were tested. In mode 1 the robots advanced

constantly in predefined steps and made a bearing angle measurement after each step. In mode 2 the robots drove at a constant speed while scanning for a landmark. When a landmark was detected, the robot stopped and measured the bearing. Then it advanced in predefined steps as in mode 1 until it could not detect the landmark anymore. After four unsuccessful bearing angle measurements the robot changed to a constant speed again until the next landmark was detected.

In mode 1 the landmarks were detected slightly earlier, which led to a higher number of measurements per landmark on average. There was also considerable variation between the robots in terms of the probability of a landmark being detected. The servos and antennas of each robot had slightly different characteristics. Additionally, the mounting height of the antenna with respect to the metal body of the robot ranged from 10 cm to 15 cm. Hence, the landmark detection distance, detection probability and measurement accuracy were different for each robot. The fourth robot ("Hugo") had the antenna mounted higher, because it was also carrying a laser scanner for reference localization purposes. "Hugo" also had an older model of the RFID reader, which had slightly poorer receiving sensitivity. The characteristics of each robot are shown in Table 6.3. More robot-specific data can be found in Appendix D. The noise parameters of each robot are shown in Table D.1 and the average number of measurements per landmark for the different robots is shown in Table D.2.

Table 6.3: Bearing angle measurement characteristics of the different robots. The second row shows the average number of successful measurements, when passing a landmark in operation mode 1. The third row is the same quantity for operation mode 2.

	Robots			
	Danny	Emma	Fiona	Hugo
Number of test runs	8	8	8	8
Measurements in mode 1	6.0	6.2	6.5	5.0
Measurements in mode 2	5.5	5.1	5.6	4.1
Antenna mounting height	10 cm	11.5 cm	12 cm	15 cm
Std deviation in calibration	8.0°	7.8°	5.6°	5.9°

The RFID tags serving as landmarks were placed on different kinds of surface materials and had different surroundings. Thus the detection ranges and probabilities of the landmarks were different. Table 6.4 shows the detection probability and the average number of successful measurements during one pass of a robot for each landmark. The detection probability means that with this percentage the robot made at least one successful measurement to a landmark while passing it. The average number of measurements

Table 6.4: Landmark detection probability percentage (Row 1), average number of successful measurements during one pass, if the landmark was detected (Row 2) and average position error in meters after ten localization runs (Row 3) for each landmark in the test environment.

Landmark	1	2	3	4	5	6	7	8	9	10
Row 1	89	95	95	97	98	100	72	100	63	100
Row 2	5.2	6.0	5.6	6.9	6.5	7.9	3.7	6.5	3.7	5.7
Row 3	0.16	0.18	0.10	0.12	0.10	0.12	0.28	0.14	0.13	0.24

is the average number of successful measurements when the robot has detected the landmark. The values are the combined averages of all four robots using both operating modes. The total number of measurement runs used for the computations was 32, so each landmark was passed 64 times. As can be seen, Landmarks 7 and 9 have clearly lower numbers of successful measurements than the average of all the landmarks. This is due to the unpredictable disturbances in a real environment and cannot be completely avoided, but with a suitable landmark density the effects can be reduced.

The average estimation error in the landmark position estimate is also listed in Table 6.4. The landmark position estimates were recorded after ten localization runs had been made in multi-robot mode, i.e. a group of ten robots had completed their localization mission. The runs were selected from the measurement database so that each of our four robots contributed 2.5 runs on average. Landmark 7 has the highest average error. Along with the low measurement count, this implies that the environment around the landmark causes disturbances to the bearing angle measurements. Landmark 9 also had an average number of measurements that was well below average. With ten robots making a total of 20 passes, Landmark 9 is expected to be detected 12.6 times. The average number of measurements to Landmark 9, when detected, was 3.7 giving approximately 47 as the total number of measurements. This is sufficient to localize the landmark when the measurement accuracy is reasonable, i.e. the environment does not cause significant disturbances. However, the average of 3.7 measurements offers little correction to the pose estimate of the passing robot and many times the robots do not even detect this landmark. As the heading angle estimate of the robot does not receive sufficient correction the accumulated error in the position of the robot keeps increasing and is inherited by the following landmarks. This can be seen in the higher position error of Landmark 10. The localization accuracy of Landmark 9 is close to the average, even though the number of measurements is low. This implies that the environment reduces the detection range of the landmark, but does not cause reflections that would increase the measurement noise, as happens with Landmark 7.

The placement of a landmark relative to other landmarks and critical locations such as intersections and room entrances affects the localization accuracy. A greater distance between two landmarks means a greater accumulated position error when driving from one landmark to the other. This is due to the inaccuracies in the heading angle estimate of the robot. The accumulated error then affects the position estimate of the landmark. When a robot turns at an intersection its heading angle estimate becomes less accurate as it is subject to the measurement error of the odometry system. In order to correct the heading angle estimate and, in consequence, keep the accumulated position error as low as possible it is important that a landmark is visible right after turning. In these experiments this can be seen when comparing Landmarks 6 and 9. When a robot turns into the side corridor it can immediately correct its pose estimate with the measurements to Landmark 6. Consequently the estimation error in the position of Landmark 8 is close to the average value. However, when a robot turns from the side corridor back into the main corridor and advances towards Landmark 9 it does not get measurements correcting its position until after several meters. Additionally, the poor detection reliability of Landmark 9 results in very few measurements. Hence, the accuracy of the robot pose estimate decreases, which causes Landmark 10 to be localized less accurately than Landmark 8, even though they are at the same distance from the starting point of the robots.

Node position estimation with a single robot

Five runs of a single robot were used to localize the nodes of the localization network. This is a close approximation of the case where a single robot is sent to traverse predefined area five times and localize the nodes found in that area. Before each run the robot gets its initial position estimate from a reference system. In this case the reference came from a marker on the floor, over which the robot was positioned manually. This allowed the initial pose of the robot to be set with a certain accuracy. The landmark position estimates and related covariances are preserved between each run. The same test was performed with all four robots. The results are shown in Table 6.5

There was no noticeable difference in the average error of the final position of a robot that depended on its order number. The first and the last robot had approximately the same estimation error in their position coordinates after they had completed the measurement run.

Each of the four different robots had approximately the same average position error in the end, but there is considerable variation in the accuracy of the landmark position estimates. This suggests that there is systematic error in the initial estimate of the robot's heading angle or in the bearing angle measurement system. Close examination of the measurement data revealed that the error in the initial heading angle causes most of the differences. The

Table 6.5: Results of single-robot localization. The average error in the landmark position is the average error distance between the absolute position and the final position estimate of the landmark after the robot had made all five runs. The average error in robot position is the average estimation error in the position of a robot after it has completed a measurement run.

	Robots			
	Danny	Emma	Fiona	Hugo
Number of runs for a robot	5	5	5	5
Avg error in landmark position	0.39 m	0.27 m	0.12 m	0.17 m
Avg error in robot position	0.34 m	0.35 m	0.33 m	0.31 m

marker that aligns a robot with the corridor was askew, more so for some robots than for others. This causes a systematic position error that increases when the robot moves further away from the starting point, but decreases again when the robot returns. Hence, the error in the final position of a robot can be small, even though the position estimates of the landmarks further away have inherited a considerable error from the robots passing by.

Node position estimation with multiple robots

When multiple robots are operating simultaneously, the position estimate of each robot is based on the measurement data of all the robots sharing information. The first robots exploring an area with no a priori information about the landmark positions would normally have to rely on their odometry only. Through sharing information they get corrections to their position estimates from the robots following them and making measurements to the same landmarks as the first robots have passed. This helps to keep the maximum accumulated error in the position of the robots smaller than in a single-robot approach.

The same measurement data that were used in the previous chapter were used when running the algorithm in multi-robot mode. The landmark position converges towards the correct position as the number of localization runs increases. When estimating the landmark position with one robot making one run, the position accuracy of the landmark depends heavily on the distance from the starting point of the robot. When the number of localization runs increases, the location dependency of the error in the final landmark position estimate decreases. Figure 6.6 illustrates the localization of five landmarks at different distances from the starting point of the robots. Measurement data were available from four different robots, so multiple runs per robot were used in order to observe the convergence with groups larger than four robots. Hence, the results do not describe a true multi-robot experiment, but indicate how the simulator should be tuned to match the real experiments as closely as possible. It can be observed that a landmark

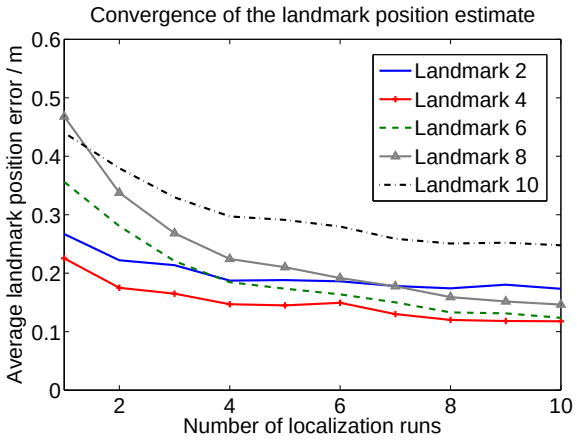

Figure 6.6: Accuracy of the final position estimates of Landmarks 2, 4, 6, 8 and 10 as a function of the number of robots in the group localizing the landmarks.

closest to the starting point is not necessarily localized most accurately. The environment and the landmark characteristics may affect the localization accuracy. This will explain the slow convergence of Landmark 2.

The average estimation error in a landmark position in a five-run multi-robot experiment was 0.20 m and the average estimation error in the position of a robot was 0.36 m. These are approximately the same as with single-robot localization, where the average of all robots is 0.24 m for landmark position error and 0.33 m for the final position error of the robot. When the number of runs was increased to ten, the values for landmark and robot position errors were 0.16 m and 0.34 m.

The position estimates of the landmarks are based on approximately the same number of measurements in the experiments with single or multiple robots. Therefore, the measurement error should be the same. The overall position accuracy of the robots is expected to be slightly better when multiple robots are cooperating and, in consequence, the landmark estimates are expected to converge faster. The error distance between the absolute and estimated positions was only measured in the final position of the robot. As the robot returns to its starting position this error does not reflect the average error during the localization run accurately. Thus the accuracy of the position estimate of the robot requires a closer look.

6.2.3 Robot position estimate

The ability of the bearing-only SLAM algorithm to keep track of the pose of a robot cannot be observed by recording the position error at a single point only. Hence, five different methods are used to illustrate the behavior of the pose estimate of a robot.

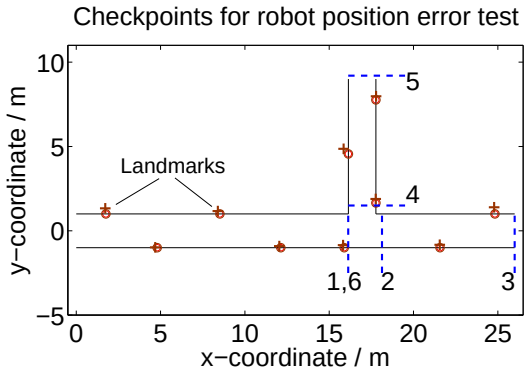

Figure 6.7: Checkpoints 1-6, where the robot position error comparison was made. True landmark positions are marked with circles and the estimates with average error are marked with crosses.

Sensitivity to landmark position error

The effect of the inaccuracies in the landmark position estimate on the position estimate of a robot was tested. In the node position estimation experiment groups of ten robots, randomly picked from the measurement database, were used to localize the landmarks. The average error for the landmark position estimates was calculated. For this experiment one localization run was selected, so that the average error of the ten landmarks was close to the overall average error of all the test runs in the previous experiment. The position estimate of each landmark after this selected localization run was stored. The error in the estimated position of each landmark close to the selected checkpoints is presented in Table 6.6.

The recorded values of the landmark position coordinates were programmed into the Kalman filter state vector before another group of robots started navigating. The estimated position of each robot was recorded at six different points. Then the correct location of each landmark was programmed into the Kalman filter state vector and exactly the same group was used for a reference test. The differences in the position estimates between these two runs were computed at the six selected locations (Figure 6.7). The test was repeated 500 times with different groups of robots in order to get an average value for each location. Another identical test was run with the errors in the landmark position coordinates doubled. The results are presented in Table 6.7.

The effect of the inaccuracies in the landmark position estimate seems to have a direct impact on the position estimate of the robot. At the ends of the corridors, where the landmark position estimates have a larger error, the position estimates of robots with perfectly localized landmarks and erroneous landmarks differ more from each other. At Check-point 6 the difference is smaller than at the ends of the corridors, even though the robot has traveled a longer trajectory. This implies that the robot position estimate depends

Table 6.6: Error in the estimated position of landmarks close to the checkpoints. The average error of all the landmarks is presented in the last column.

Landmark	5	6	7	8	9	10	all
Average error / m	0.05	0.20	0.29	0.18	0.12	0.27	0.16
Double error / m	0.10	0.41	0.57	0.37	0.24	0.54	0.32

Table 6.7: Difference in robot position estimate on the basis of perfectly placed landmarks and erroneous position estimates of landmarks. Difference 1 is calculated with landmarks that have approximately the average error after ten-robot localization. For Difference 2 the errors were doubled. The path lengths to points 2-5 depend on the direction in which the robot is following the path. The first values are for a robot driving in a counter-clockwise direction, i.e. driving to the end of the long corridor first.

Checkpoint	1	2	3	4	5	6
Path from start/m	16	18/36	26/44	36/18	44/26	54
Nearest landmark	5	5/6	10	6	8	5
Difference 1 /m	0.02	0.08	0.15	0.08	0.14	0.12
Difference 2 /m	0.03	0.12	0.24	0.13	0.24	0.22

more on the accuracy of the landmark position estimate than on the length of the robot's trajectory.

When the error in the position coordinates of the landmarks is doubled, the robot position estimate difference increases by 70% on average. Even poorly localized landmarks offer support for a robot, but accurate localization of the landmarks clearly results in more accurate estimation of the robot's position, even if the bearing angle measurements have considerable noise.

Measured robot position error at five locations

A test run was made, during which the robot was stopped at five different locations during the localization run and its true position was recorded. The path followed was the same as in the previous experiments. The checkpoints where the robot position was measured were approximately the same as Checkpoints 1,3,4,5 and 6 in the previous example (Figure 6.7). The reference robot, with a known position at the checkpoints, was always the last robot of the group. The tests were performed with different types of robot groups. Each test was repeated 1000 times and the other robots, except the last robot, were randomly picked for each run. The results are presented in Table 6.8.

Table 6.8: Error distance between the absolute and estimated position of a reference robot at selected checkpoints. The measurements were made on the last run of a five run set, except in the last test, where a group of ten robots was used. Both single-robot and multi-robot (or CL) approaches were tested.

Checkpoint	1	3	4	5	6	End
Trajectory length / m	16	26	36	45	56	72
Error with odometry only / m	0.11	0.18	0.19	0.48	0.20	0.73
Emma after 4 runs of Danny / m	0.12	0.30	0.22	0.35	0.34	0.18
Error of 5th run of Emma / m	0.12	0.27	0.21	0.31	0.30	0.17
Error of 5th robot with CL / m	0.12	0.22	0.25	0.27	0.27	0.21
Error of 10th robot with CL / m	0.12	0.19	0.25	0.22	0.26	0.19

The position estimates based on odometry only show that the error in the initial heading angle was very small. Checkpoint 2 is at the end of the 26-meter-long corridor, but the robot error at this checkpoint is only 18cm. When the robot makes two turns and reaches Checkpoint 5 at the end of the side corridor, the error is already 48 cm and after two more turns and a complete trajectory of 72 meters the error is already 73 cm. This implies that the accuracy of the heading angle estimate of the robot decreases along the way and the position error grows out of bounds, even if the initial angle estimate is accurate.

When the robots use the landmarks as reference points, the accuracy of the position estimate of the robot decreases towards the ends of the corridors as the landmark position estimates furthest away are less accurate on average. However, with cooperative localization (CL) the error distance between the absolute and estimated position of the robot stays below 30 cm all the time and decreases when the robot returns towards the starting position.

In single-robot mode the error depends on the odometry accuracy of the robot doing the four runs before the reference robot makes the fifth run. If a robot with an odometry accuracy less than the average is used (e.g. Danny), the position error of the reference robot is slightly higher, but it is still 35 cm at maximum and it decreases when the robot returns towards the starting point. With an average robot (Emma) doing all the runs the position error is approximately the same as with the cooperative approach. As a result of the small differences in the position errors and the heavy dependency on the odometry accuracy of the robots that are chosen, it is impossible to make a comparison of the localization accuracy of the single-robot and multi-robot approaches. However, the multi-robot system is a lot faster if the localization of the landmarks needs to be done within a certain time window.

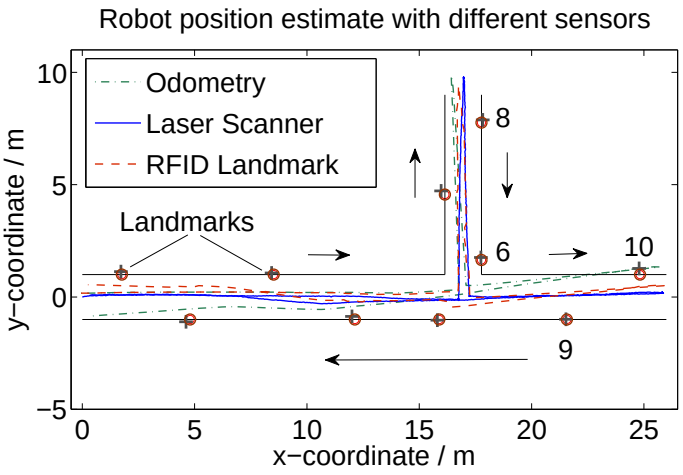

Figure 6.8: Robot position estimate with different sensors. Odometry (green) shows the estimate based on wheel encoders. Laser scan matching (blue) serves as the reference for ground truth. The RFID landmark-based estimate (red) shows the performance of the bearing-only localization. True landmark positions are marked with circles and current estimates with crosses. The arrows indicate the direction of the robot trajectory.

Comparison of a robot position estimate to a reference position

One of the robots ("Hugo") was equipped with a laser scanner in order to record its true position throughout a localization run. The test environment was made optimal for laser scan matching by placing cardboard boxes along the walls of the corridors. The boxes did not interfere with the bearing angle measurements. The reference trajectory of the robot was computed with a scan matching algorithm. A comparison between the robot position estimate based on bearing-only SLAM and the reference position is illustrated in Figure 6.8. The robot that is illustrated was the last robot in a group of eight robots.

The correction of the error in the heading angle of a robot depends on the number of measurements to the landmarks. When a robot passes multiple well-positioned landmarks along a straight trajectory, the heading angle gets corrected. However, when the robot turns from the side corridor into the main corridor and heads towards Landmark 10 (the furthest one on the right), the heading angle error does not get corrected and it causes noticeable inaccuracies in the robot position estimate. This is because the robot did not manage to make any successful measurements to Landmark 9.

Long-distance test

In this experiment a robot drove six loops continuously while making measurements to the landmarks. The first five loops followed the standard path

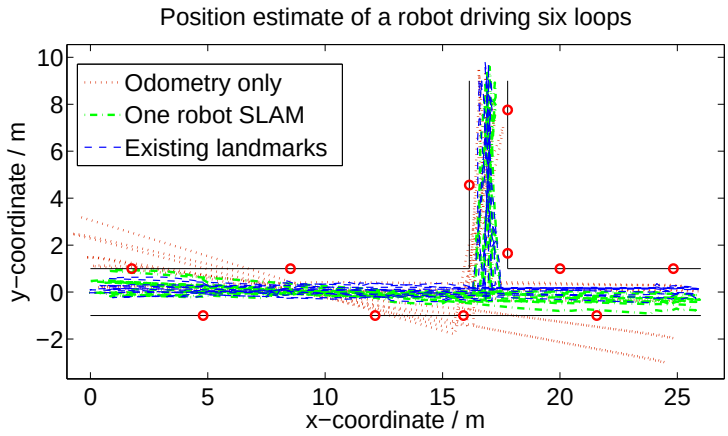

Figure 6.9: A robot driving six rounds in the office environment and estimating its position with odometry only (red, dotted line), with bearing-only SLAM (green, dash-dot line) and with landmarks that have already been localized (blue, dashed line).

used in the previous experiments. The sixth loop was an L-shaped path from the starting area to the end of the side corridor and back. The results of the experiment are presented in Figure 6.9.

When the robot was deployed, it was carefully aligned with the marker at the starting point in order to have an accurate initial heading angle estimate. If the robot is not using the bearing angle measurements, but only navigates with the odometry sensors, it can complete two loops without a problem. During the third loop the accumulated heading angle error starts to cause significant estimation error to the position of the robot and by the end of the third loop the robot would hit a wall.

If the robot is localizing landmarks simultaneously, the position estimate of the robot remains significantly more accurate. The accumulated error in the odometry still causes uncertainty in the position estimate of the robot. At two points the position estimate is close to the walls of the corridor, while the true position of the robot was close to the middle of the corridor.

Landmarks localized with ten robots give very good support for the robot driving six loops. The position estimate of the robot stays close to the middle of the corridor all the time, except at the beginning of the side corridor. This is partly because the true path of the robot also went close to the walls at this point. When the robot was moving along the long corridor, its true position was always in a one-meter-wide strip in the middle of the corridor, which matches well with the estimated position. Additionally, no significant differences between the loops can be seen, which implies that the localization error would be bounded.

The long test drive was performed with the robot (“Hugo”) equipped with the older model of the RFID reader. The average number of measure-

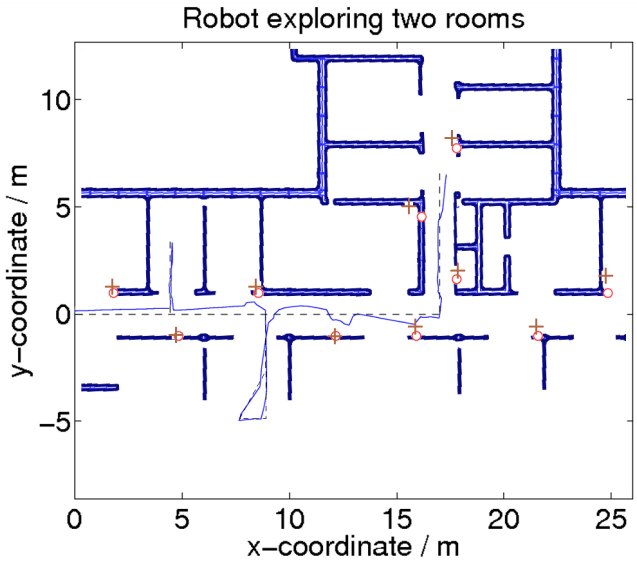

Figure 6.10: Position estimate of a robot visiting two rooms and then continuing along the corridors. The dashed line indicates the intended path of the robot. True landmark positions are marked with circles and current estimates with crosses.

ments to a landmark while passing it was only 3.96. This implies that the algorithm works even with a relatively small number of measurements and can keep the error distance between the absolute and the estimated position of the robot within bounds.

Robot following a complex path

A few test runs were made with a robot visiting one or two rooms in the office environment. The estimated path of a robot visiting two rooms is illustrated in Figure 6.10. As there are no landmarks in the rooms, the robot has to rely on its odometry until it returns to the corridor. After the second room the heading angle estimate of the robot is far from accurate, but when the robot passes landmarks the heading angle estimate becomes more and more accurate. The rate at which the heading angle gets corrected depends on many things, such as the number of successful measurements to landmarks and the uncertainty of the landmark position estimates. With this kind of localization system, where the measurement error and the heading angle error cannot easily be distinguished, the error in the heading angle of a robot cannot be expected to be corrected with a low number of measurements. Therefore, it is important that a sufficient landmark density is used in environments, where considerable error in the heading angle of a robot is expected to accumulate.

6.2.4 Summary

The experiments with the bearing angle measurement unit indicate that the accuracy of the unit depends on the environment. The measurements in the anechoic chamber had very good accuracy, but in the office environment the standard deviation grows. All the conductive surfaces cause reflections, which may bias the bearing angle measurement. The detection probability of the landmark is also sensitive to the environment.

The estimation of unknown node positions with robots equipped with a bearing angle measurement unit and odometry sensors was tested. With bearing-only SLAM the robots were able to localize the nodes of the localization network while simultaneously keeping track of their own pose. The algorithm is robust enough to work even with relatively inaccurate bearing angle measurements. The accuracy of the localization system is shown to be sufficient for indoor localization. The estimation error in the position of a localization node is shown to converge fast when the initial position estimate of each robot and the odometry system have good but realistic accuracy.

When a robot was exploring rooms with no localization nodes, error accumulated and its pose estimate became inaccurate. However, when the robot returned to the corridor it was able to correct its pose estimate with the help of the localization nodes already localized by previous robots.

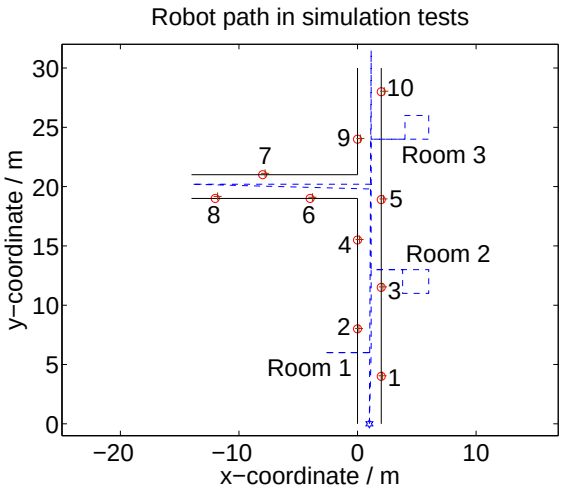

Figure 6.11: The simulation environment with ten landmarks and the path of the robots. The rooms were only visited in certain tests. The true locations of the landmarks are marked with small circles. Estimated landmark locations with average position error are marked with crosses.

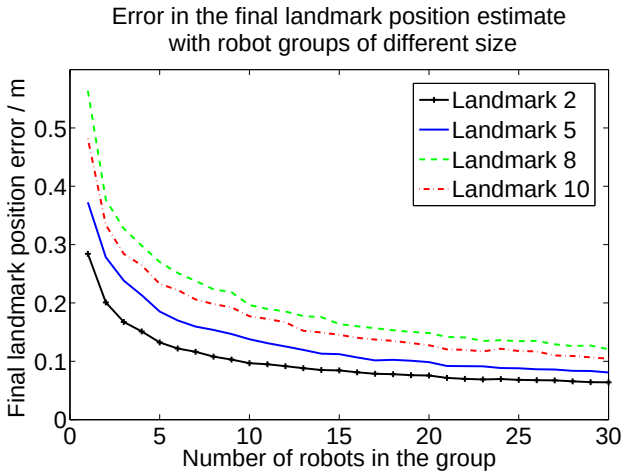

Figure 6.12: Landmark position error as a function of the number of robots. The convergence of the position estimates for four different landmarks is shown.

6.3 System performance simulations

The performance of the system in various environments and with robot groups of different sizes was tested with simulations. The simulation environment and robot parameters were set in a such manner that the simulator would match a real-world application as closely as possible. The robot error parameters were adjusted according to the information found during the laboratory experiments. The values used are listed in Table C.1, which can be found in Appendix C. The noise parameters used in the simulations are presented in Table C.2.

6.3.1 Node position estimation

The magnitude of the landmark (node) position error as a function of its relative position (i.e. the distance from the starting point of the robots) was tested with simulations. In this simulation, the environment was designed to resemble the environment of the real laboratory experiments with two perpendicular corridors and ten landmarks (Figure 6.11). The dimensions of the working area of the robots and the locations of the landmarks were approximately the same as in the laboratory experiments.

The convergence of the landmark position estimate was tested with robot groups of different sizes. All the robots followed approximately the same trajectory as the robots in the laboratory experiments. The robots followed the path in alternating directions. The error distance between the absolute position and the final position estimate of a landmark, as a function of the number of robots participating in the localization task, is illustrated in Figure 6.12.

The main source of error in the landmark localization is the accumulated estimation error in the position of a robot as a result of the inaccurate heading angle estimate. As the robot moves further away, the position error of a localized landmark increases. When the number of robots increases, the average heading angle error converges towards zero and the position estimate of a landmark becomes more accurate. For landmarks close to the starting point of the robots (e.g. Landmark 2) the position estimate converges fast as the accumulated estimation error in the robot position is small. Landmarks 8 and 10 are approximately at the same distance from the starting point and consequently have approximately the same convergence rate. This implies that for the reasonably fast convergence of landmark position estimates, it is crucial to have an accurate estimate of the heading angle of a robot when the robot is deployed. What is even more important is that the remaining inaccuracies in the heading angle estimate are non-systematic. Otherwise the landmarks will have a distance-dependent offset.

When the convergence of the position estimate in the simulations is compared with Figure 6.6, which illustrates the convergence in the laboratory experiments, a similarity can be observed. Both figures indicate that the accuracy of the landmark position estimate increases as the number of robots increases. Additionally, the accuracy of the position estimate is less sensitive to the distance from the starting point of the robots when a greater number of robots is used. The simulation results are based on a larger number of test runs and thus have a smoother appearance.

6.3.2 Robot position estimate

When the robots are able to use the landmarks for localization, the accuracy of the position estimate of a robot is expected to be bounded, i.e. independent of the time and distance the robot has traveled in the working area covered by the landmarks. The bounds of the estimation error in the position estimate of a robot are set by the accuracy of the landmark position estimates and the measurement error of the bearing angle measurements.

The accuracy of the robot position estimate was observed while a robot did eight consecutive laps following the same path as described in the previous experiment. The robot did every second lap in a clockwise direction and the others in a counter-clockwise direction. The simulations were repeated 1000 times in order to have average values for the errors. The results of three different scenarios are illustrated in Figure 6.13. The black lines show the average error distance between the absolute and estimated position of the robot after it has passed Landmark 8 at the end of the side corridor. The red lines show the average error distance after the robot has passed Landmark 10 at the end of the long corridor.

In the first scenario the robot relies on its odometry only. The position error of the robot grows with each lap as there are no measurements to correct

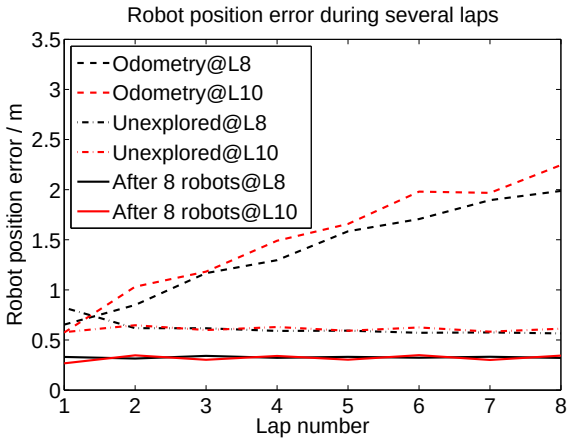

Figure 6.13: Accuracy of the position estimate of a robot doing 8 laps in the office environment. Three different localization scenarios were tested. Black lines show the position error after Landmark 8 and the red lines after Landmark 10.

it. There is only a small difference between the errors at the two observation points.

In the second scenario the robot uses bearing-only SLAM. There is no a priori information about the locations of the landmarks. As can be seen, the landmarks stabilize the robot position estimate and the error stays at a constant level. As the landmarks are localized by one robot only, the initial and systematic errors cause considerable inaccuracies in the position estimates of the landmarks. Hence the accuracy of the robot position estimate is mediocre at the two observation points 34 meters (Landmark 8) and 30 meters (Landmark 10) away from the starting point.

The landmarks are localized in advance for the third scenario. A simulation run with a group of eight robots is used to localize the landmarks. The simulation is repeated 1000 times to get an average position error and variance for each landmark. These values are then used to compute a priori values for the state vector and covariance matrix, before a robot is ordered to drive eight laps, just like in the previous scenario. Now that the landmarks are positioned more accurately, the position estimate of the robot stays fairly accurate during each lap.

The same setup was used for a robot visiting rooms. The landmarks had the position estimates and variances with average values when a robot was ordered to follow a path through two or three rooms. The path of the robot is shown in Figure 6.11. The rooms were visited in ascending order. Therefore, a robot visiting only two rooms did not visit room number three. The error distance between the absolute and the estimated position of the robot was recorded at the final position close to the starting point, at the end of the long corridor (after Landmark 10) and at the end of the side corridor. The results are presented in Tables 6.9 and 6.10. The position errors that are

Table 6.9: A robot visiting two rooms

	Odometry	SLAM
Position error after Landmark 8 / m	0.86	0.34
Position error after Landmark 10 / m	1.08	0.39
Position error at final point / m	0.92	0.20

Table 6.10: A robot visiting three rooms

	Odometry	SLAM
Position error after Landmark 8 / m	0.86	0.33
Position error after Landmark 10 / m	1.11	0.46
Position error at final point / m	1.08	0.21

presented are average values of 1000 test runs.

The results of the two-room simulation show that a robot navigating with its odometry sensors only has considerable inaccuracies in the position estimate at all the checkpoints. With the landmarks the robot is able to correct the accumulated error and improve the accuracy of the position estimate to approximately the same level as a robot roaming along the corridor had in the previous experiment.

The interesting observation in the three-room test is the accuracy of the position estimate of the robot after the Landmark 10. The third room is just before that landmark, so the error accumulated during the visit to the third room is reflected in the measured position error. Even though the position error after the Landmark 10 is higher than in the two-room test, the error in the final position of the robot is approximately the same in both experiments. This implies that the accumulated error is corrected when the number of measurements to landmarks increases and does not grow out of bounds.

6.3.3 Comparison between one robot and multi-robot systems

The localization of the landmarks with a single robot was compared to the localization with multiple robots. A single robot made 10 consecutive localization runs. For each run the robot was repositioned, so the odometry error only accumulated over one run and was then set back to the initial values.

A group of ten robots was used to observe the localization accuracy with multiple robots. Each robot made one localization run. The robots of the group started from the same position with short intervals. Therefore, there

Table 6.11: Landmark and robot position error with single- and multi-robot localization

	Single-robot		Multi-robot	
	Error	Std dev	Error	Std dev
Landmark final position	0.15 m	0.04 m	0.14 m	0.04 m
Robot final position	0.25 m	0.30 m	0.22 m	0.14 m
Robot after Landmark 10	0.37 m	0.24 m	0.31 m	0.19 m
Robot after Landmark 8	0.41 m	0.26 m	0.33 m	0.18 m

were multiple robots operating simultaneously.

The average position error of the landmarks, the average error of a robot after each test run and the average error of a robot when it was at the ends of both corridors (i.e. by Landmarks 10 and 8, 30 m and 34 m from the starting point) were recorded. The results are presented in Table 6.11.

On average, the landmarks are positioned equally well in both tests. There is approximately the same number of measurements to the landmarks, which means that the effect of the error in the bearing angle measurements is the same for both tests. The accuracy of the position estimates of the landmarks depends mostly on the accuracy of the initial heading angle estimates of the robots. As this can be expected to be approximately the same for a single robot launched ten times as it is for ten different robots launched one by one, it does not cause a significant difference to the localization accuracy between the two tests.

As stated earlier, in the case where the robot returns to its starting point, the accuracy of the final position estimate of the robot does not give a clear picture of the effects of the accumulated estimation error in the pose of the robot at various locations. Thus it is important to observe the accuracy of the robot position estimate at the points some distance away from the starting point. With multiple robots the average position estimates at the ends of the corridors seem to be more accurate. As the robots cooperate, even the first robot gets its position estimate corrected while heading towards the end of a corridor. Hence, the position estimate of the robot stays more accurate, which affects the average position error of all the robots. Additionally, the more accurate position estimate of the first robot results in slightly better initial position estimates of the landmarks. This is the main reason why the landmark position estimates are slightly more accurate with the multi-robot system. As the number of robots (or measurement runs) increases, the importance of the initial estimate decreases and so does the difference in the estimation error of the landmark position between the two systems that were tested (Figure 6.14).

The standard deviation indicates how much the position errors of the

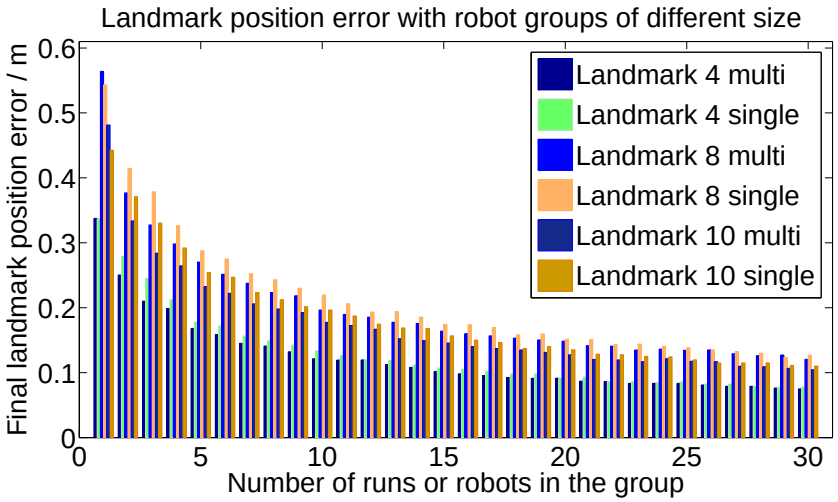

Figure 6.14: The estimation error in the final position estimate of the landmarks with robot groups of different sizes and with different numbers of runs in single-robot mode. The results of the multi-robot experiments are shown with dark bars and those of the single-robot experiments with light colors.

individual robots differ from the average position error. A smaller standard deviation in multi-robot localization means that there is less difference in the position errors of individual robots and in consequence, they have a better estimate of the relative positions between robots.

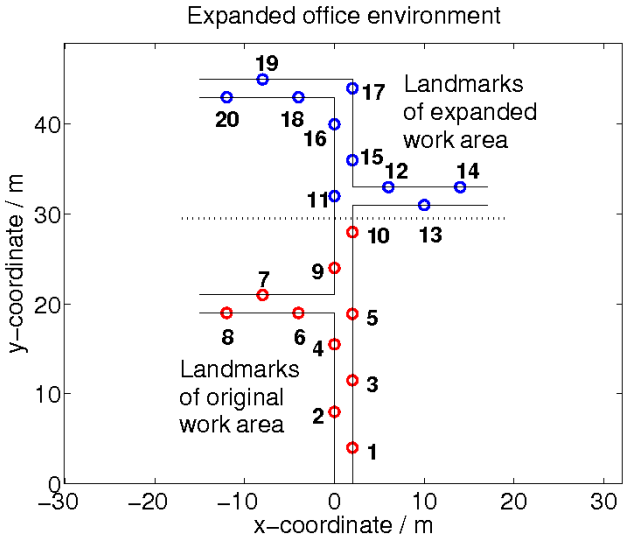

Figure 6.15: The expanded office-like environment for simulations. The landmarks (1-10) of the original work area are marked with red circles and the landmarks (11-20) of the extension of the work area are marked with blue circles.

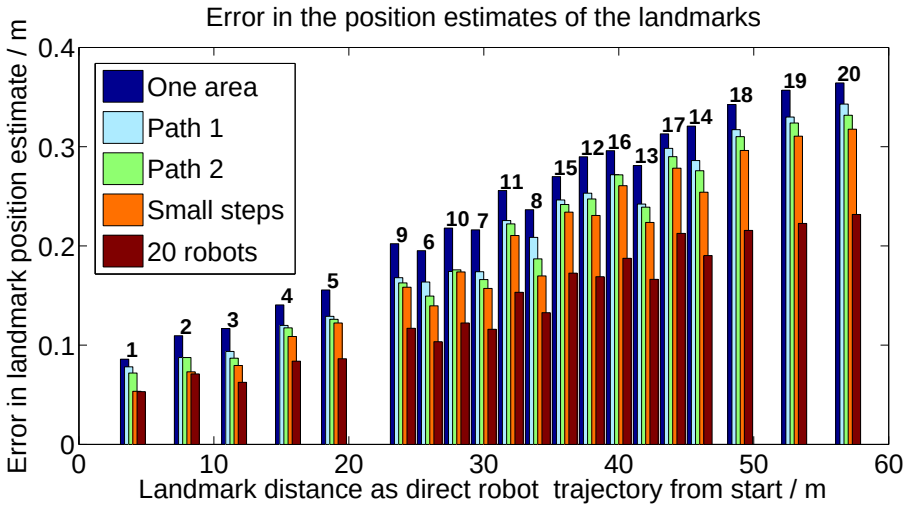

Figure 6.16: The error in the estimated position of a landmark. In order to avoid the overlapping of the bars, the landmarks in the first two side corridors (6,7,8,12,13 and 14) have been plotted 1 m further away than their real distance from the start.

6.3.4 Robots expanding the work area

The work area of the robots may change over time. Simulation runs were used to observe the capability of the robots to expand their work area after first localizing the landmarks of the original work area. The original work area was the same as that used in the previous simulations. The expanded environment is illustrated in Figure 6.15.

As the heading angle error causes considerable inaccuracies to the robot position estimate, which in turn is inherited by the new landmarks, the robots tried to minimize the inaccuracy of their heading angle estimates before advancing into uncharted territory. Therefore, the robots returned to their starting point and then headed straight to the new work area. In this way the robots get measurements to several old landmarks along a straight trajectory before they arrive in the new area without well-localized landmarks. A group of ten robots was used, unless mentioned otherwise.

For reference, a simulation was run, in which the whole area was just one work area and the robots localized the tags by first driving to the end of the long corridor and then exploring the side corridors on their way back. The results of this simulation are illustrated in Figure 6.16 with the bars labeled "One area".

Another simulation was run, in which the robots first localized the ten original landmarks with one loop trajectory and then made another loop covering the last ten landmarks. This is marked as "Path 1". In the next simulation the robots made two loops in the original area and then two loops in the extended area ("Path 2"). The latter approach gives slightly

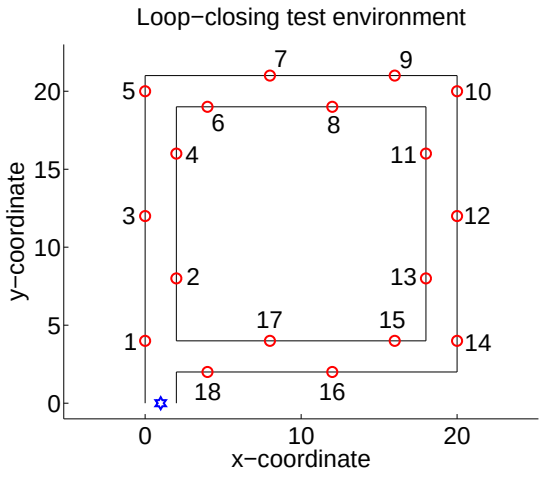

Figure 6.17: Circular environment for the loop-closing simulations. Landmarks are marked with small red circles and are numbered. The starting position of the robots is marked with a blue hexagon at (1,0).

better results due to the greater number of measurements. The same path was then used for another simulation, but this time the robots made measurements every 10 cm ("Small steps"), which resulted in approximately twice as many measurements as before. Once again there is just a slight increase in the landmark position accuracy. Overall these three aforementioned methods are clearly better than the reference run, where the robots directly localized all the landmarks. However, the accuracy of the landmark position estimate decreases as the distance from the starting point increases.

One more simulation was made with a group of 20 robots. The robots followed Path 2, which included two loops in the original and extended areas. Even though the accuracy of the landmark position estimate still decreases as the distance increases, the slope is less steep. With a larger number of robots, the average error in the initial heading angle error of a robot is closer to zero and thus the landmark position estimates are less sensitive to the distance from the start.

6.3.5 Circular environment

Three different simulations were conducted in the circular environment illustrated in Figure 6.17. The robots always started from the same location, but the paths they followed were different for each simulation test. Figure 6.18 shows the accuracy of the position estimate of each landmark for all three simulations.

In the first simulation ("no closing"), all the robots followed the same path along the corridor until they reached the last landmark (Landmark 18). After the last landmark the robots stopped. Thus each robot passed each landmark only once. The accuracy of the position estimates of the land-

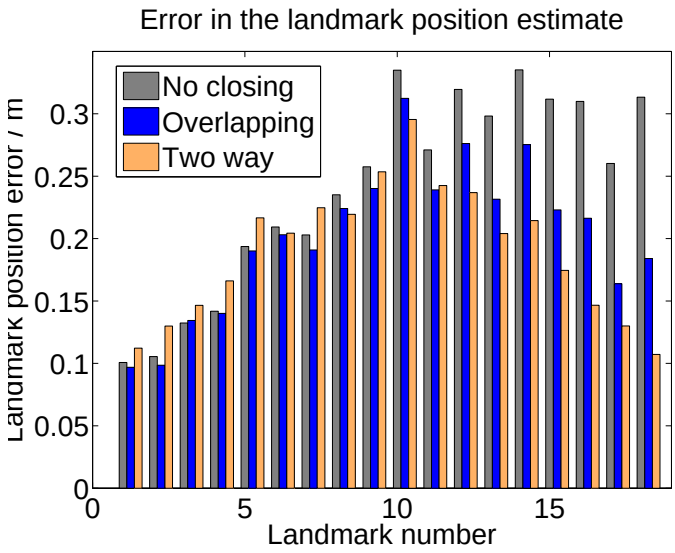

Figure 6.18: Landmark position error in circular environment with no overlap (left), with two-tag overlap and with half of the robots driving in the opposite direction.

marks decreases as the robot moves away from the starting point. This is due to the accumulated estimation error in the position of the robots. As the robots reach the landmark furthest away (Landmark 10) and start to move towards the starting point again, the position error caused by the initial inaccuracies in the heading angle estimate of a robot starts to decrease. However, the other error sources still reduce the accuracy of the position estimate of a robot. Hence, the overall accuracy of the position estimate of a robot may remain almost static, as happened in this simulation. The accuracy of the position estimates of the remaining landmarks reflects the almost unvarying robot position accuracy.

In the second simulation ("overlapping"), all the robots followed the same path again, but this time they did one full circle and then continued past Landmark 2. Thus they got another set of measurements to Landmarks 1 and 2, which they had already localized during the first round. These measurements apply a correction to the pose estimate of a robot, which is then propagated to the landmark position estimates through the covariances in the covariance matrix of the Kalman filter. As the covariances between a robot and the landmarks passed most recently are the strongest, the effect of the correction is most visible in the position estimates of the last landmarks of the circular environment.

In the third simulation ("two way"), half of the robots circled the corridors in a clockwise direction and the other half circled them in a counterclockwise direction. As expected the landmark position estimates have decreasing accuracy towards the landmark that is furthest away, starting from both ends of the landmark series.

6.3.6 Summary

The simulation experiments with robot groups of different sizes show that the accuracy of the final position estimates of the landmarks increases as the number of robots increases. However, when the robot odometry is fairly accurate, the effect is significant only for relatively small groups of robots and for groups larger than 15 robots the addition of an extra robot has very little effect.

The landmark localization is shown to be more accurate with a multi-robot system than with a single robot if the same number of measurement runs is used. The multi-robot system is also significantly faster than the single-robot approach, as all the robots of the multi-robot system operate simultaneously.

The accuracy of the robot position estimate is shown to be bounded when the landmarks are used for localization. The bounds depend on the accuracy of the landmark position estimates.

It is also shown that the so-called loop-closing is not a problem, but an advantage, when landmarks with unique IDs are used. When a robot returns to a place it visited earlier and detects a landmark, it can considerably reduce the accumulated estimation error in its position estimate. This correction can be propagated to the recent landmark position estimates.

Chapter 7

Conclusions

The aim of this research was to develop a new method for autonomous landmark localization with mobile robots. Properly localized landmarks would provide support for the localization of the robots operating within the coverage area. Accurate localization of the landmarks in a common coordinate frame may be difficult for humans as the necessary information may not all be readily available. In any case, human involvement would take time and effort, which may be costly.

For the localization of landmarks with a group of robots, a novel method was implemented and tested. The experiments were performed on mobile robots equipped with basic odometry sensors and another sensor for measuring bearing angles to static, identifiable landmarks. It is shown that these robots can estimate the a priori unknown positions of the landmarks while keeping track of their own pose simultaneously. As the absolute position of both the landmarks and robots is estimated and the estimates are based on bearing angle measurements, the method is called bearing-only SLAM.

The implementation of bearing-only SLAM is realized with a centralized Kalman filter. As the system may contain several robots and numerous landmarks, the correlation between the entities is trivial only if all the data are maintained in one place. As the measurement equation is non-linear, the Extended Kalman Filter (EKF) algorithm was used. EKF uses linear approximation at the related operation point in order to update the covariance matrix. Thus the computation of the full algorithm is necessary for each measurement update and no constant values can be used for the uncertainties or for the Kalman gain. Normally, the robots make measurements to only one landmark at a time. Therefore, the number of simultaneous measurements is low and the complexity of the algorithm is not a problem for real-time operation.

The performance of the localization method was tested with laboratory experiments and simulations. The laboratory experiments indicate that the robots are able to localize the landmarks with the proposed method. Even sparsely distributed landmarks offer support for the long-term operation of the robots. The accuracy of the position estimate of the robots is of the same order of magnitude as the position accuracy of the localized landmarks. Four small robots were used for the laboratory experiments. Each robot

had slightly different characteristics as a result of small mechanical differences. The robots had wheel encoders and a bearing angle measurement unit. The accuracy of the bearing angle sensor was found to be mediocre in an office environment. However, on average the robots managed to make five to six measurements to a landmark while passing it. Hence, even uncertain measurements were enough for the localization system to operate with sufficient accuracy. The sparse distribution of the landmarks was possible partly because the odometry systems of the robots were very accurate. Less accurate odometry can be compensated for with a denser distribution of landmarks and with a greater number of measurements to the landmarks.

It was also shown that the landmarks clearly support the localization of the robots. When a robot visited two rooms without any landmarks, its position estimate became inaccurate. However, when the robot returned to the corridor, it was able to correct its position estimate with the bearing angle measurements to the landmarks. After the robot had passed a few landmarks, its position estimate was approximately at the same level as that of the robots that had never left the corridor. In another experiment, a robot followed a 70-meter-long loop path for several rounds. When landmarks were used to support the localization, there was no noticeable difference in the accuracy of the position estimate of the robot between different rounds. This indicates that the accuracy of the position estimate of the robot does not change over time. The landmark position estimates converge fast and the remaining uncertainty is reflected in the position estimate of a robot using the landmarks for navigation.

Simulations were used to observe the performance of the system with an arbitrary number of robots. A comparison between approaches using one or multiple robots was also performed. The simulation parameters were set according to the observations made during the laboratory experiments. The landmark position accuracy clearly increased when the number of measurement runs increased from one to ten. Additional measurement runs offer a smaller improvement in the position accuracy, but it may still be considerable, especially for landmarks far away from the starting point of the measurement runs. If the odometry system of a robot is less accurate than that simulated here, the number of measurement runs required for a certain localization accuracy may be somewhat higher. A group of robots can localize the landmarks significantly faster than a single robot as they execute the measurement runs simultaneously. Additionally, the convergence of the landmark position estimates is faster as the robot position estimates stay within tighter bounds with a group of cooperating robots.

It was also observed that a more accurate localization of landmarks can be obtained when the robots first localize landmarks in one part of the accessible area and then expand the localization to another part. Even if the landmarks are not perfectly localized, they help the robots to correct the accumulated error in their position and heading angle estimates. Additionally,

the detection of a landmark that has been localized earlier may significantly increase the accuracy of the position estimates of the landmarks that the robot has just passed. This was observed when the robots completed a loop in a circular environment and detected again the landmarks that they had passed at the beginning of the measurement run.

The bearing angle measurement was based on the RFID technology. Passive tags were used as landmarks. The bearing angle to a landmark was measured by turning the reader antenna and marking the sector where the landmark responded. The bearing angle to the landmark was then estimated, using the center angle of the sector and antenna-specific calibration parameters. The accuracy of the bearing angle measurement unit was found to be good in an anechoic chamber, but in an office environment it was less accurate than expected. This was due to various disturbances, mostly caused by reflections of the radio waves from conductive surfaces. However, the localization algorithm was found to be robust enough for efficient operation, even when the uncertainty in the bearing angle measurement is set to over 40°.

A hobby servo was used to turn the RFID reader antenna. The accuracy of the servo was found to be adequate, but the measurement process was slow. The mechanical turning of the antenna also causes design constraints and it is subject to wear. As the algorithm was shown to work even when the bearing angle measurement system is relatively inaccurate, an alternative method for bearing angle measurement could be found. This is one major topic for the further development of the system. There are at least two possible candidates for a new measurement method. An array of antennas can form a directed beam of radiation which is controlled by the signals fed to each antenna. The turning of the beam happens instantaneously and no mechanical movement is required. The dimensions of the antenna array depend on the operating frequency of the system. The size of the robots and the availability of technology on different frequencies affect the feasibility of this approach. Another possibility is sensor fusion. For example, in some environments, the landmarks can be made observable by a camera. Hence, the bearing angle could be measured with a panoramic view of a camera, whereas the identification and the data transfer could be realized with the RFID technology.

Another topic for future research is the distribution of the localization algorithm. The availability of a reliable communication method to a central computer cannot always be assumed. The distribution of the algorithm and implementation of robot-specific sub-filters would allow the robots to navigate independently and use the cooperation to correct their own pose estimates when communication between other entities becomes possible. Additionally, the optimal distribution of the landmarks can be studied. If the robots are expected to distribute the landmarks when they explore uncharted territories, they need a method for selecting where to position the

landmarks. This method can be based, for example, on the analysis of the robot path and the surrounding environment.

The localization system was only tested in an office building, but the concept might be useful in other environments too. It may not be feasible for outdoor localization, where GPS is readily available, but this is not the case everywhere. Underground applications or search and rescue operations in collapsed buildings may require an infrastructure-independent localization system that can support autonomous vehicles. In a rescue scenario, the localization system could also provide important information on the approximate position of human beings, even if they did not have accurate measurement devices, but could still detect the landmarks within a short range. In the future, planetary rovers may also need accurate localization within a constrained working area. In general, a localization system that can be set up by robots is needed where the participation of humans would be expensive, dangerous or practically impossible.

Bibliography

Lars A. A. Andersson and Jonas Nygards. On utilizing geometric formations for minimizing uncertainty in 3 robot teams. Technical report, Robotics / Autonomous Mechanical Systems, Linköping University, 2008.

A. Bais, R. Sablatnig, and J. Gu. Single landmark based self-localization of mobile robots. In *Computer and Robot Vision, 2006. The 3rd Canadian Conference on*, pages 67–67, 2006.

Jürgen Bohn. Prototypical implementation of location-aware services based on super-distributed RFID tags. In *Proceedings of the 19th International Conference on Architecture of Computing Systems (ARCS'06), Frankfurt am Main, Germany. Number 3894 in LNCS, Springer-Verlag*, pages 69–83. Springer, 2006.

J. Borenstein, H. R. Everett, and L. Feng. *Where am I? Sensors and Methods for Mobile Robot Positioning*. University of Michigan, USA, 1996.

K. Briechle and U. D. Hanebeck. Localization of a mobile robot using relative bearing measurements. *Robotics and Automation, IEEE Transactions on*, 20(1):36–44, 2004.

W. Burgard, M. Moors, D. Fox, R. Simmons, and S. Thrun. Collaborative multi-robot exploration. In *Robotics and Automation, 2000. Proceedings. ICRA '00. IEEE International Conference on*, volume 1, pages 476–481, 2000.

V. Cevher and J. H. McClellan. Sensor array calibration via tracking with the extended kalman filter. In *Acoustics, Speech, and Signal Processing, 2001. Proceedings. (ICASSP '01). 2001 IEEE International Conference on*, volume 5, pages 2817–2820, 2001.

H. J. Chang, C. S. G. Lee, Y. C. Hu, and Yung-Hsiang Lu. Multi-robot SLAM with topological/metric maps. In *Intelligent Robots and Systems, 2007. IROS 2007. IEEE/RSJ International Conference on*, pages 1467–1472, 2007.

Charles Cohen and Frank V. Koss. A comprehensive study of three object triangulation. In *Proceedings of the 1993 SPIE Conference on Mobile Robots*, pages 95–106, 1992.

Matthew Deans and Martial Hebert. Experimental comparison of techniques for localization and mapping using a bearing-only sensor. In *ISER '00: Experimental Robotics VII*, pages 395–404, London, UK, 2001. Springer-Verlag. ISBN 3-540-42104-1.

Frank Dellaert, Tucker Balch, Michael Kaess, Ram Ravichandran, Fernando Alegre, Marc Berhault, Robert McGuire, Ernest Merrill, Lilia Moshkina, and Daniel Walker. The Georgia Tech Yellow Jackets: A marsupial team for urban search and rescue. In *Proc. of AAAI Mobile Robot Competition & Exhibition Workshop*, pages pp. 44–52. AAAI Press, 2002.

Gregory Dudek, Michael R. M. Jenkin, and David Wilkes. A taxonomy for multi-agent robotics. *Autonomous Robots*, 3:375–397, 1996.

Mikko Elomaa and Aarne Halme. *Distributed Estimation of Unknown Beacon Positions in a Localization Network*, pages 147–162. Contemporary Robotics - Challenges and Solutions. In-Teh, 2009. ISBN 978-953-307-038-4.

Mikko Elomaa and Aarne Halme. Estimating localization network node positions with a multi-robot system. In *Proceedings of the International Conference on Computer, Electrical, and Systems Science, and Engineering*, 2010.

Mikko Elomaa, Aarne Halme, and François Vacherand. Cooperative localization - self-configuring procedure of a multi-robot localization system with passive RFID technology. In *Proceedings of the Fifth International Conference on Informatics in Control, Automation and Robotics, Robotics and Automation*. INSTICC Press, 2008.

J. W. Fenwick, P. M. Newman, and J. J. Leonard. Cooperative concurrent mapping and localization. In *Robotics and Automation, 2002. Proceedings. ICRA '02. IEEE International Conference on*, volume 2, pages 1810–1817 vol.2, 2002.

D. Fox, J. Ko, K. Konolige, B. Limketkai, D. Schulz, and B. Stewart. Distributed multirobot exploration and mapping. *Proceedings of the IEEE*, 94 (7):1325–1339, 2006.

A. Galstyan, B. Krishnamachari, K. Lerman, and S. Pattem. Distributed online localization in sensor networks using a moving target. In *Information Processing in Sensor Networks, 2004. IPSN 2004. Third International Symposium on*, pages 61–70, 2004.

Robert Grabowski, Luis E. Navarro-serment, Christiaan J. J. Paredis, and Pradeep K. Khosla. Heterogeneous teams of modular robots for mapping and exploration. *Autonomous Robots*, 8:293–308, 2000.

D. Hahnel, W. Burgard, D. Fox, K. Fishkin, and M. Philipose. Mapping and localization with RFID technology. In *Robotics and Automation, 2004. Proceedings. ICRA '04. 2004 IEEE International Conference on*, volume 1, pages 1015–1020 Vol.1, 2004. ISBN 1050-4729.

Seppo Heikkilä. Development of laser based localisation methods for personal navigation system - PeNa. Master's thesis, Helsinki University of Technology, 2005.

Herianto, Toshiki Sakakibara, and Daisuke Kurabayashi. Artificial pheromone system using RFID for navigation of autonomous robots. *Journal of Bionic Engineering*, 4(4):245 – 253, 2007. ISSN 1672-6529.

Y. S. Hidaka, A. I. Mourikis, and S. I. Roumeliotis. Optimal formations for cooperative localization of mobile robots. In *Robotics and Automation, 2005. ICRA 2005. Proceedings of the 2005 IEEE International Conference on*, pages 4126–4131, 2005.

J. Hightower, R. Want, and G. Borriello. Spoton: An indoor 3d location sensing technology based on RF signal strength. Technical report, UW CSE 00-02-02, University of Washington, Department of Computer Science and Engineering, Seattle, WA, February, 2000.

A. Howard, M. J. Mataric, and G. S. Sukhatme. Putting the 'I' in 'team': an ego-centric approach to cooperative localization. In *Robotics and Automation, 2003. Proceedings. ICRA '03. IEEE International Conference on*, volume 1, pages 868–874, 2003. ISBN 1050-4729.

Andrew Howard, Lynne E. Parker, and Gaurav S. Sukhatme. The SDR experience: Experiments with a large-scale heterogenous mobile robot team. In *9th International Symposium on Experimental Robotics*, 2004.

Kyoung-Hwan Jo and Jihong Lee. Multi-robot cooperative localization with optimally fused information of odometer and gps. In *Control, Automation and Systems, 2007. ICCAS '07. International Conference on*, pages 601 –605, 17-20 2007.

Jijoong Kim and Hatem Hmam. Landmark-based navigation of an unmanned ground vehicle (UGV). Technical report, Weapons Systems Division, DSTO Defence Science and Technology Organisation, 2009.

M. Kim, Tsunenori Takeuchi T, and N. Y. Chong. *A 3-axis Orthogonal Antenna for Indoor Localization*, pages 923–1292. Robotics Lab., Japan Advanced Institute of Science and Technology, 2004.

Myungsik Kim and Nak Young Chong. Direction sensing RFID reader for mobile robot navigation. *Automation Science and Engineering,*

IEEE Transactions on, 6(1):44 –54, jan. 2009. ISSN 1545-5955. doi: 10.1109/TASE.2008.2006858.

Alexander Kleiner, Johann Prediger, and Bernhard Nebel. RFID technology-based exploration and SLAM for search and rescue. In *Intelligent Robots and Systems, 2006 IEEE/RSJ International Conference on*, pages 4054–4059, 2006.

J. Ko, B. Stewart, D. Fox, K. Konolige, and B. Limketkai. A practical, decision-theoretic approach to multi-robot mapping and exploration. In *Intelligent Robots and Systems, 2003. (IROS 2003). Proceedings. 2003 IEEE/RSJ International Conference on*, volume 4, pages 3232–3238, 2003.

D. Kroetsch and C. Clark. Towards gaussian multi-robot SLAM for underwater robotics. In *Proceedings of the 2005 International Symposium on Unmanned Untethered Submersible Technology*, 2005.

O. Kubitz, M.O. Berger, M. Perlick, and R. Dumoulin. Application of radio frequency identification devices to support navigation of autonomous mobile robots. In *Vehicular Technology Conference, 1997 IEEE 47th*, volume 1, pages 126 –130, 1997.

V. Kulyukin, C. Gharpure, J. Nicholson, and S. Pavithran. RFID in robot-assisted indoor navigation for the visually impaired. In *Intelligent Robots and Systems, 2004. (IROS 2004). Proceedings. 2004 IEEE/RSJ International Conference on*, volume 2, pages 1979–1984, 2004.

R. Kurazume, S. Nagata, and S. Hirose. Cooperative positioning with multiple robots. In *Robotics and Automation, 1994. Proceedings., 1994 IEEE International Conference on*, pages 1250–1257 vol.2, 1994.

D. Kurth, G. Kantor, and S. Singh. Experimental results in range-only localization with radio. In *Intelligent Robots and Systems, 2003. (IROS 2003). Proceedings. 2003 IEEE/RSJ International Conference on*, volume 1, pages 974 – 979, 2003.

Koen Langendoen and Niels Reijers. Distributed localization in wireless sensor networks: A quantitative comparison. *Computer Networks*, 43(4): 499–518, 2003.

Yufeng Liu and S. Thrun. Results for outdoor-SLAM using sparse extended information filters. In *Robotics and Automation, 2003. Proceedings. ICRA '03. IEEE International Conference on*, volume 1, pages 1227–1233, 2003. ISBN 1050-4729.

F. Lu and E. Milios. Globally consistent range scan alignment for environment mapping. *Autonomous Robots*, 4:333–349, 1997.

P. Marantos, Y. Koveos, J. Stergiopoulos, A. Panousopoulou, and A. Tzes. Mobile robot odometry relying on data fusion from RF and ultrasound measurements in a wireless sensor framework. In *Control and Automation, 2008 16th Mediterranean Conference on*, pages 523–528, 2008.

M. Di Marco, A. Garulli, A. Giannitrapani, and A. Vicino. Simultaneous localization and map building for a team of cooperating robots: A set membership approach. *Robotics and Automation, IEEE Transactions on*, 19 (2):238–249, 2003.

R. Martinez-Cantin, J. A. Castellanos, and N. de Freitas. Multi-robot marginal-SLAM. *IJCAI Workshop on Multi-Robotic Systems for Societal Applications*, 2007.

P. S. Maybeck. *Stochastic Models, Estimation and Control*, pages pp. 1–16. Academic Press, New York, 1979.

James McLurkin. The ants: A community of microrobots. Technical report, 1995. Bachelor's Thesis, MIT, 1995.

Michael Montemerlo. FastSLAM: A factored solution to the simultaneous localization and mapping problem. In *Proceedings of the AAAI National Conference on Artificial Intelligence*, pages 593–598. AAAI, 2002.

Michael Montemerlo, Sebastian Thrun, Daphne Koller, and Ben Wegbreit. FastSLAM 2.0: An improved particle filtering algorithm for simultaneous localization and mapping that provably converges. In *Proceedings of the International Conference on Artificial Intelligence (IJCAI*, pages 1151–1156, 2003.

E. D. Nerurkar and S. I. Roumeliotis. Power-SLAM: A linear-complexity, consistent algorithm for SLAM. In *International Conference on Intelligent Robots and Systems, 2007. IROS 2007*, pages 636–643, 2007.

P. Newman and Kin Ho. SLAM-loop closing with visually salient features. In *Robotics and Automation, 2005. ICRA 2005. Proceedings of the 2005 IEEE International Conference on*, pages 635–642, 2005.

Lionel M. Ni and Yunhao Liu. Landmarc: Indoor location sensing using active RFID. *Wireless Networks*, (10):701–710, 2004.

Edwin Olson, John J. Leonard, and Seth Teller. Robust range-only beacon localization. *Oceanic Engineering, IEEE Journal of*, 31(4):949–958, 2006.

E. Papadopoulos and M. Misailidis. On differential drive robot odometry with application to path planning. In *Proceedings of the European Control Conference, Kos, Greece*, page 5492, 2007.

L. E. Parker. Alliance: an architecture for fault tolerant multirobot cooperation. *Robotics and Automation, IEEE Transactions on*, 14(2):220–240, 1998.

L. E. Parker, B. Kannan, Xiaoquan Fu, and Yifan Tang. Heterogeneous mobile sensor net deployment using robot herding and line-of-sight formations. In *Intelligent Robots and Systems, 2003. (IROS 2003). Proceedings. 2003 IEEE/RSJ International Conference on*, volume 3, pages 2488–2493, 2003.

L. E. Parker, B. Kannan, Fang Tang, and M. Bailey. Tightly-coupled navigation assistance in heterogeneous multi-robot teams. In *Intelligent Robots and Systems, 2004. (IROS 2004). Proceedings. 2004 IEEE/RSJ International Conference on*, volume 1, pages 1016–1022, 2004.

P. N. Pathirana, N. Bulusu, A. V. Savkin, and S. Jha. Node localization using mobile robots in delay-tolerant sensor networks. *Mobile Computing, IEEE Transactions on*, 4(3):285–296, 2005.

Nissanka B. Priyantha, Anit Chakraborty, and Hari Balakrishnan. The cricket location-support system. In *Proceedings of Sixth Annual ACM International Conference on Mobile Computing and Networking*, 2000.

I. M. Rekleitis, G. Dudek, and E. E. Milios. Probabilistic cooperative localization and mapping in practice. In *Robotics and Automation, 2003. Proceedings. ICRA '03. IEEE International Conference on*, volume 2, pages 1907–1912, 2003. ISBN 1050-4729.

Ioannis M. Rekleitis, Gregory Dudek, and Evangelos E. Milios. Multi-robot exploration of an unknown environment, efficiently reducing the odometry error. *In Proceedings of the International Joint Conference on Artificial Intelligence (IJCAI)*, 1997.

S. I. Roumeliotis and G. A. Bekey. Distributed multirobot localization. *Robotics and Automation, IEEE Transactions on*, 18(5):781–795, 2002.

I. Shimshoni. On mobile robot localization from landmark bearings. *Robotics and Automation, IEEE Transactions on*, 18(6):971–976, 2002.

Reid Simmons, David Apfelbaum, Wolfram Burgard, Dieter Fox, and Mark Moors. Coordination for multi-robot exploration and mapping. In *Proceedings of the AAAI National Conference on Artificial Intelligence*, page 852. AAAI, 2000.

R. Smith, M. Self, and P. Cheeseman. *Estimating uncertain spatial relationships in robotics*, pages 167–193. Autonomous robot vehicles. Springer-Verlag New York, Inc., 1990. ISBN 0-387-97240-4.

J. R. Spletzer and C. J. Taylor. A bounded uncertainty approach to multi-robot localization. In *Intelligent Robots and Systems, 2003. (IROS 2003). Proceedings. 2003 IEEE/RSJ International Conference on*, volume 2, pages 1258–1265 vol.2, 2003.

C. Taylor, A. Rahimi, J. Bachrach, H. Shrobe, and A. Grue. Simultaneous localization, calibration, and tracking in an ad hoc sensor network. In *Information Processing in Sensor Networks, 2006. IPSN 2006. The Fifth International Conference on*, pages 27–33, 2006.

S. Thrun and Y. Liu. Multi-robot SLAM with sparse extended information filers. In *Proceedings of the 11th International Symposium of Robotics Research (ISRR'03)*, Sienna, Italy, 2003. Springer.

G. Welch and G. Bishop. An introduction to the kalman filter. *University of North Carolina at Chapel Hill, Chapel Hill, NC*, 1995.

S. B. Williams, G. Dissanayake, and H. Durrant-Whyte. An efficient approach to the simultaneous localisation and mapping problem. In *Robotics and Automation, 2002. Proceedings. ICRA '02. IEEE International Conference on*, volume 1, pages 406–411, 2002a.

S. B. Williams, G. Dissanayake, and H. Durrant-Whyte. Towards multi-vehicle simultaneous localisation and mapping. In *Robotics and Automation, 2002. Proceedings. ICRA '02. IEEE International Conference on*, volume 3, pages 2743–2748, 2002b.

X. S. Zhou and S. I. Roumeliotis. Multi-robot SLAM with unknown initial correspondence: The robot rendezvous case. In *Intelligent Robots and Systems, 2006 IEEE/RSJ International Conference on*, pages 1785–1792, 2006.

Appendices

Appendix A

Extended Kalman filter

In this application, during the prediction step of the Kalman filter, the values of the variables in the state vector are estimated on the basis of the previous estimate and the motion measured with the odometry system.

$$\hat{x}_k^- = \hat{x}_{k-1} + u_k$$

For two robots and two landmarks the predicted value for the state vector can be computed as follows:

$$\begin{bmatrix} {}^1_r\hat{x}_k^- \\ {}^1_r\hat{y}_k^- \\ {}^1_r\hat{\theta}^- \\ {}^2_r\hat{x}_k^- \\ {}^2_r\hat{y}_k^- \\ {}^2_r\hat{\theta}^- \\ {}^1_t\hat{x}_k^- \\ {}^1_t\hat{y}_k^- \\ {}^2_t\hat{x}_k^- \\ {}^2_t\hat{y}_k^- \end{bmatrix} = \begin{bmatrix} {}^1_r\hat{x}_{k-1} \\ {}^1_r\hat{y}_{k-1} \\ {}^1_r\hat{\theta}_{k-1} \\ {}^2_r\hat{x}_{k-1} \\ {}^2_r\hat{y}_{k-1} \\ {}^2_r\hat{\theta}_{k-1} \\ {}^1_t\hat{x}_{k-1} \\ {}^1_t\hat{y}_{k-1} \\ {}^2_t\hat{x}_{k-1} \\ {}^2_t\hat{y}_{k-1} \end{bmatrix} + \begin{bmatrix} {}^1_r\Delta x_k \\ {}^1_r\Delta y_k \\ {}^1_r\Delta\theta_k \\ {}^2_r\Delta x_k \\ {}^2_r\Delta y_k \\ {}^2_r\Delta\theta_k \\ 0 \\ 0 \\ 0 \\ 0 \end{bmatrix},$$

where the index in the upper left-hand corner indicates the order number of the entity and the index in the bottom left-hand corner shows the type of the entity (r=robot, t=landmark). The estimated change in the pose of a robot $(\Delta x_k, \Delta y_k, \Delta\theta_k)$ is obtained from the odometry system. However, the uncertainties of the measured changes in the position coordinates depend on the estimated heading angle and thus make the calculation of the predicted covariance matrix more complex.

As explained in Chapter 3 the measured movement of the robot can be presented as a vector with length d_k and angle ψ_k relative to the heading angle estimate θ_{k-1}. This makes the calculation of the predicted covariance matrix simpler as the variables are independent of each other.

$$u_k = \begin{bmatrix} {}^1_r d_k \\ {}^1_r \psi_k \\ {}^1_r \Delta\theta \\ {}^2_r d_k \\ {}^2_r \psi_k \\ {}^2_r \Delta\theta \\ 0 \\ 0 \\ 0 \\ 0 \end{bmatrix}$$

The prediction of the state vector using the aforementioned form of the control vector is computed with these functions:

$$\begin{aligned}
{}^1_r\hat{x}_k^- = f_x(\hat{x}_{k-1}, u_k) &= {}^1_r\hat{x}_{k-1} + {}^1_r d_k \cdot cos({}^1_r\hat{\theta}_{k-1} + {}^1_r\psi_k) \\
{}^1_r\hat{y}_k^- = f_y(\hat{x}_{k-1}, u_k) &= {}^1_r\hat{y}_{k-1} + {}^1_r d_k \cdot sin({}^1_r\hat{\theta}_{k-1} + {}^1_r\psi_k) \\
{}^1_r\hat{\theta}_k^- = f_\theta(\hat{x}_{k-1}, u_k) &= {}^1_r\hat{\theta}_{k-1} + {}^1_r\Delta\theta \\
{}^2_r\hat{x}_k^- = f_x(\hat{x}_{k-1}, u_k) &= {}^2_r\hat{x}_{k-1} + {}^2_r d_k \cdot cos({}^2_r\hat{\theta}_{k-1} + {}^2_r\psi_k) \\
{}^2_r\hat{y}_k^- = f_y(\hat{x}_{k-1}, u_k) &= {}^2_r\hat{y}_{k-1} + {}^2_r d_k \cdot sin({}^2_r\hat{\theta}_{k-1} + {}^2_r\psi_k) \\
{}^2_r\hat{\theta}_k^- = f_\theta(\hat{x}_{k-1}, u_k) &= {}^2_r\hat{\theta}_{k-1} + {}^2_r\Delta\theta
\end{aligned}$$

The landmarks are static and thus their position estimates do not change during the prediction step.

The prediction step for the covariance matrix contains movement- and measurement-related parts. The movement of the robot affects the covariances, as does the measurement uncertainty of the odometry system.

$$P_k^- = A_k P_{k-1} A_k^T + B_k U_k B_k^T$$

The accumulated inaccuracies in the heading angle estimate of the robot cause uncertainties in the position coordinates of the robot. Thus the non-diagonal elements of the system matrix A relate the heading angle uncertainty of each robot to the position coordinates of the robot:

$$A = \begin{bmatrix}
1 & 0 & -{}^1_r\Delta y_k & 0 & 0 & 0 & 0 & 0 & 0 & 0 \\
0 & 1 & {}^1_r\Delta x_k & 0 & 0 & 0 & 0 & 0 & 0 & 0 \\
0 & 0 & 1 & 0 & 0 & 0 & 0 & 0 & 0 & 0 \\
0 & 0 & 0 & 1 & 0 & -{}^2_r\Delta y_k & 0 & 0 & 0 & 0 \\
0 & 0 & 0 & 0 & 1 & {}^2_r\Delta x_k & 0 & 0 & 0 & 0 \\
0 & 0 & 0 & 0 & 0 & 1 & 0 & 0 & 0 & 0 \\
0 & 0 & 0 & 0 & 0 & 0 & 1 & 0 & 0 & 0 \\
0 & 0 & 0 & 0 & 0 & 0 & 0 & 1 & 0 & 0 \\
0 & 0 & 0 & 0 & 0 & 0 & 0 & 0 & 1 & 0 \\
0 & 0 & 0 & 0 & 0 & 0 & 0 & 0 & 0 & 1
\end{bmatrix}$$

The measurement uncertainties contained as diagonal elements in the matrix U are multiplied by the matrix B:

$$B_k = \begin{bmatrix} \cos({}^1_r\theta_{k-1} + {}^1_r\psi_k) & -{}^1_r\Delta y_k & 0 & 0 & 0 & 0 & 0 & 0 & 0 & 0 \\ \sin({}^1_r\theta_{k-1} + {}^1_r\psi_k) & {}^1_r\Delta x_k & 0 & 0 & 0 & 0 & 0 & 0 & 0 & 0 \\ 0 & 0 & 1 & 0 & 0 & 0 & 0 & 0 & 0 & 0 \\ 0 & 0 & 0 & \cos({}^2_r\theta_{k-1} + {}^2_r\psi_k) & -{}^2_r\Delta y_k & 0 & 0 & 0 & 0 & 0 \\ 0 & 0 & 0 & \sin({}^2_r\theta_{k-1} + {}^2_r\psi_k) & {}^2_r\Delta x_k & 0 & 0 & 0 & 0 & 0 \\ 0 & 0 & 0 & 0 & 0 & 1 & 0 & 0 & 0 & 0 \\ 0 & 0 & 0 & 0 & 0 & 0 & 0 & 0 & 0 & 0 \\ 0 & 0 & 0 & 0 & 0 & 0 & 0 & 0 & 0 & 0 \\ 0 & 0 & 0 & 0 & 0 & 0 & 0 & 0 & 0 & 0 \\ 0 & 0 & 0 & 0 & 0 & 0 & 0 & 0 & 0 & 0 \end{bmatrix}$$

which is a Jacobian matrix of the functions $f(\hat{x}_{k-1}, u_k)$ with respect to the input vector u_k.

If a robot makes a successful bearing measurement to a landmark, a correction can be applied to the predicted values of the state vector. The residual between the measured bearing and the expected value computed with the function $h(\hat{x}_k^-)$ is used to correct the estimated values of the variables in the state vector. The residual is a vector with as many rows as there are measurements. When Robot 1 makes one measurement to Landmark 2 and Robot 2 makes one measurement to Landmark 1, the expected values for the bearing angle measurements are calculated as follows:

$$\begin{aligned} h_1(\hat{x}_k^-) &= atan2\left(\frac{{}^2_t\hat{y}_k^- - {}^1_r\hat{y}_k^-}{{}^2_t\hat{x}_k^- - {}^1_r\hat{x}_k^-}\right) - {}^1_r\hat{\theta}_k^- \\ h_2(\hat{x}_k^-) &= atan2\left(\frac{{}^1_t\hat{y}_k^- - {}^2_r\hat{y}_k^-}{{}^1_t\hat{x}_k^- - {}^2_r\hat{x}_k^-}\right) - {}^2_r\hat{\theta}_k^- \end{aligned}$$

In the aforementioned case of two robots making one measurement each, the measurement matrix H is:

$$H = \begin{bmatrix} \frac{-\Delta y_1}{(\Delta y_1)^2+(\Delta x_1)^2} & \frac{\Delta x_1}{(\Delta y_1)^2+(\Delta x_1)^2} & -1 & 0 & 0 & 0 \\ 0 & 0 & 0 & \frac{-\Delta y_2}{(\Delta y_2)^2+(\Delta x_2)^2} & \frac{\Delta x_2}{(\Delta y_2)^2+(\Delta x_2)^2} & -1 \end{bmatrix}$$

$$\begin{bmatrix} 0 & 0 & \frac{\Delta y_1}{(\Delta y_1)^2+(\Delta x_1)^2} & \frac{-\Delta x_1}{(\Delta y_1)^2+(\Delta x_1)^2} \\ \frac{\Delta y_2}{(\Delta y_2)^2+(\Delta x_2)^2} & \frac{-\Delta x_2}{(\Delta y_2)^2+(\Delta x_2)^2} & 0 & 0 \end{bmatrix}$$

where the difference in the x coordinates of a robot and a landmark is marked $\Delta x_1 = {}^2_t\hat{x}_k^- - {}^1_r\hat{x}_k^-$ and $\Delta x_2 = {}^1_t\hat{x}_k^- - {}^2_r\hat{x}_k^-$. The difference in the y-coordinates

is marked respectively. The number of rows in the matrix H is defined by the number of measurements. The number of columns is the same as the number of elements in the state vector.

If there are two measurements the denominator in the Kalman gain equation becomes a 2 x 2 matrix:

$$K_k = P_k^- H_k^T (H_k P_k^- H_k^T + R_k)^{-1}$$

As the number of measurements increases, so do the dimensions of the denominator matrix, which increases the computational complexity of the update phase. The matrix R is a square matrix with the measurement uncertainty of each measurement on its diagonal. The resulting Kalman gain has as many rows as the state vector. The number of columns is defined by the number of measurements.

The update phase is only computed when there is at least one measurement. For two measurements the state vector is updated as follows:

$$\hat{x}_k = \hat{x}_k^- + \begin{bmatrix} {}^1_{r,x}\mathcal{G}1 & {}^1_{r,x}\mathcal{G}2 \\ {}^1_{r,y}\mathcal{G}1 & {}^1_{r,y}\mathcal{G}2 \\ {}^1_{r,\theta}\mathcal{G}1 & {}^1_{r,\theta}\mathcal{G}2 \\ {}^2_{r,x}\mathcal{G}1 & {}^2_{r,x}\mathcal{G}2 \\ {}^2_{r,y}\mathcal{G}1 & {}^2_{r,y}\mathcal{G}2 \\ {}^2_{r,\theta}\mathcal{G}1 & {}^2_{r,\theta}\mathcal{G}2 \\ {}^1_{t,x}\mathcal{G}1 & {}^1_{t,x}\mathcal{G}2 \\ {}^1_{t,y}\mathcal{G}1 & {}^1_{t,y}\mathcal{G}2 \\ {}^2_{t,x}\mathcal{G}1 & {}^2_{t,x}\mathcal{G}2 \\ {}^2_{t,y}\mathcal{G}1 & {}^2_{t,y}\mathcal{G}2 \end{bmatrix} \left(\begin{bmatrix} z_1 \\ z_2 \end{bmatrix} - \begin{bmatrix} h_1 \\ h_2 \end{bmatrix} \right)$$

The Kalman gain matrix has coefficients that relate each measurement residual to the elements of the state vector. For example, the residual of the first measurement $(z_1 - h_1)$ affects the x-coordinate of the first robot according to the Kalman gain variable ${}^1_{r,x}\mathcal{G}1$. Some of the gain variables may be zeros if there is no correlation between some variable in the state vector and the variables directly involved in the measurement.

The covariance matrix P is a square matrix with dimensions according to the number of elements in the state vector. The update of the covariance matrix is calculated as follows:

$$P_k = (I - K_k H_k) P_k^-$$

As the Kalman gain always has as many rows as the state vector and the measurement matrix H has the same number of columns, the product $K_k H_k$ used in the update of the covariance matrix, always results in a matrix with the same dimensions as the matrix P_k^-.

Appendix B

Software architecture

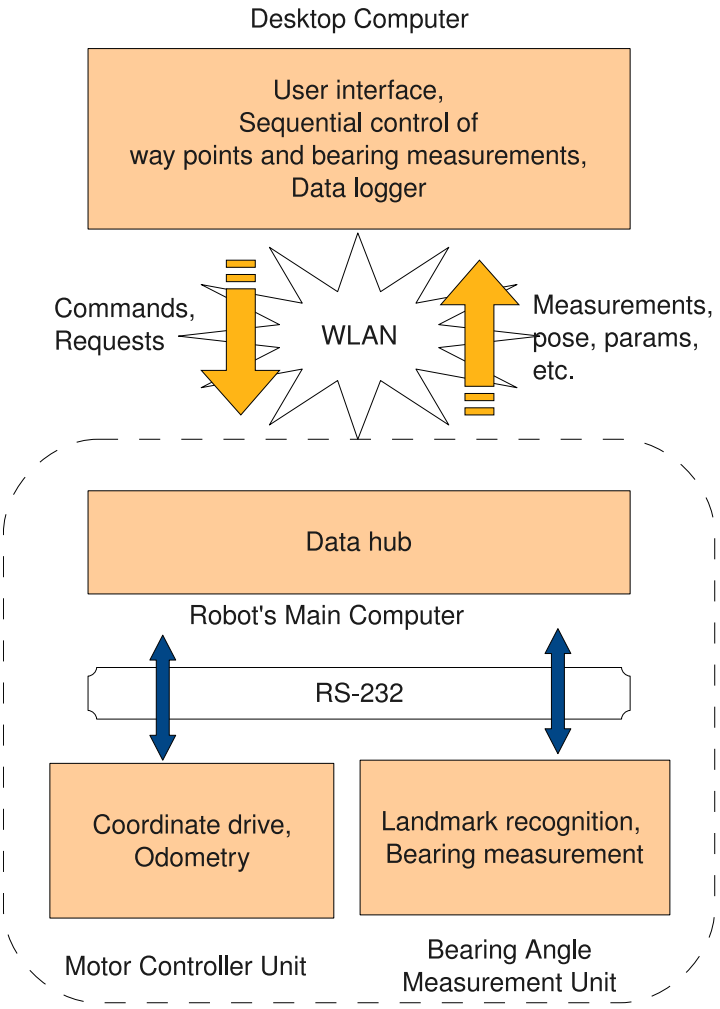

Figure B.1: The high-level architecture of the system software. The software is divided between the two computers and the two microcontrollers. The parts within the dashed lines are mounted on the robot.

Appendix C

Simulation parameters

Table C.1: The default values for the parameters in the system performance simulations

Standard deviation of original error in robot's x-coordinate	ϵ_{orig_x}	0.01 m
Standard deviation of original error in robot's y-coordinate	ϵ_{orig_y}	0.01 m
Standard deviation of original error in robot's heading	ϵ_{orig_θ}	0.025 rad (1.4°)
Standard deviation in the measured bearing angle	ϵ_λ	0.30 rad (17.2°)
Standard deviation of heading angle error introduced when turning 2π	ϵ_θ	0.050 rad (2.9°)
Standard deviation of systematic heading angle error introduced when turning 2π	ϵ_{sys}	0.012 rad (0.7°)
Distance between consecutive measurements	*step*	0.2 m

Table C.2: The default values for noise parameters in the system performance simulations

Initial position uncertainty	$4.0 \cdot 10^{-4} m^2$
Initial heading angle uncertainty	$1.0 \cdot 10^{-3} rad^2$
Odometry noise for position coordinates	$1.6 \cdot 10^{-5} m^2$
Odometry noise for heading angle	$1.6 \cdot 10^{-3} rad^2$
Measurement noise for bearing angle	$0.14 rad^2$

Appendix D

Laboratory experiments

Table D.1: The robot-specific noise parameters used in the laboratory experiments.

	Robots			
	Danny	Emma	Fiona	Hugo
Initial position variance / m^2	0.0016	0.0016	0.0016	0.0016
Initial angle variance / rad^2	0.001	0.001	0.0006	0.0006
Variance in odometry distance for one meter / m^2	$4 \cdot 10^{-6}$	$4 \cdot 10^{-6}$	$4 \cdot 10^{-6}$	$4 \cdot 10^{-6}$
Variance in measured heading angle change of one rad / rad^2	$9 \cdot 10^{-4}$	$9 \cdot 10^{-4}$	$2.25 \cdot 10^{-4}$	$9 \cdot 10^{-4}$
Variance in the bearing angle measurement / rad^2	0.6	0.6	0.35	0.3

Table D.2: Average number of measurements (during one pass) to each tag with different robots. The low number of measurements to Landmarks 7 and 9 is partly because these landmarks were often not detected at all.

	Landmarks									
	1	2	3	4	5	6	7	8	9	10
Danny	5.14	5.21	5.29	4.79	5.21	7.64	2.86	6.36	3.07	5.00
Emma	6.14	5.71	6.86	5.14	5.71	7.57	2.21	6.50	1.57	5.93
Fiona	5.71	6.79	5.64	8.07	7.36	8.43	3.07	7.29	2.64	7.07
Hugo	4.0	5.00	5.57	5.79	5.57	6.93	1.21	5.43	0.71	3.79

HELSINKI UNIVERSITY OF TECHNOLOGY AUTOMATION TECHNOLOGY RESEARCH REPORTS

No. 22 Appelqvist, P.,
Mechatronics design of a robot society – A case study of minimalist underwater robots for distributed perception and task execution, November 2000.

No. 23 Forsman, P.,
Three-dimensional localization and mapping of static environments by means of mobile perception, November 2001.

No. 24 Selkäinaho, J.,
Adaptive autonomous navigation of mobile robots in unknown environments, December 2002.

No. 25 Oksanen, T.,
Nelijalkainen nelipyöräinen robotti liikkuvana systeeminä, February 2003.

No. 26 Suomela, J.,
From teleoperation to the cognitive human-robot interface, November 2004.

No. 27 Aalto, H.,
Real-time receding horizon optimization of gas pipeline networks, April 2005.

No. 28 Ylönen, S.,
Modularity in service robotics – Techno-economic justification through a case study, December 2006.

No. 29 Appelqvist, A.,
Development of a biocatalytic fuel cell system for low-power electronic applications, December 2006.

No. 30 Leppänen, I.,
Automatic Locomotion Mode Control of Wheel-Legged Robots, September 2007.

No. 31 Oksanen, T.,
Path Planning Algorithms for Agricultural Field Machines, December 2007.

No. 32 Pirttioja, T.,
Applying Agent Technology to Constructing Flexible Monitoring Systems in Process Automation, December 2008.

No. 33 Saarinen, J.,
A sensor-based personal navigation system and its applications for incorporating humans into a human-robot team June 2009.

No. 34 Heikkilä, M.,
Configuration of skilled tasks for execution in multipurpose and collaborative service robots, December 2009.

No. 35 Taipalus, T.,
ActionPool: A Novel Dynamic Task Scheduling Method for Service Robots, November 2010.

ISBN 978-952-60-3440-9 (print)
ISBN 978-952-60-3441-6 (pdf)
ISSN 0783-5477